GEOWISSENSCHAFTLICHE MITTEILUNGEN

Heft Nr. 78, 2007

Research Projects at IGG
- Reports -

Gintcho Kostov, Géraldine Bourda,
Laura Fernandez, Tetsuro Kondo

Veröffentlichung des
Instituts für Geodäsie und Geophysik (IGG)

ISSN 1811-8380

Schriftenreihe der Studienrichtung VERMESSUNG UND GEOINFORMATION
TECHNISCHE UNIVERSITÄT WIEN

Project:

Assessment of the Quality of Geodetic Networks Using Fuzzy Logic

Gintcho Kostov

Guest scientist at the IGG from

01-10-2004 to 31-05-2005

Abstract

One of the main tasks when dealing with the adjustment of geodetic networks is to estimate their accuracy and condition. Generally two distinct ways exist for the assessment of the quality of geodetic networks: either a pure mathematical approach with exact criteria or fuzzy logic, where linguistic terms are used. In order to produce reliable results in the case of many parameters and conditions, the networks under investigation are assessed with fuzzy logic. For this study a software for processing the results of the adjustment used as input variables for the fuzzy logic application has been developed. Its final task is computing rating values in the interval [0,1] showing the quality of the system, i.e. in our case the adjusted geodetic network. Conclusions are made, taking in mind the computed rating values for various geodetic networks.

1. Introduction

The classical way for assessing geodetic networks is based on various criteria (described in the next chapter), derived within the adjustment procedure. The human expert should decide which system amongst others has the best quality, based on each criterion. The technical problem is that some of the mathematical criteria known from literature are derived in parallel with the processing, whereas for others additional computations are necessary. Due to this reason and because of the complexity of the problems in some occasions the geodesists use only a few criteria, neglecting the others. However, for a complete network analysis all available criteria for accuracy and condition should be considered in order to get reliable results.

Generally, using fuzzy logic is a way to assess a system, which has a number of parameters varying between large and small values. It is in particular useful when no exact deterministic model exists for the problem, but rules can be found by human experts, solving the problem by their experience. In this case, fuzzy logic is an alternative for assessing both condition and accuracy of geodetic networks. One of the important questions in geodesy is the choice of appropriate weights. In some of the articles the application of fuzzy logic in geodesy is treated only under the assumption of equal weights. As it will be shown here, in fuzzy logic weights have their significance, too. An application has been developed, which reads the variables, values, rules and after finishing all processes calculates the rating value for the given system.

2. Fuzzy logic

2.1 Some general information

The general concept of fuzzy logic is described e.g. by Wieser (2001). A fuzzy set consists of pairs of values of a given variable and relevant values of a characteristic membership function , often abbreviated as MF. The value of MF is in the range of [0,1], indicating the so-called degree of membership. Value "0" indicates non-membership, while "1" indicates full membership. The difference to the classical

concept of set theory is that with fuzzy sets, also degrees of membership between 0 and 1 are possible.

The main idea of fuzzy variables is linguistic: e.g. "small", "not big", "rather big", "big". For example, one can treat a number around 0.1 as "small", a number around 0.6 as "not big" and a number around 0.9 as "big". The general scheme for the so-called fuzzy controller is:

Input>Fuzzification>Inference>Defuzzification

In the first part certain values are entered, which are then fuzzified, this means with the relevant MF they get their value for the degree of membership. In the inference part the weights are given and the relevant operator ("and", "or") is applied. The final part called defuzzification is used to obtain a crisp value for the rating. There are several methods to perform this final part of the calculation, but the most appropriate and commonly used one is the *centroid* method of defuzzification.

Fuzzy logic is a simple way to "plot" an input region into an output region. An example: *if I know how good was the lunch at your favourite restaurant today, I could tell you what is the tip you should give.*

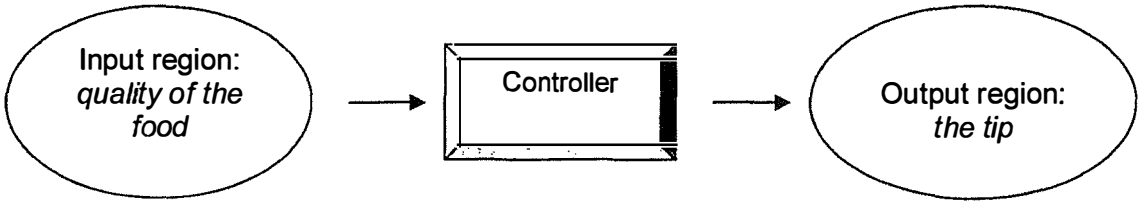

Figure 1: Graphical example for a fuzzy logic system

The common structure of a rule is: input variables, resulting MF, weight, logical operator ("and (1)", "or (2)"). For example, if the user defines a, b, and c as input variables, the rules may look in the following way:

a	b	c	resulting MF	weight	logical operator
-1	0	0	1	0,4	2
0	-1	0	1	0,85	2
0	0	-1	1	0,9	2
1	0	0	2	0,4	2
0	1	0	2	0,85	2
0	0	1	2	0,9	2

Figure 1a: Example and description for six rules

In natural language the last rule has the following meaning: If (c is small) then the network is *goodnetwork*, (weight).

After the calculation, the user will get a value between [0,1], telling the quality of the system. In this particular case, for example if we derive a rating of 0.85 we can say that the system is *goodnetwork*. In case we get 0.95 it can be said that the system is also *goodnetwork*, but much better. But if the rating is 0.25, the system is considered as *badnetwork.* One can assess any kind of system, with given input variables and user-constructed rules.

2.2 Applications of fuzzy logic in geodesy

The possible use of fuzzy logic for various geodetic tasks (GPS, data processing, landslide monitoring, etc.) has been described in several publications, e.g. by Heine (2001), Kutterer (2001), Leinen (2001), Wieser (2001), Haberler (2003), Wieser (2003). Many more applications of this logic might be possible in geodesy, depending on the specific needs. One new additional possible usage for the assessment of the quality of geodetic networks will be given in this paper.

3. Application of fuzzy logic for assessing geodetic networks

3.1 Mathematical Basics

A brief explanation of the used symbols in the article will be given here:

N - Normal equation matrix;
Q - Co-factor matrix;
$\mathrm{cond}(.)$ - Condition number of a matrix;
$\mathrm{Tr}()$ - Trace of a matrix;
$\mathrm{Det}()$ - Determinant of a matrix;
Mar - Mean arithmetic error for the whole network;
Msq - Mean quadratic error for the whole network;
m_P - Mean error in the position of a new point;
nn - Number of the new-determined points;
n - Dimension of a matrix;
a_{ij} - Element of a matrix;
λ_i - Eigenvalue of the Q matrix;
B_i - Hyper ellipsoid semi-axis.

In this research the following criteria for assessing the quality of geodetic networks are used, all of them based on parameters obtained by a standard least-squares fit:

Sum Tr(Q) of the diagonal elements of the co-factor matrix of parameters:

$$\mathrm{Tr}(Q) = \sum_{i=1}^{n} Q(i,i) \tag{1}$$

Determinant Det(Q) of the inverse matrix Q of the normal equation matrix N :

$$\mathrm{Det}(Q) = \prod_{i=1}^{n} \lambda_i \tag{2}$$

Mean arithmetic error Mar for the whole network:

$$\mathrm{Mar} = \frac{\sum m_{P_i}}{nn} \tag{3}$$

Mean quadratic error Msq for the whole network:

$$\mathrm{Msq} = \sqrt{\frac{\sum m_{P_i}^2}{nn}} \tag{4}$$

Semi-axes B_i of the ellipse, respectively hyper ellipsoid of errors:

$$B_i = \mu\sqrt{\lambda_i} \tag{5}$$

where μ is the RMS for weight 1. This criterion is both used locally, i.e. for each new point, and globally, i.e. for the whole network.

The product:

$$\varepsilon \cdot \mathrm{cond}(N) \tag{6}$$

described by Konstantinov and Vulchanov (1987), where $\varepsilon = 2.2204e-016$ and N is the normal equation matrix. It is known, that if $\varepsilon \cdot \mathrm{cond}(N) << 1$, the matrix N is well conditioned. With $\mathrm{cond}(N) = \|N\|\|N^{-1}\|$ the condition number of the matrix under investigation is denoted.

We also use the criteria Nnumber and Mnumber, given in Faddeev and Faddeeva (1963), using the design matrix A :

$$\mathrm{Nnumber} = \frac{1}{n} N(N_A) N(N_A^{-1}); \quad \mathrm{Mnumber} = \frac{1}{n} M(N_A) M(N_A^{-1}); \tag{7}$$

$$N(N_A) = \sqrt{\mathrm{Tr}(N_A^T N_A)}, \; M(N_A) = n \cdot \max_{ij} |a_{ij}| \tag{8}$$

It must be noted, that in order to avoid confusion, only in (7) and (8) the normal equation matrix is denoted with N_A.

P number:

$$P = \frac{\max|\lambda_i|}{\min|\lambda_i|} \tag{9}$$

All criteria are derived from the adjustment process of the geodetic networks. Later on they will be used as input variables in fuzzy logic.

3.2 Software information

In order to customize, ease and mechanize the calculation of the rating values, especially for geodetic purposes an application has been developed in the OS Windows XP environment. The actual aim of the application is to assess the quality of a given

geodetic network (measured by triangulation and trilateration), based on the computed rating with appropriately assigned weights for each input variable.

The main characteristics and capabilities of the application are:

a) It is possible to enter the names of the variables and their values by hand or from file.
b) A check for inconsistency of the input parameters is performed.
c) Appropriate weights are calculated for each variable, as will be demonstrated in section 3.3.
d) Construction can easily be performed, editing, addition and removal of the rules, more than one simultaneously.
e) A check for blunders in the rules is also done.
f) It is possible to perform sequential computations after changing the necessary parameters.
g) The last computations are optionally saved for further referencing.
h) The rating of any given system can be evaluated with minimum effort.
i) For the current needs the case is considered with two linguistic terms, describing the output i.e. *badnetwork* and *goodnetwork* (see section 3.4).

The input and editing of the rules is organized in a memo box, which allows the user to easily change the parameters of the rules, including the weights.

In case the user enters the data from the adjustment *by hand*, the following is required:

- names of input variables;
- their values;
- type of the input membership function - either ZMF (function, which has a shape as the letter "Z", figure 2);
- or SMF (function, which has a shape as the letter "S", figure 3), the default is set to ZMF.

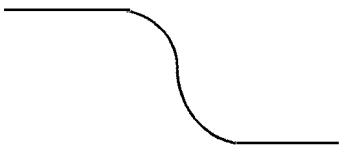

Figure 2: View of the ZMF function

Figure 3: View of the SMF function

- minimum and maximum input range;
- required parameters for each input function, corresponding to each variable;
- names of the linguistic terms, two are necessary for current purposes;
- values of the output parameters, there are default set values;
- rules, simply with –1, 0, 1;
- weight for each rule, one by default;
- resulting variable (*badnetwork* or *goodnetwork)*;
- logical operator in the rule: or/and.

3.3 Weights of the rules

The weights p_i can be calculated using the equation:

$$p_i = \frac{\text{MinParameter}}{\text{Value}_i}, \text{ for } \text{Value}_i \neq 0 \qquad (10)$$

where MinParameter is the smallest parameter of the relevant membership function used for the calculations. The values of the weights will be between [0,1]. Thus, every variable will get its most-appropriate weight and the system (in our case the network) will be assessed in a strict way.

In our investigation the weights were determined according to one of three different options, in order to compare the results:

1. Each rule has the weight 1;
2. Each rule has a weight calculated according to equation (10);
3. Each rule, consisting of different variables has a weight determined by the human expert.

3.4 Assessment of geodetic networks

The following studies were done within this research:

1. Construction of the rules with a single variable according to section 3.3.
2. Including only certain variables in the rules in order to investigate specific characteristics of a given network.
3. Investigating the quality of specific small networks and also of a big network based on sets of variables and the geographical positions of certain fixed points within the geodetic network.

In order to decide which network variant from a given set has a good quality in terms of accuracy and condition, the values of the relevant criteria were determined according to section 3.1. The key moment for the user is to define the rules, based on human experience, with appropriate weights.

For example:

If Tr(Q) is small then system is goodnetwork -> high weight,

If Tr(Q) is small or Det(Q) is small then system is goodnetwork -> medium weight,

If Tr(Q) is big then system is badnetwork -> small weight,

where "*badnetwork*" and "*goodnetwork*" are the linguistic terms, describing the quality of the system. From the input data (values of variables, rules, etc.), the application computes the rating value.

Experiments were performed with geodetic networks having various geometry and different number of fixed points which all are part of a big network (figure 4) – along the parallel (figure 5), along the meridian (figure 6), and in a square area (figure 7). The tests were done in order to explore certain characteristics of the networks and also to detect eventual differences of the rating values depending on certain input data. In some of the variants coordinates, treated as measurements, were added to the usual angular and distance measurements to improve the quality.

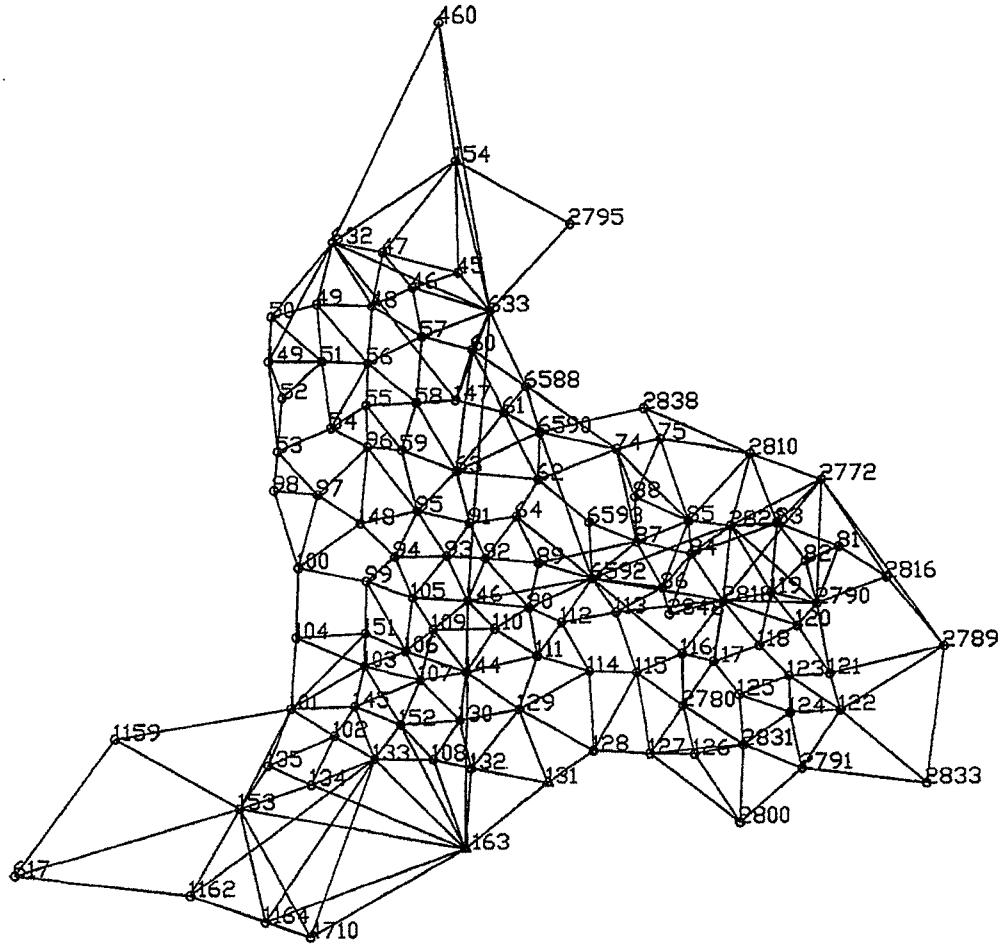

Figure 4: Plan of the network; M ≈ 1 : 300 000

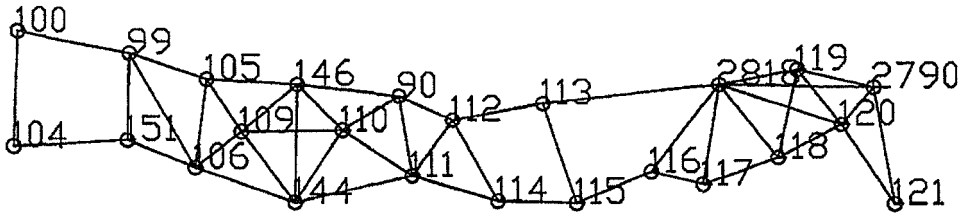

Figure 5: Plan of the network along the parallel; M ≈ 1 : 200 000

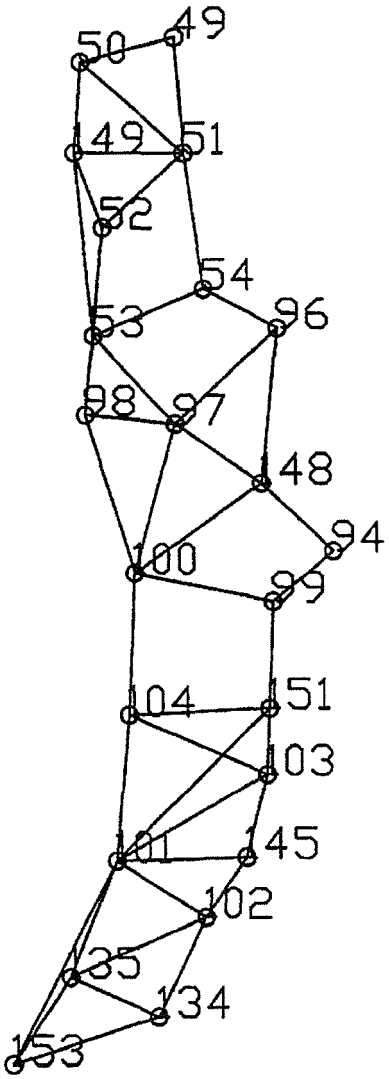

Figure 6: Plan of the network along the meridian; M ≈ 1 : 200 000

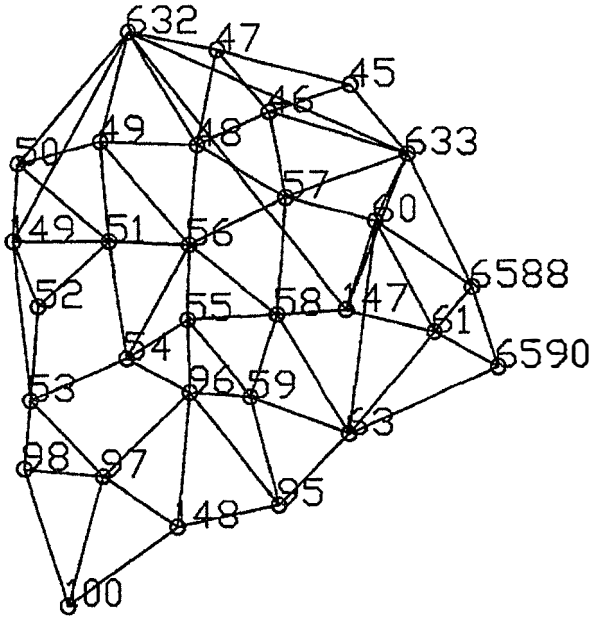

Figure 7: Plan of the network with a square area shape; M ≈ 1 : 200 000

3.5 Results and remarks

The comparison of the rating values using either equal weights or appropriately assigned weights is given in figure 8.

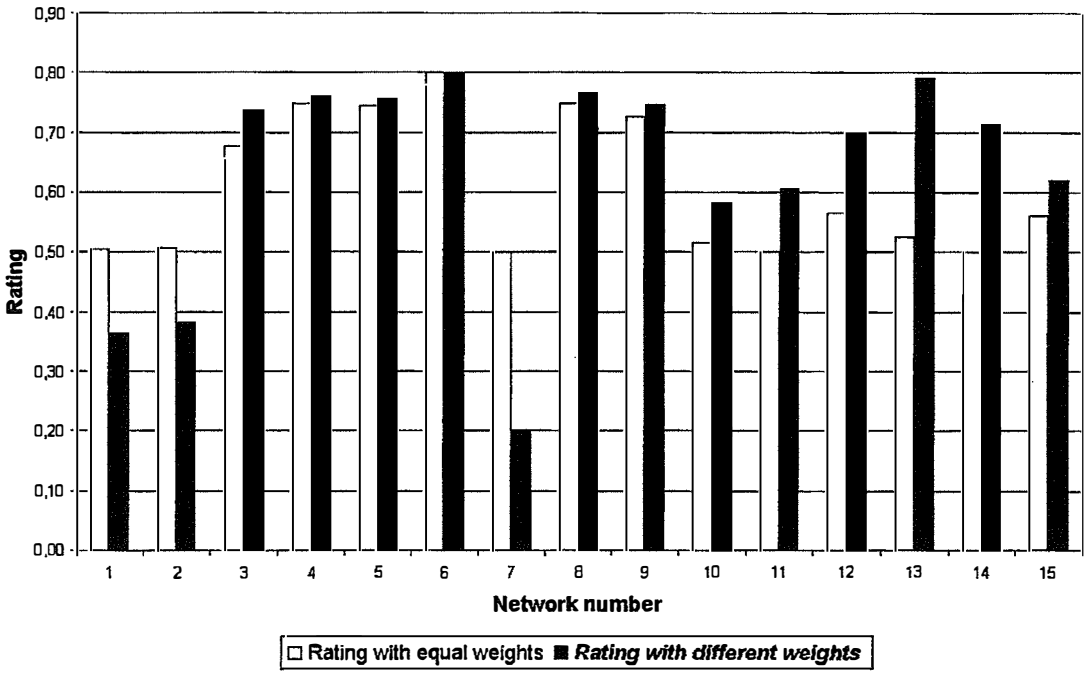

Figure 8: Rating of the meridian network, parallel network and network with a square area shape (see Table 1). Calculated with Tr (Q), Det (Q), maximum hyper ellipsoid semi-axis, eps*cond(N), Mnumber.

Detailed descriptions of the various solutions, the variables and the rating values are given in table 1. For network M3 (fixed points 134, 153 from the network along the meridian with additional coordinate measurements) and also for network M4 (fixed points 99, 100 from the network along the meridian) the rating is higher in comparison with network M1 (fixed points 49, 50 from the network along the meridian) and network M2 (fixed points 134, 153 from the network along the meridian). The difference between the rating values with equal or appropriately assigned weights in network M1 and M2 is due to the fact that they were not suitably chosen. Similar results are valid for networks P1 to P5. A high value is obtained when coordinate measurements were added, e.g. in P4, compared to P3, or when the fixed points are positioned in the opposite part of the network, see P2. From estimating the network with a square area shape it can be concluded, that the highest rating is derived when the fixed points are positioned in the central part of the network. As a result it can be said that there is a slight change in the rating values when using different weights instead of equal weights.

Number of network	Kind of sub-network	Coordinates fixed for points	Criteria (variables)					Rating	
			Tr(Q)	Det(Q)	Max Hyper Ellipsoid Semiaxis [mm]	Eps*cond(N)	Mnumber	Rating with equal weights	Rating with different weights
M1	Meridian Net	49, 50	2,03E+04	3,82E+35	1,41E+03	1,77E-11	1,45E+05	0,50	0,36
M2		134, 153	1,95E+04	8,73E+35	1,37E+03	1,72E-11	1,35E+05	0,51	0,38
M3		134, 153 and added additional measurements	5,17E+03	1,14E+30	7,21E+02	4,99E-12	6,24E+04	0,68	0,74
M4		99, 100	4,96E+03	1,06E+35	5,53E+02	2,80E-12	2,80E+04	0,75	0,76
P1	Parallel net	100, 104, 112, 114	4,51E+03	1,31E+33	5,66E+02	2,65E-12	4,78E+04	0,74	0,76
P2		100, 104, 121, 2790	2,27E+03	3,31E+31	3,12E+02	1,14E-12	5,64E+03	0,80	0,80
P3		100, 104	4,26E+04	2,16E+40	1,85E+03	3,35E-11	3,31E+05	0,50	0,20
P4		100, 104 and added additional measurements	2,89E+03	3,45E+31	5,55E+02	2,14E-12	3,55E+04	0,75	0,77
P5		112, 114	8,83E+03	4,78E+40	6,07E+02	3,78E-12	5,45E+04	0,73	0,75
A1	Area net	98, 100	2,66E+04	1,07E+60	9,57E+02	9,12E-12	3,21E+04	0,52	0,58
A2		50, 149	2,23E+04	1,36E+61	9,16E+02	7,80E-12	3,88E+04	0,50	0,61
A3		50, 149 and added additional measurements	3,66E+03	1,09E+53	1,00E+03	1,20E-12	2,18E+04	0,57	0,69
A4		58, 59	6,76E+03	9,31E+60	4,03E+02	1,64E-12	8,63E+03	0,53	0,79
A5		60, 633	1,49E+04	1,68E+61	6,91E+02	4,66E-12	2,71E+04	0,50	0,72
A6		47, 632	2,08E+04	7,50E+60	8,90E+02	7,47E-12	4,10E+04	0,56	0,62

Table 1: Rating values (with equal and appropiriate weights) of the networks with five variables

The quality of a big classical network (figure 4) was investigated within nine variants with various locations of the fixed points (table 2 and figure 9). Major differences of the rating values can be observed in network variant N6. The reason for this low rating are mainly the large values of the used criteria and the position of the fixed points on the western edge of the network.

Number of variant	Fixed points	Criteria (variables)						Rating	
								First set	Second set
		Tr(Q)	Mnumber	Nnumber	eps*cond(N)	Msq	Mar	used variables: Tr(Q), Mnumber, Nnumber,	used variables: Tr(Q), Mnumber, Nnumber, eps*cond(N), Msq, Mar
N1	154, 632	9058,5	1193759,2	1178,3	5,91E-11	117,4	100,5	0,80	0,76
N2	131, 1163 and added additional measurements I-st set	2809,7	1078695,7	306,4	1,54E-11	159,8	97,0	0,80	0,76
N3	131, 1163 and added additional measurements II-nd set	2784,7	1076700,2	304,8	1,53E-11	101,5	63,3	0,80	0,79
N4	131, 1163	6384,0	1078788,9	739,5	3,71E-11	99,1	62,1	0,80	0,79
N5	90, 112	7809,4	1125876,9	964,0	4,84E-11	109,0	90,0	0,80	0,79
N6	617, 1159	185305,3	4170793,6	32735,9	1,64E-09	631,1	503,3	0,20	0,20
N7	49-50 and added additional measurements	2790,6	1087574,8	303,3	1,52E-11	66,5	41,0	0,80	0,80
N8	45-633	15946,0	1345421,4	2367,8	1,19E-10	155,8	137,7	0,79	0,76
N9	100, 104	10642,7	1126818,5	1467,2	7,36E-11	127,3	110,4	0,80	0,78

Table 2: Input variables and rating values of the big network (Figure 4) with nine variants, using two sets of variables.

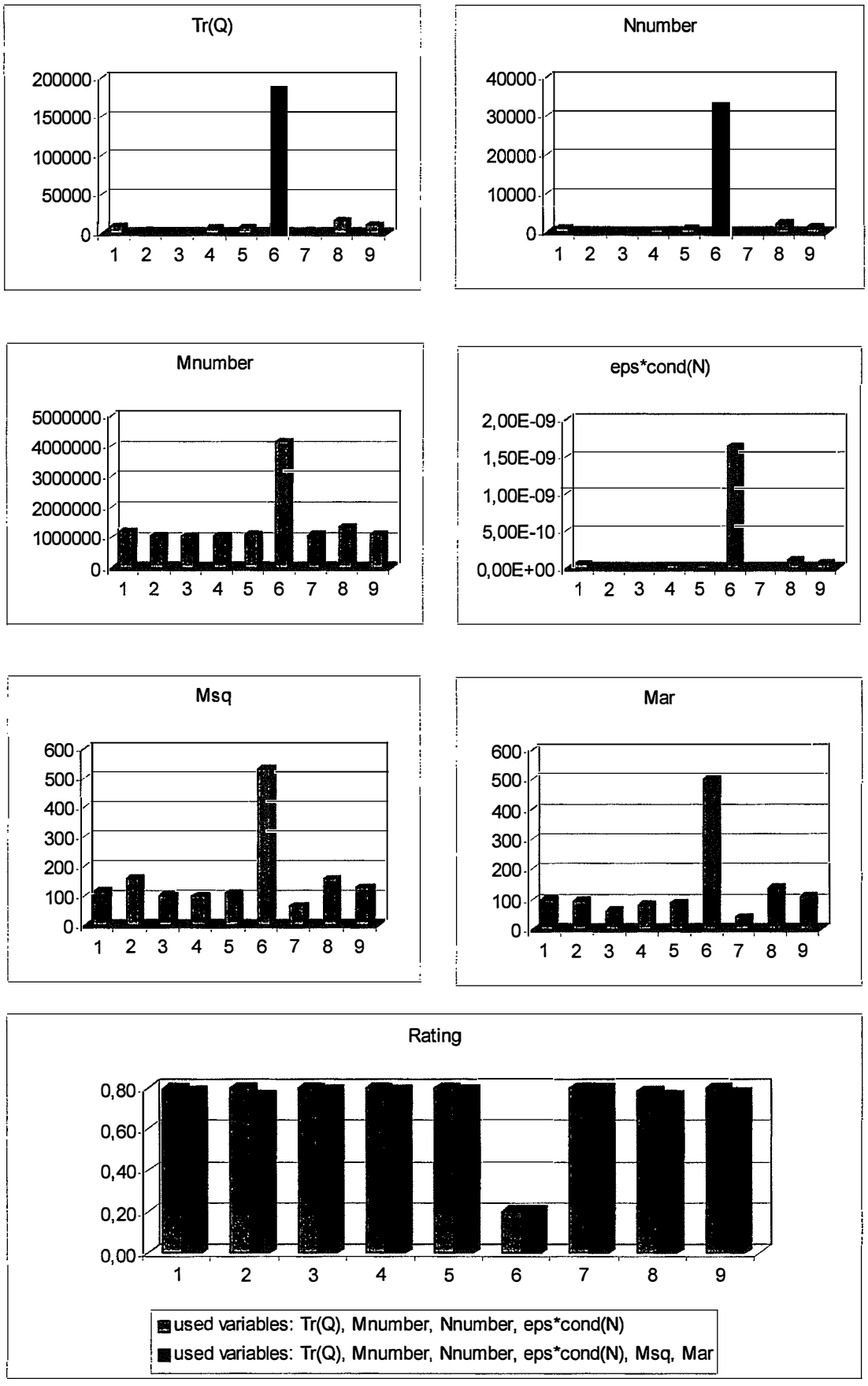

Figure 9: Values of the input variables and fuzzy logic rating for investigating the condition of the big network with nine variants.

The network with a square area shape (figure 7) was under investigation with variables and rating values summarized in table 3 and figure 10. For this case six input variables were used. The reason for the low rating of networks 1, 5, 7, 10 might be due to the small number of fixed points or their specific position. High rating between 0.74 and 0.79 was obtained when coordinates were added as "measurements" for improving the quality of the network. It should be noted that there is no significant difference in the rating when the coordinate measurements were increased even to 8 (network 12-15). As a result it can be said that almost the same rating was obtained when no coordinate measurements were added, but the fixed points are at the periphery of the network according to variant 11. Thus, the quality of a network can be assessed with fuzzy logic to decide about the number of coordinates to be added.

		Variables						
	Fixed points	*Tr(Q)*	*Mnumber*	*Nnumber*	*eps*cond(N)*	*Det(Q)*	*P number*	**Rating**
1	45, 47	14568,2	29409,2	369,8	4,60E-12	1,43E+60	6817,5	0,63
2	45, 47 and added coordinates I-st case	2586,8	18908,7	56,8	7,06E-13	3,43E+53	1066,2	0,78
3	45, 47and added coordinates II-nd case	4248,9	29666,2	126,8	1,58E-12	2,41E+52	2493,9	0,74
4	45, 47 and added coordinates III-rd case	2234,6	18818,4	48,8	6,06E-13	7,94E+50	934,6	0,78
5	53, 98	26869,9	40976,6	787,3	9,79E-12	1,93E+61	15757,2	0,43
6	53, 98 and added coordinates	2344,9	16911,1	47,0	5,84E-13	3,58E+52	834,2	0,78
7	60, 633	14879,6	27033,9	375,0	4,66E-12	1,67E+61	7090,7	0,64
8	60, 633 and added coordinates	2358,2	16447,8	47,5	5,91E-13	1,48E+53	878,4	0,78
9	59, 95	10866,8	15983,2	246,4	3,06E-12	3,26E+60	4173,7	0,75
10	61, 6590	44028,1	71679,3	1306,2	1,62E-11	1,98E+61	25250,8	0,20
11	45, 47, 53, 59, 61, 95, 98, 6590	883,7	1783,8	12,2	1,19E-13	1,58E+40	159,7	0,80
12	45, 47 and added two coordinates	3194,0	20139,8	78,6	9,77E-13	6,54E+53	1317,4	0,77
13	45, 47 and added four coordinates	1554,8	13739,4	35,8	4,45E-13	2,05E+47	493,4	0,79
14	45, 47 and added six coordinates	1178,4	13184,4	32,8	4,07E-13	1,10E+41	460,2	0,79
15	45, 47 and added eight coordinates	917,6	13128,7	31,7	3,94E-13	4,58E+35	454,6	0,79

Table 3: Investigating the condition of a network with a square area shape, fifteen variants

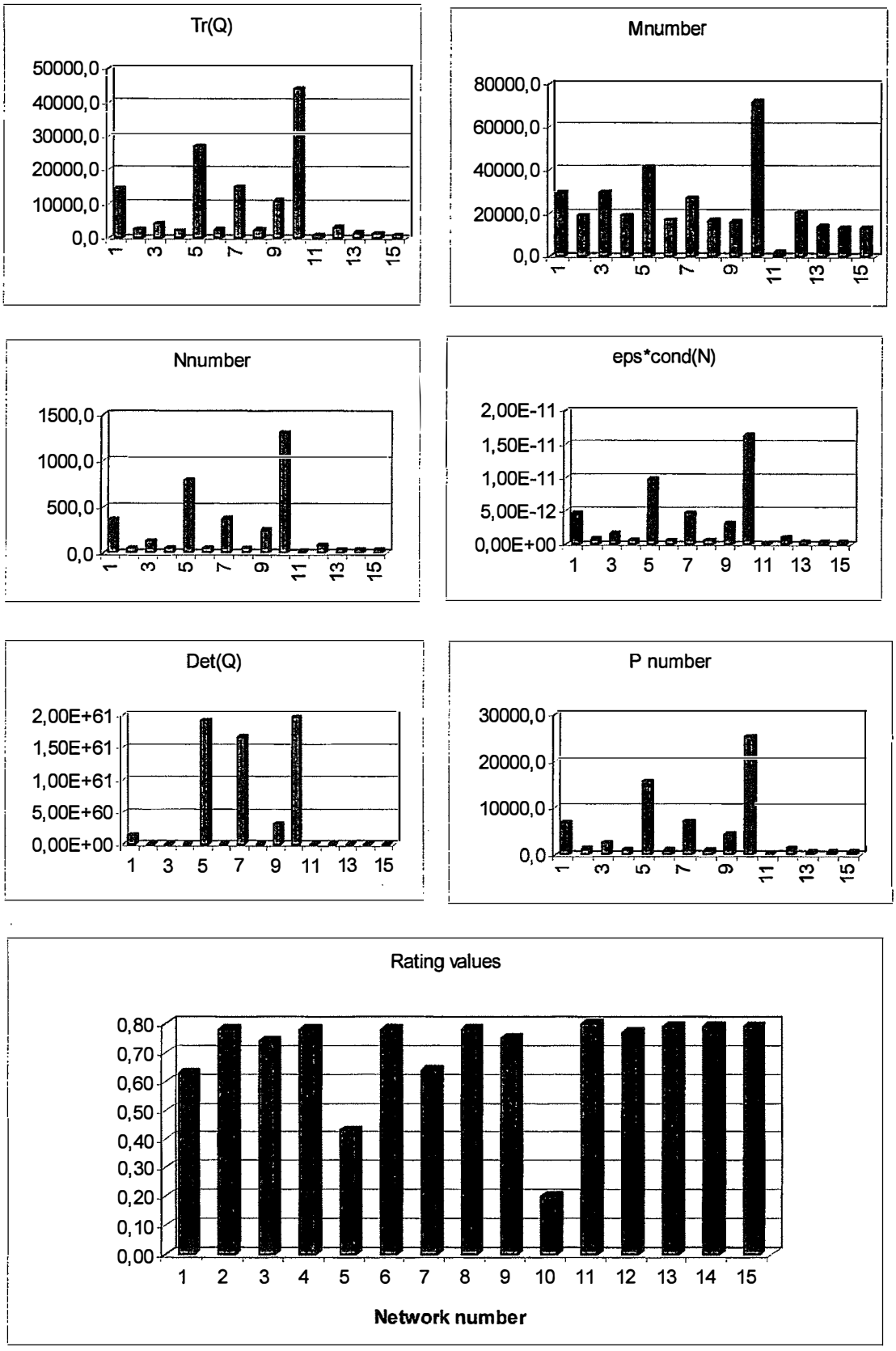

Figure 10: Values of the input variables and fuzzy logic rating of a network with a square area shape, fifteen variants

It should be noted that the rating value for an assessment with fuzzy logic might vary, if the input parameters of the functions are changed by entering additional results from the adjustment. In order to avoid such a casual change, all basic variables should be entered at once. Fuzzy logic should produce similar results as those derived by the human expert, as the rules are created from the user. However, fuzzy logic is more reliable than the human expert, when there are a lot of variables and conditions.

4. Conclusions

From the calculations and experiments done in this study, it can be summarized:

When performing an assessment of a network, one should use all available variables and avoid construction of a sophisticated system of rules. In this case it is preferably that the rules are simple with one variable in each rule. It is proposed not to compose multiple variables-rules.

Weights should be determined precisely, according to section 3.3. The user should not determine the weights by her/himself. It is recommended that the human expert examines whether the rating corresponds to reality. The output generally depends on the value of each variable and/or of the logical operator when using rules with many variables. It is proposed to apply both classical and fuzzy methods in order to get a complete and reliable network analysis.

In this way a well-conditioned system can be quickly and easily chosen among others. Rating values derived with fuzzy logic could be used as an additional information for the geodesists.

Acknowledgements:

This study was funded by Austrian Exchange Service (ÖAD).

Special gratitude is expressed to Prof. Schuh for his strong support and his advices when writing, editing and improving this article.

Used software:

Matlab fuzzy logic toolbox;

Vienna_fuzzy (Application developed for the needs of this research);

PhDSf (Application, subject to the PhD thesis of the author).

References

Faddeev, D.K., Faddeeva, V.N., Calculation methods of Linear Algebra. Physical-Mathematical Literature State Publishing House. Moscow, 1963. (Фаддеев, Д.К., Фаддеева, В. Н., Въйчислительныіе методы линейной алгебры. Государственное издательство физико-математической литературы. Москва 1963 г.) (in Russian)

Haberler, M. A Fuzzy System for the Assessment of Landslide Monitoring Data. VGI, 1/2003, Wien, pp 92-98

Heine, K. Potential application of fuzzy methods in geodetic fields. First International Symposium on Robust Statistics and Fuzzy Techniques in Geodesy and GIS. Organised by IAG-SSG 4.190 Non-probabilistic data analysis. Proceedings. March 12-16, 2001. Institute of Geodesy and Photogrammetry. Swiss Federal Institute of Technology. ETH Hoenggerberg. CH-8093 Zürich. ISBN 3-906467-29-5, pp 87-93

Kutterer, H. Uncertainty assessment in geodetic data analysis. First International Symposium on Robust Statistics and Fuzzy Techniques in Geodesy and GIS. Organised by IAG-SSG 4.190 Non-probabilistic data analysis. Proceedings. March 12-16, 2001. Institute of Geodesy and Photogrammetry. Swiss Federal Institute of Technology. ETH Hoenggerberg. CH-8093 Zürich. ISBN 3-906467-29-5, pp 7-12

M. Konstantinov and N. Vulchanov. Modern Mathematical Methods for Computer Calculations. Part 2 - Numerical Linear Algebra. BIAR Studies in Math. Sci., vol. 2, Sofia, 1997, ISBN 954-8949-02-4, MR 2001g:65004 (in Bulgarian).

S. Leinen. Fuzzy-Logic based GPS On-The-Fly Ambiguity Search. First International Symposium on Robust Statistics and Fuzzy Techniques in Geodesy and GIS. Organised by IAG-SSG 4.190 Non-probabilistic data analysis. Proceedings. March 12-16, 2001. Institute of Geodesy and Photogrammetry. Swiss Federal Institute of Technology. ETH Hoenggerberg. CH-8093 Zürich. ISBN 3-906467-29-5, pp 209-214

Wieser, A. Robust and fuzzy techniques for parameter estimation and quality assessment in GPS. Dissertation Technische Universität Graz. Shaker Verlag. Graz, July 2001. ISBN 3-8265-9807-5. ISSN 1618-6303, pp 49-80

Wieser, A. Benefitting from Uncertainty. GPS WORLD. March 2003

DESCARTES Project:

Study of the influence of changes in the gravity field on the Earth orientation parameters

Géraldine Bourda

Guest scientist at the IGG from

01-02-2005 to 31-07-2005

1. Introduction

The IAU/IUGG (International Astronomical Union/International Union of Geodesy and Geophysics) Working Group on "Nutation for a nonrigid Earth", led by Véronique Dehant, won the european Descartes Prize in 2003, for its work developing a new model for the Precession and the Nutations of the Earth. This model (MHB2000, Mathews et al. 2002) was adopted by the IAU during the General Assembly of Manchester, in 2000. It is based (i) on some improvements for the Precession model (with respect to the previous one of Lieske et al. 1977) owing to the VLBI (Very Long Baseline Interferometry) technique, and (ii) on a very accurate nutation model, close to the observations (see Figures 1.1 and 1.2).

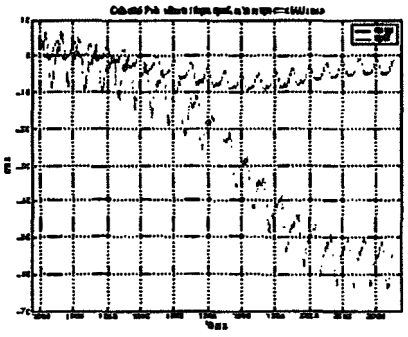

FIG. 1.1 – Celestial pole offsets ($d\psi$, $d\epsilon$), in longitude and obliquity (respectively), with respect to the IAU1980 model.

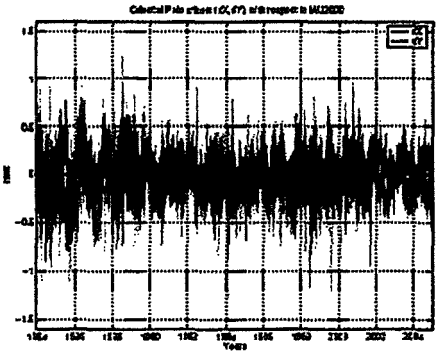

FIG. 1.2 – Celestial pole offsets (dX, dY), with respect to the IAU2000 model.

Owing to this Prize, the Nutation researcher community could offer some grants for international scientists, in the framework of the Descartes-Nutation project, that refers to further improvements of the Precession-Nutation Earth model. The fields being implied in such an effort have been pointed out (see Report of the WG Precession-Nutation):

- The atmosphere and related ocean effects should be better taken into account,
- The strategy for VLBI data based on more stable radio-sources should be considered (Feissel-Vernier 2003),
- New couplings mechanisms at the core boundaries should be considered, such as the viscous coupling,
- The effects of differential rotation between the inner core and the mantle, and the liquid core and the mantle, should be considered,
- The free mode excitations by the atmosphere or any other phenomena should be considered (this is particularly the case for the Free Core Nutation (FCN) and the Free Inner Core Nutation (FICN)),
- The coupling between the three components of the Earth rotation should be considered (e.g. effect of Length-Of-the-Day (LOD) variations on the nutations).

In the framework of this Descartes-prize, I arrived on Monday 31st of January 2005 at the University of Technology of Vienna (TU Vienna). I spent six months at the Institute of Geodesy and Geophysics (IGG), managed by Professor Harald Schuh. We decided that our contribution to

the improvement of the Precession-Nutation model could be part of the Nutations observation effort. At the IGG, the OCCAM software is used for analyzing the VLBI data. We decided to use it in order to compute the Earth Orientation Parameters (EOP) on the basis of the VLBI data, which is nowadays the most complete geodetic technique to determine Earth Rotation:

- First I had to deal with this new software and the VLBI data to use.
- Then I computed some tests for the models and options of fitting considered during the solving for the EOP.
- I solved for the EOP (more particularly the nutations in which the Descartes-Nutation project is involved) with the version 6.1 of OCCAM.
- Finally, I compared our results with the other IVS (International VLBI Service) analysis centers.

The goal was to allow the IGG to compute the IVS VLBI sessions (with the OCCAM software) for the whole data span available. This step was the first one for: (i) the submission of the results to the IVS Analysis Coordinator, and (ii) the combination of the results for the EOP coming from OCCAM with the ones obtained with the Bernese GPS software used at the Institute. The combination would be even more interesting in an a priori way (lets say on Sinex level). In the future, these results could be used with the Galileo ones and combinations at Sinex level could be undertaken.

In this paper we present first our studies and results related to the EOP computed with OCCAM software and VLBI data. Then we focuss on the various seminars, talks and posters presented during these six months and finally we conclude about this collaboration.

2. Project on EOP computed with OCCAM and VLBI data

2.1 Preliminary tests

First we began to make some tests of the OCCAM options considered during the computation of a VLBI session, solving for the EOP (see Table 2.1). We considered two options for these preliminary tests: free solution or not for the station network (see Fig 2.1). The results are in good agreement.

```
SIGMA ADDED 0.005   TEST   3.50  BIB/SNO S   REF.STOCH  Y
TROPOSPHERIC MODEL:  VMF  MMF  IMF  I+N  G+N  G+I  1/C
MMF
CUTOFF ELEVATION:  5.0
NO   DOWNWEIGHTING FOR LOW ELEVATIONS:  COSZ    COSZ**2
20.0  COSZ**2
EOP        OFFSET  RATE  PL CONSTRNT OFFSET CONSTRNT RATE
NUT         99.99  0.00   N     0.000 [mas]      0.000 [mas/h]
XPOL/YPOL   99.99 99.99   N     0.000 [mas]      0.000 [mas/h]
DUT1        99.99 99.99   N     0.000 [ms]       0.000 [ms/h]
N6   FREE SOLUTION
NO. STATIONS  5   V  N  E  CONSTRNT  __N_ECC  __E_ECC  __H_ECC
STATION     0.000  Y  Y  Y   0.00000   0.000    0.000    0.000
CONSTRAINED DIRECTIONS   0
-------------------------------------------------------------
AUXILIARY PARAMETERS
TIME INT.       ZD   ZDR   ZRS    CO    CR   CRS    GR   GRR
STATION      99.99  1.00  0.00 99.99  1.00 99.99 99.99  0.00
PIECEWISE LINEAR FUNCTIONS AND CONSTRAINTS
INVERSE FRACTIONAL WEIGHT OF CONSTRAINTS: 99999
#RATES      RW  ZDR PL   RW  CLR PL   RW  GRR PL
            MM/SQRT(H)   MM/SQRT(H)   MM/SQRT(H)
STATION      10.000  Y    30.000  Y     0.000  N
#OFFSETS    SIG ZDO EX   SIG CLO EX   SIG GRO EX
            MM           MM           MM
STATION       0.000  N     0.000  N     0.500  N
-------------------------------------------------------------
N ESTIMATION OF SOURCES (NNR/FIX) NNR (ALL/SET) ALL
N ADDITIONAL LOOSE CONSTRAINTS ON ALL 99.000 [mas]
```

FIG. 2.1 – Input file for running OCCAM software.

TAB. 2.1 – Comparison of the EOP results for the OCCAM solution (at the mjd date 52573.00), depending on various options : (1) No free solution, and (2) Free solution for the network (always "no estimation of source positions"). The celestial pole offsets results are given with respect to MHB2000.

	$d\epsilon$	$d\psi$	x_p		y_p		$UT1$	
	μas		μas	μas/d	μas	μas/d	μs	μs/d
1	-356.1	-2.9	129434.1	-4180.1	157138.1	-1496.8	-246630.5	-239.9
	± 41.5	± 94.6	± 67.9	± 182.1	± 51.5	± 141.6	± 2.2	± 5.5
2	-363.4	-56.4	129480.8	-4198.1	157137.0	-1432.1	-246635.2	-238.6
	± 40.1	± 91.9	± 85.9	± 175.7	± 61.9	± 136.9	± 2.5	± 5.3

Then we undertook to make some tests with the new version of OCCAM (OCCAM 6.1), implemented recently at the Institute. Indeed, Volker Tesmer from DGFI (Deutsches Geodätisches Forschungsinstitut, München, Germany) came to the Institute to implement this new OCCAM version. Then I began using it to solve for the Earth Orientation Parameters (EOP).

First of all, I present here the comparisons investigated for the EOP results between the old and new versions of OCCAM software. Then, I show some tests made taking into account various options and models during the OCCAM 6.1 computation. Finally, I compare our solution for the EOP obtained with OCCAM 6.1 with the ones of the analysis centers.

2.2 EOP offsets solutions: OCCAM 6.0 versus OCCAM 6.1

We computed OCCAM 6.0 and OCCAM 6.1 for the IVS (International VLBI Service) R1 and R4 sessions from the first half part of the year 2004:

- The limit for the precision of our computation is 5 sigmas.
- For the troposphere, we use the Vienna Mapping Function (VMF) during the computation (Boehm & Schuh 2004).
- The cut-off elevation angle for the troposphere is set to 5.0 degrees.
- We solve each day for:

  (i) the celestial pole offsets ($d\varepsilon$, $d\psi$), with respect to IAU2000 model,

  (ii) the pole coordinates (x_p, y_p) and the corresponding rates, with respect to the C04 series of the IERS (International Earth Rotation and Reference Systems Service),

  (iii) the angle UT1 and its rate, with respect to C04 series.
- At the same time solving for the EOP, we solve for some auxiliary parameters:

  (i) a zenith delay, a clock parameter and an atmospheric gradient each day,

  (ii) a zenith delay rate and a clock parameter rate each hour, and an atmospheric gradient rate each day,

  (iii) a second order clock parameter each day.
- We do not solve for the station network nor for the radio source positions.

The results are compared for each EOP in Figure 2.2. Taking into account the error bars of the figures, we can determine the mean precision of the computation for each EOP (see Table 2.2). We must add that there are some errors in terms of error statistics with the old version of OCCAM. We will use now OCCAM 6.1, with the input settings described above (the corresponding solution is named *"classical solution"*).

TAB. 2.2 – Mean EOP sigmas (using the IVS R1 and R4 VLBI sessions from the beginning of the year 2004), for the computations with OCCAM 6.1 ("rms" means root-mean-square) : we added up all the session sigmas for each EOP, and we divided by the number of sessions computed.

	OCCAM 6.1 computation
Mean rms of the residual delays (cms)	1.12
Mean $d\epsilon$ sigma (μas)	51.29
Mean $d\psi$ sigma (μas)	121.47
Mean x_p sigma (μas)	78.03
Mean y_p sigma (μas)	73.86
Mean UT1 sigma (μs)	2.71
Mean UT1 rate sigma (μs/day)	6.38

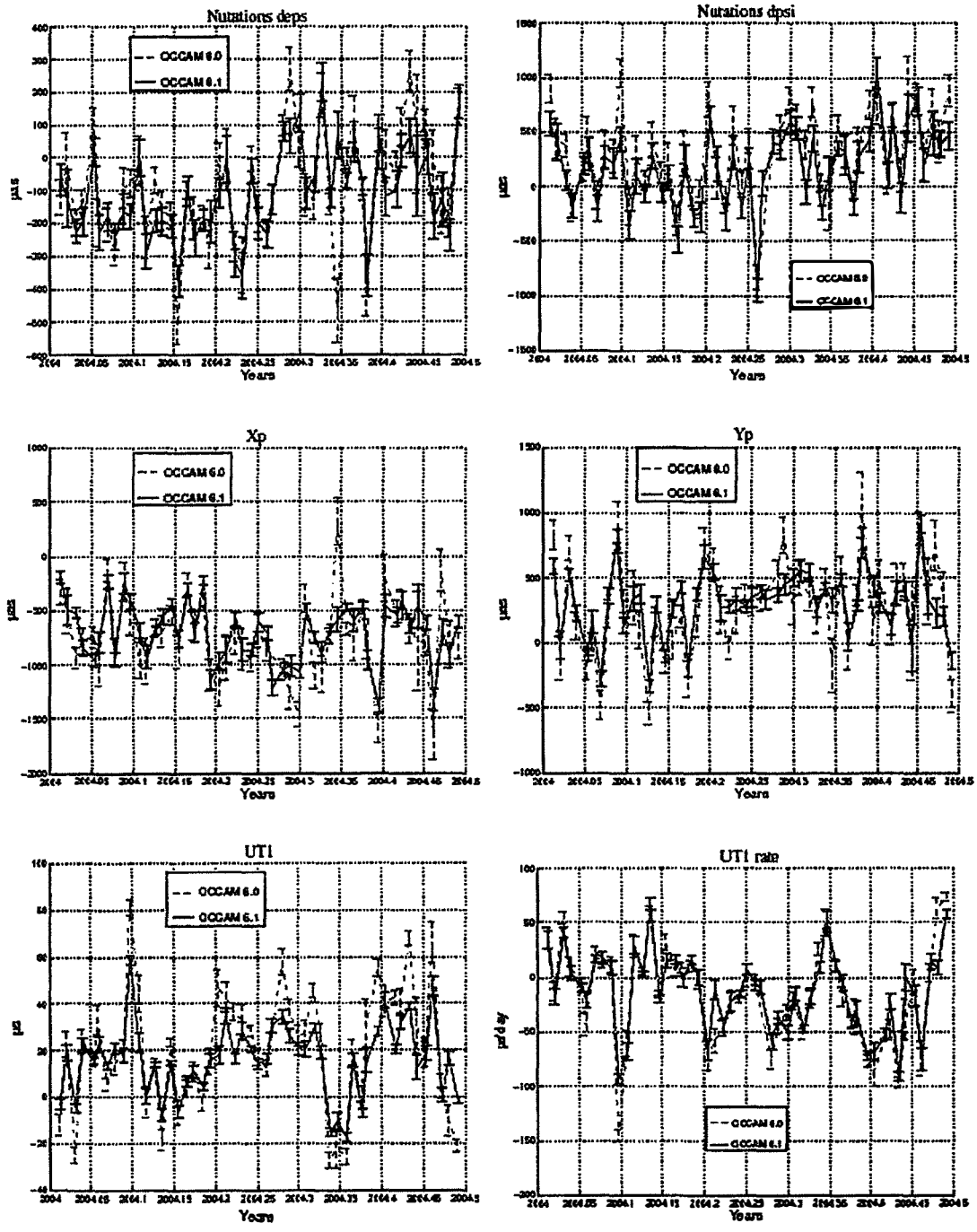

FIG. 2.2 – Comparison of the EOP offsets obtained with OCCAM 6.0 and OCCAM 6.1 : celestial pole offsets (deps, dpsi) are given with respect to IAU2000 model, and pole coordinates as well as UT1 angle and rates are given with respect to C04 IERS series.

2.3 Tests for the OCCAM 6.1 options and models

Table 2.3 shows some comparisons for the EOP results obtained computing OCCAM 6.1 with various input settings (the source positions are never estimated):

(1) We do not estimate the station network (this corresponds to the "classical solution").

(2) We solve for the station network.

(3) We do not solve for the atmospheric gradients.

(4) We use a Lagrange interpolation (and not a linear one anymore) for estimating the EOP at each time interval.

TAB. 2.3 – Comparison of the EOP results for the OCCAM 6.1 solution (at the mjd date 52573.00), depending on various options : (1) No free solution, or (2) Free solution for the network (always "no estimation of source positions"). Not solving for the atmospheric gradients is also checked in (3), and a Lagrange interpolation (not a linear one anymore) for the EOP is tested in (4) (with no free solution and no estimation for the source positions in both case). The celestial pole offsets are given with respect to IAU2000 model.

	$d\epsilon$	$d\psi$	x_p		y_p		UT1	
	μas		μas	μas/d	μas	μas/d	μs	μs/d
1	-356.1	-2.9	129434.1	-4180.1	157138.1	-1496.8	-246630.5	-239.9
	± 41.5	± 94.6	± 67.9	± 182.1	± 51.5	± 141.6	± 2.2	± 5.5
2	-363.4	-56.4	129480.8	-4198.1	157137.0	-1432.1	-246635.2	-238.6
	± 40.1	± 91.9	± 85.9	± 175.7	± 61.9	± 136.9	± 2.5	± 5.3
3	-362.5	-147.3	129459.5	-4074.4	157213.2	-1352.7	-246629.1	-240.1
	± 42.6	± 96.6	± 64.4	± 187.8	± 45.7	± 145.3	± 2.1	± 5.6
4	-357.4	-17.9	129432.2	-4163.0	157153.4	-1494.8	-246630.9	-238.2
	± 41.5	± -17.9	± 67.9	± 182.1	± 51.5	± 141.7	± 2.2	± 5.5

We can see that the results are in good agreement, but for having a better idea of the settings to really implement, we compute OCCAM 6.1 for a dozen of IVS R1 and R4 VLBI sessions in the beginning of the year 2004 (see Fig. 2.3 - Fig. 2.8).

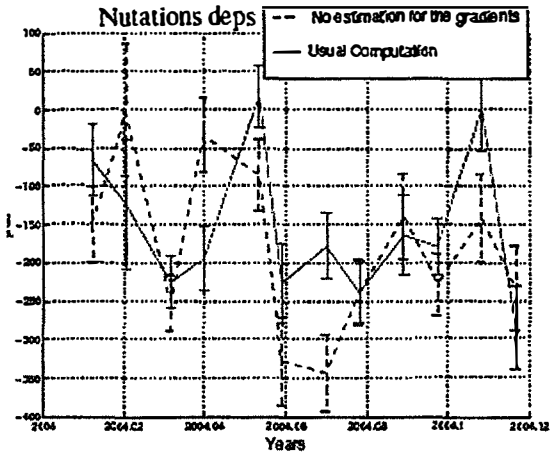

(a) Estimation or not for the atmospheric gradients.

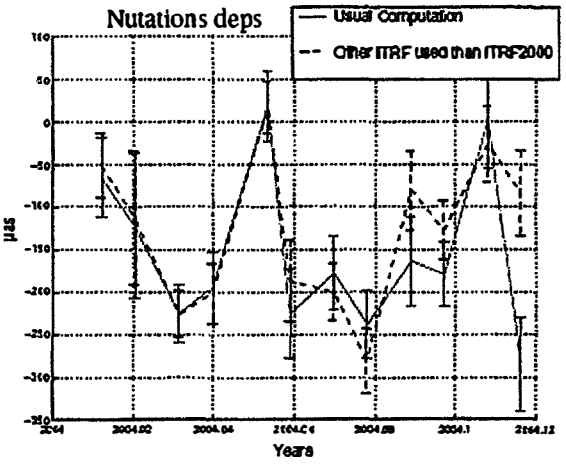

(b) Use of ITRF2000 or another terrestrial frame.

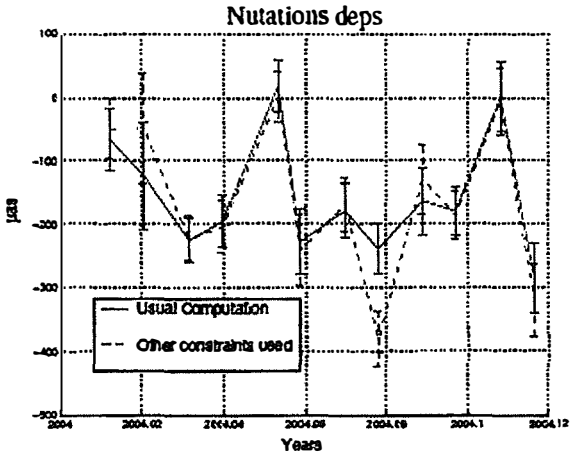

(c) Use of various constraints for the zenith delay, clock and atmospheric gradient offsets (less constraints than in the *classical computation*).

FIG. 2.3 – Celestial pole offset $d\epsilon$, with respect to the MHB2000 model, obtained with OCCAM (version 6.1).

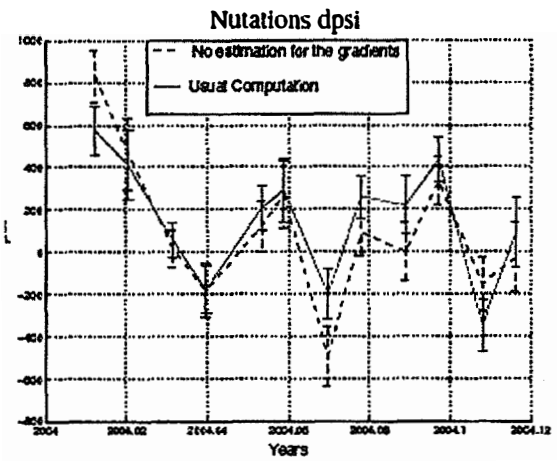

(a) Estimation or not for the atmospheric gradients.

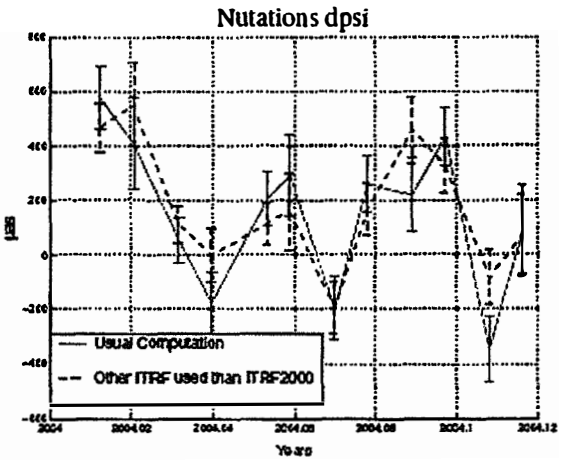

(b) Use of ITRF2000 or another terrestrial frame.

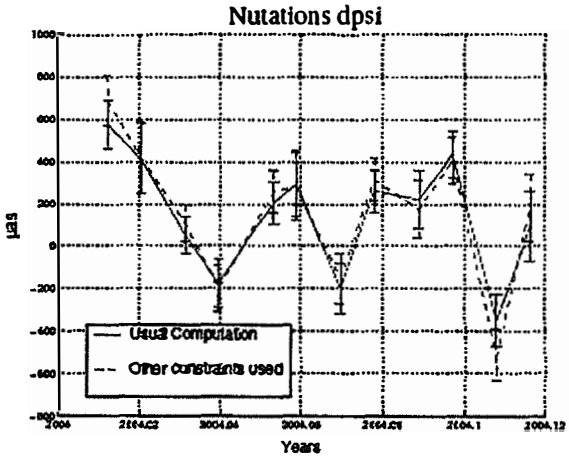

(c) Use of various constraints for the zenith delay, clock and atmospheric gradient offsets (less constraints than in the *classical computation*).

FIG. 2.4 – Celestial pole offset $d\psi$, with respect to the MHB2000 model, obtained with OCCAM (version 6.1).

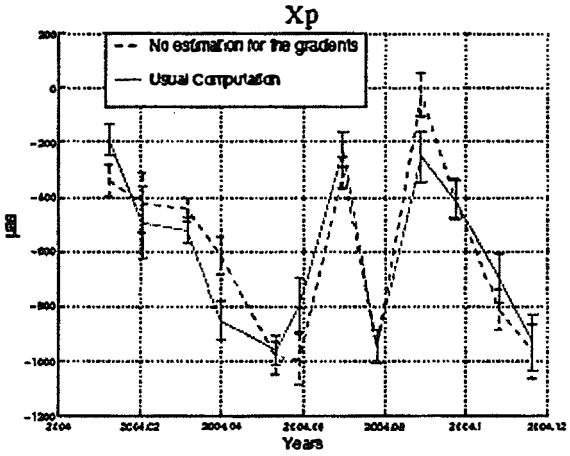

(a) Estimation or not for the atmospheric gradients.

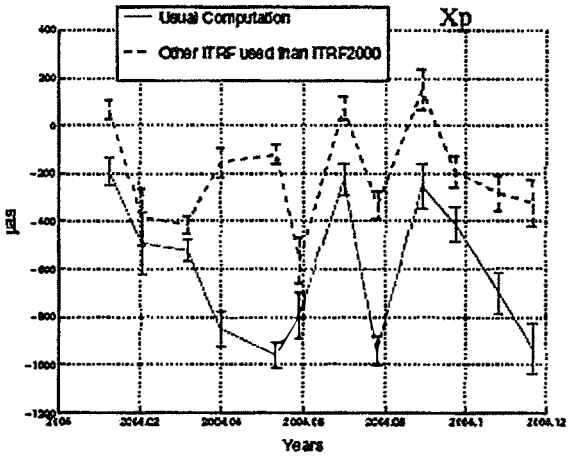

(b) Use of ITRF2000 or another terrestrial frame.

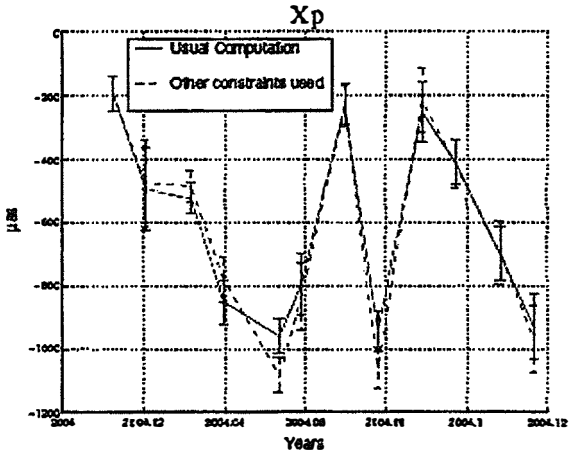

(c) Use of various constraints for the zenith delay, clock and atmospheric gradient offsets (less constraints than in the *classical computation*).

FIG. 2.5 – Polar Motion x_p coordinate, obtained with OCCAM (version 6.1) : offset with respect to C04 series.

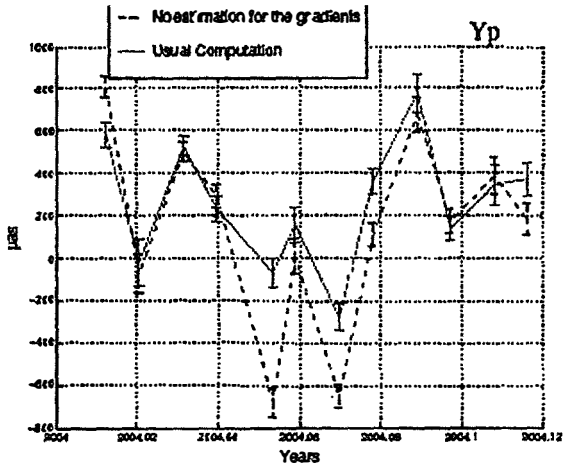

(a) Estimation or not for the atmospheric gradients.

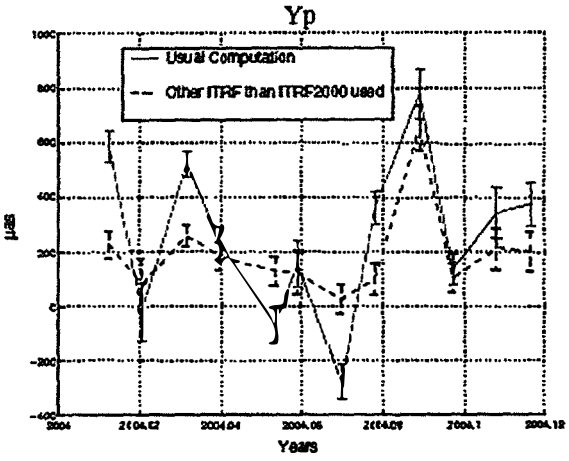

(b) Use of ITRF2000 or another terrestrial frame.

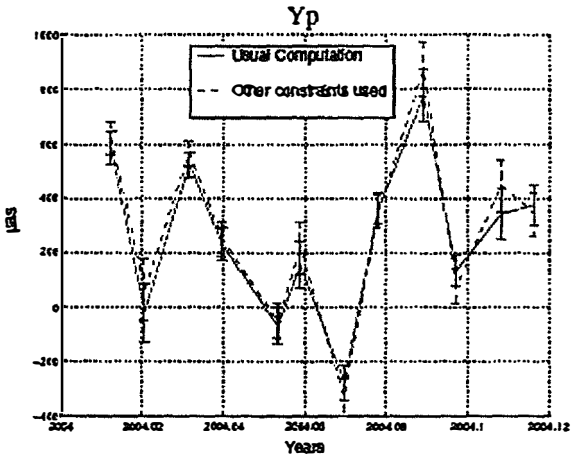

(c) Use of various constraints for the zenith delay, clock and atmospheric gradient offsets (less constraints than in the *classical computation*).

FIG. 2.6 – Polar Motion y_p coordinate, obtained with OCCAM (version 6.1) : offset with respect to C04 series.

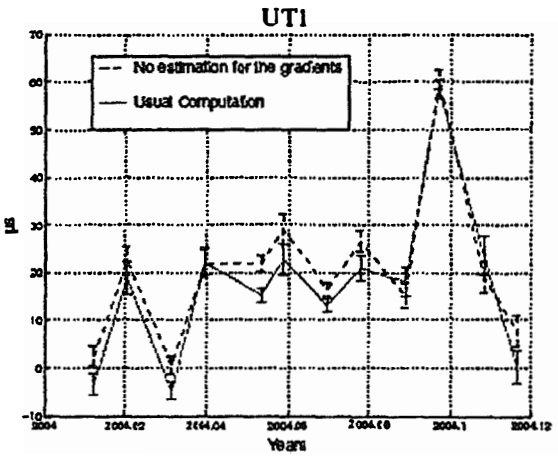

(a) Estimation or not for the atmospheric gradients.

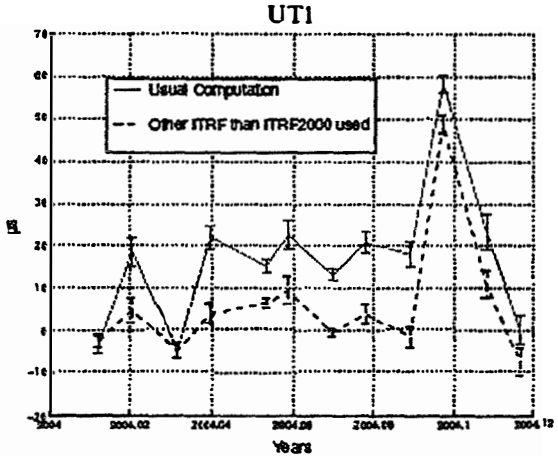

(b) Use of ITRF2000 or another terrestrial frame.

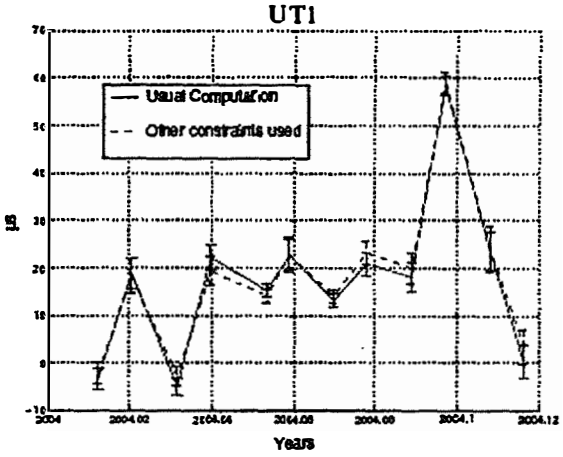

(c) Use of various constraints for the zenith delay, clock and atmospheric gradient offsets (less constraints than in the *classical computation*).

FIG. 2.7 – Time UT1, obtained with OCCAM (version 6.1) : offset with respect to C04 series.

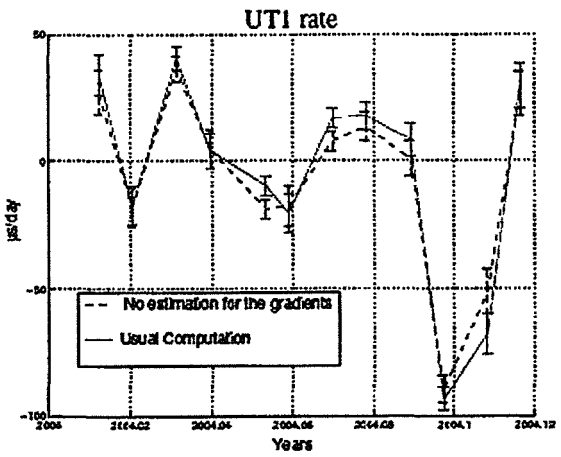

(a) Estimation or not for the atmospheric gradients.

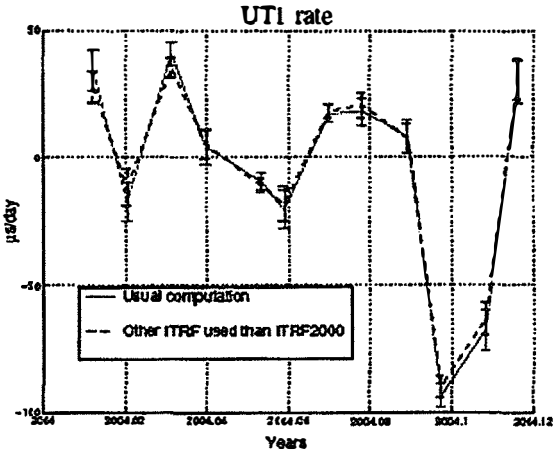

(b) Use of ITRF2000 or another terrestrial frame.

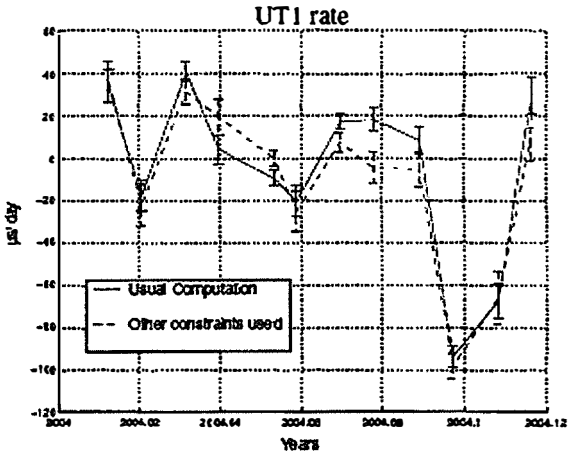

(c) Use of various constraints for the zenith delay, clock and atmospheric gradient offsets (less constraints than in the *classical computation*).

FIG. 2.8 – UT1 rate, obtained with OCCAM (version 6.1) : offset with respect to C04 series.

Figure 2.9 shows the root mean square (rms) of the residual delays during the OCCAM 6.1 computation, for each of the dozen IVS R1 and R4 VLBI sessions in the beginning of the year 2004, depending on various input settings:

- Solving for the gradients or not,
- Use of ITRF2000 or another terrestrial frame (named "05R01_PB.CAT": reference frame from DGFi global solution),
- Use of various constraints for the zenith delays, the clocks and the atmospheric gradients offsets (less constraints than in the "classical computation").

We can see that solving for the atmospheric gradients is better than not solving for them at the same time than for the EOP. The terrestrial frame used instead of ITRF2000 seems to give better results, but comparisons with the other analysis centers will be undertaken with ITRF2000 which is the classical one. And finally, the constraints implemented on the zenith delay, the clock and the atmospheric gradient offsets do not modify significantly the results for the EOP.

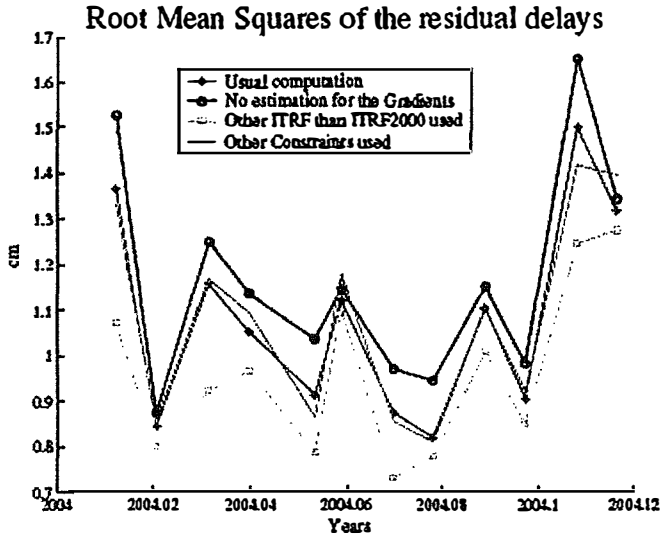

FIG. 2.9 – Root mean square (rms) of the residual delays during OCCAM 6.1 computation (in centimeters), depending on various input settings and options considered.

2.4 Comparison with the solutions of the EOP analysis centers

In order to investigate further the reliability of our results computing OCCAM 6.1 for solving the EOP, we compare our results with the ones of the IVS analysis centers. We use the series described in Table 2.4.

TAB. 2.4 – Details about the EOP series from 6 IVS analysis centers (5 used for our comparisons).

Analysis Centers	Geoscience Australia (Australia)	BKG Leipzig (Germany)	Institute of Applied Astronomy (Russia)	Main Astronomical Observatory (Ukraine)	Saint-Petersburg University (Russia)	United States Naval Observatory (USA)
Series	aus00001	bkg00004	iaao0301	mao2003o	spu00002	usn2005a
Software	OCCAM 5.0	CalcSolve 9.12	OCCAM /GROSS	SteelBreeze 2.0.2	OCCAM 5.0	CalcSolve 9.12
Solving for :						
celestial frame?	No	Yes	No	No	No	Yes
terrestrial frame?	No	Yes	No	Yes	No	Yes
A priori for :						
CRF	ICRF'2000	ICRF-Ext.1	ICRF-Ext.1	ICRF-Ext.1	ICRF-Ext.1	ICRF
TRF	ITRF'2000	ITRF2000	ITRF2000	ITRF2000	ITRF2000	ITRF2000
Precession model	IAU1976	IERS1996	IAU2000A	IAU2000A	IAU1976	IERS1996
Nutation model	IAU1980	IERS1996	IAU2000A (+ FCN from MHB)	IAU2000A	IAU198	IERS1996

Figure 2.10 shows the solution for the nutations computed with OCCAM 6.1, taking into account the three different nutation models: IAU1980 (Lieske et al., 1977), IERS1996 and IAU2000 (Mathews et al., 2002). For the comparisons with the analysis centers series, we use the IAU1980 model.

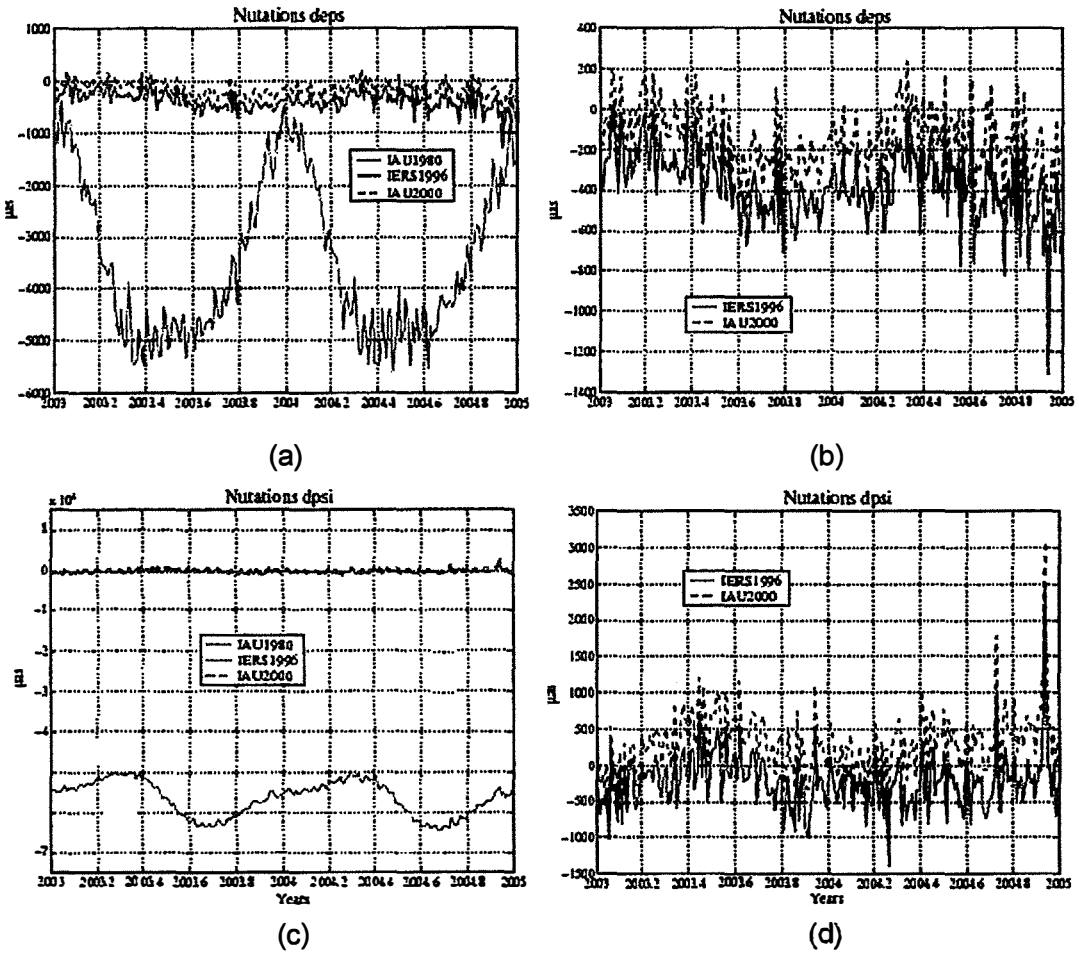

FIG. 2.10 – Celestial pole offsets computed with OCCAM 6.1 (*classical solution*), using different nutation a priori models.

Figures 2.11 and 2.12 shows then that our results with OCCAM 6.1 are in good agreement with the results of the IVS analysis centers.

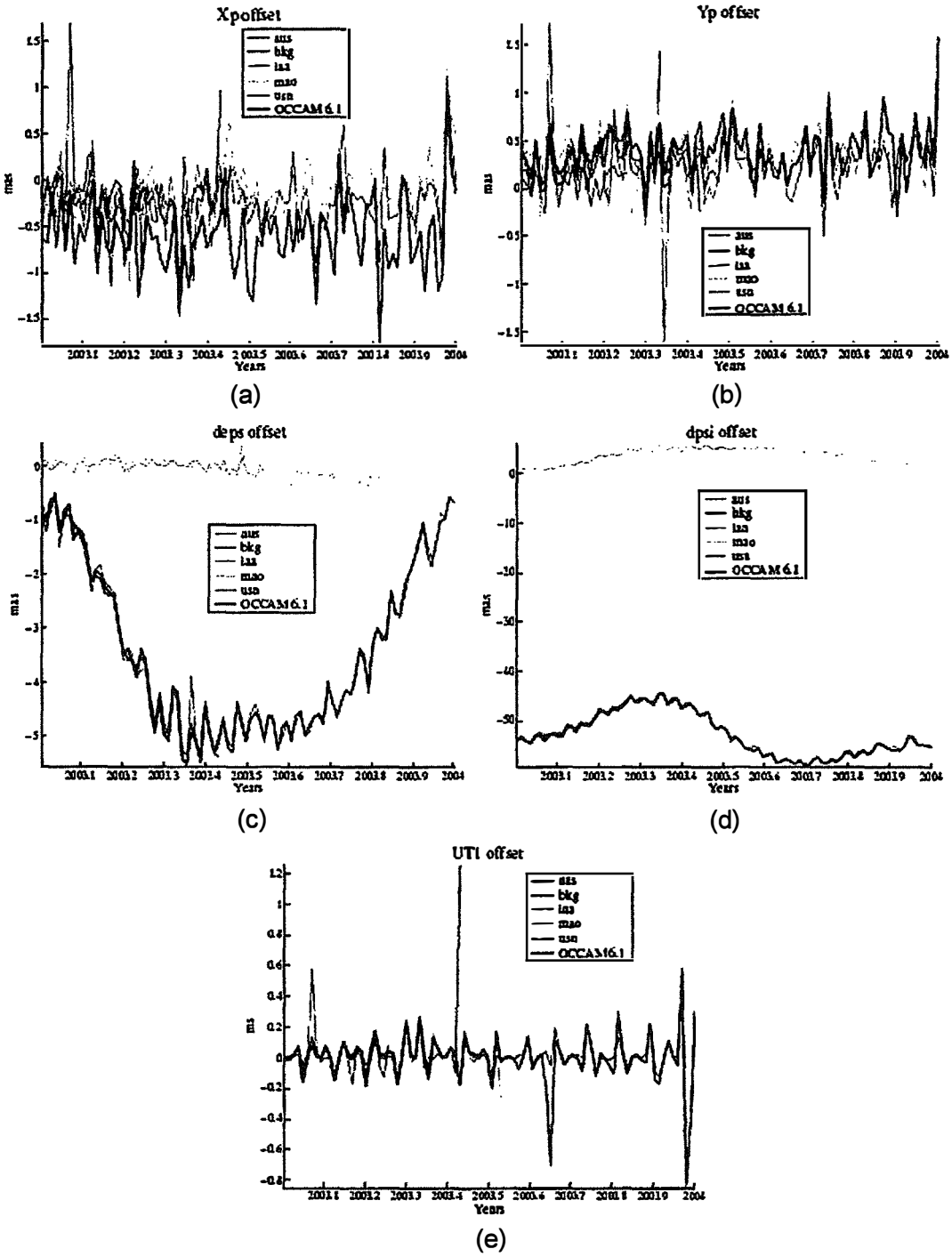

FIG. 2.11 – EOP offsets with respect to the C04 IERS series : comparison of our solution, computed owing to OCCAM 6.1, with the one of 5 IVS analysis centers.

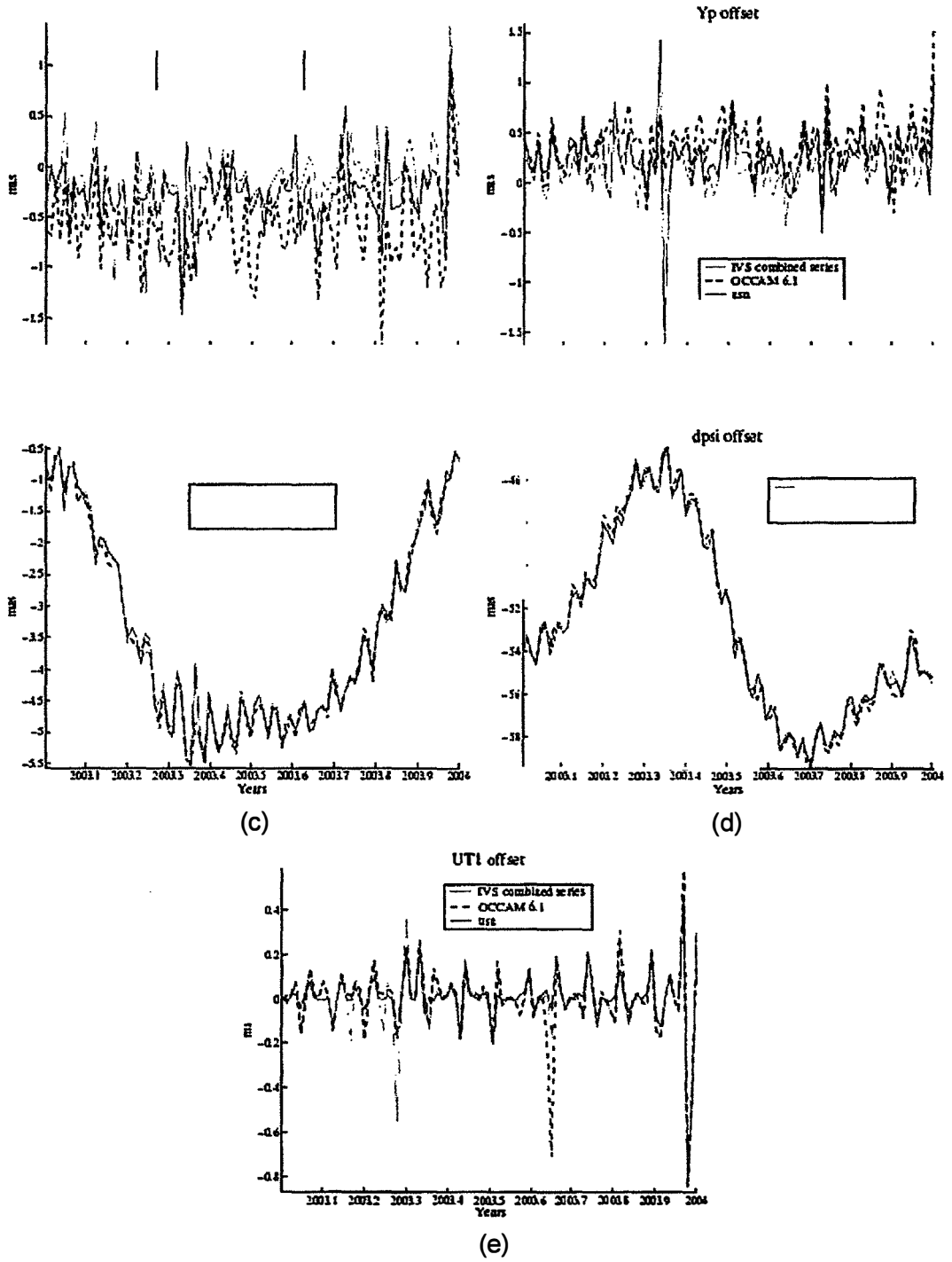

FIG. 2.12 – EOP offsets with respect to the C04 IERS series : comparison of our solution, computed owing to OCCAM 6.1, with the combined one of the IVS analysis coordinator.

To discuss further these EOP results, a point to investigate is the reason for the shifted x_p and y_p solutions (obtained with OCCAM) with respect to the other analysis centers series. This seems to come from the use of ITRF2000 coordinates for positionning the VLBI stations (more particularly for Tigoconception). Then we could use another terrestrial reference frame for solving the EOP.

3. Scientific Communications

3.1 Seminar

At the beginning of March, I gave a seminar at the Institute of Geodesy and Geophysics, which was entitled: "Earth Rotation and Variations of the Gravity Field". This talk was part of the conference series of the Institute, dealing with the modern researches done in Geodesy. I presented my PhD Thesis work and general points about Earth Rotation.

3.2 EGU General Assembly 2005

At the end of April 2005, the annual General Assembly of the EGU (European Geosciences Union) took place in Vienna. This colloquium allows the geosciences scientific community to meet. It is an important annual assembly for the international Geodesy scientists. I took part at this meeting, so during the month of April I prepared the poster I presented there. The poster was entitled "Length of day and polar motion, with respect to temporal variations of the Earth gravity field" (see Appendix A). This paper was a part of my PhD Thesis work, that I investigated further.
(PhD Thesis, http://tel.ccsd.cnrs.fr/documents/archives0/00/00/82/86/index_fr.html)

3.3 Retreat of the Institute of Geodesy and Geophysics

On Monday 30th and on Tuesday 31st of May 2005, all the scientists of the Institute of Geodesy and Geophysics went together to a cottage in the south of Vienna for a *brainstorming retreat*. The goals were to present to our colleagues the work done in the last few months, the plans for the near future and further ideas for Geodesy in general and for the Institute research way in particular (see Appendix B).

3.4 IAG Scientific Assembly Colloquium "Dynamic Planet 2005"

In the framework of the collaboration with Laura Fernandez, we obtained that the GRGS/CNES (Toulouse, France) let us use the series for the Stokes coefficients of degree 2 (order 0,1,2) for comparisons with geophysical models. Indeed, Laura is interested in the influence of the hydrology in the Earth Rotation perturbation (with some geophysical models). To compare these results with the temporal variations of the gravity field, we have the series coming from: (i) the positioning study of about 20 satellites between 1985 and 2002 (GRIM5 model; see Gruber et al.~2000 and Biancale et al. 2000), and (ii) the positioning study of Lageos I and Lageos II, between 1985 and 2004 (see my PhD manuscript and Bourda & Capitaine 2004). Then we submitted an abstract for the IAG Scientific Assembly taking place this summer in Cairns (Australia) (see Appendix D).

3.5 Journées 2005

During June 2005, I decided to submit an abstract to the Journées 2005 meeting taking place in Warsaw (Poland) in September 2005 (see Appendix E). This paper presents the work I have been doing in Vienna during six months, in the framework of the Descartes nutations prize (see Fig. 3.1 - 3.2).

ANALYSIS AND COMPARISON OF PRECISE LONG-TERM NUTATION SERIES, STRICTLY DETERMINED WITH OCCAM 6.1 VLBI SOFTWARE

G. BOURDA[1 2 3], J. BOEHM[3], R. HEINKELMANN[3], H. SCHUH[3]
[1] L3AB-UMR5804, Observatoire de Bordeaux, FRANCE
[2] SYRTE-UMR8630, Observatoire de Paris, FRANCE
[3] Institute of Geodesy and Geophysics, Vienna University of Technology, AUSTRIA
e-mail: Geraldine.Bourda@obspm.fr

1. INTRODUCTION

The IAU/IUGG Working Group on "Nutation for a non-rigid Earth", led by Véronique Dehant, won the European Descartes Prize in 2003, for its work developing a new model for the precession and the nutations of the Earth. This model (MHB2000, Mathews et al. 2002) was adopted by the IAU (International Astronomical Union) during the General Assembly in Manchester, in 2000. It is based (i) on some improvements for the precession model (with respect to the previous one of Lieske et al. 1977) owing to the VLBI technique (Very Long Baseline Interferometry), and (ii) on a very accurate nutation model, close to the observations. With this prize, the Descartes nutation project could offer for international scientists some grants, to be used for further improvements of the precession-nutation Earth model. At the IGG (Institute of Geodesy and Geophysics), with the OCCAM 6.1 VLBI analysis software and the best data and models available, we re-analyzed the whole VLBI sessions available (from 1985 till 2005) solving for the Earth Orientation Parameters (EOP). In this paper we present the results obtained for the EOP and more particularly for the nutation series. We compare them with the other IVS (International VLBI Service) analysis centers results, as well as with the IVS combined EOP series from the analysis coordinator. The series are in good agreement, except for the polar motion coordinates that show a shift with respect to the other ones and that we discuss here. Finally, we analyse the nutation series in the framework of the free core nutation (FCN) effect.

2. COMPUTATION

In this study we use 2944 VLBI sessions from 1982 till 2004, described as suitable for determining the EOP by the IVS Analysis Coordinator. They are computed at the IGG, from the NGS-format files corrected on the basis of the ECMWF meteorological data, in order to improve the height component of the stations and the determination of the tropospheric parameters. Clock breaks and reference clocks were investigated and taken into account for each session (Heinkelmann et al., 2005). The VLBI analysis software used at the IGG is OCCAM 6.1, in which the classical least-squares method based on the Gauss-Markov model (Koch, 1997) is implemented. We used (i) the terrestrial reference frame ITRF2000, (ii) the Vienna Mapping Function (VMF; Boehm & Schuh 2004), and (iii) a cut-off elevation angle for the troposphere set to 5 degrees. We estimated atmospheric gradients, clock parameters and zenith delays, as the same time we solve for the 5 EOP: one per session, and its rate for the pole and UT1. But we do not estimate the stations and sources position.

FIG. 3.1 – Proceedings of the poster presented at the Journées 2005 in Warsaw in the framework of the Descartes-Nutations prize.

3. DISCUSSION

In Figure 1, we show the results obtained for the polar motion (x_p component) compared to the IVS combined rapid solution (series ivs03r1e). This series was obtained using the IVS-R1 and R4 sessions, very good ones for determining the EOP, occuring after the year 2000. We can notice a shift in our series with respect to the IVS combined one. We wondered if this shift could be solved removing Tigoconception station. And we can realise that it is in better agreement after removing it (see Fig. 1). This can be explained by the fact that we used ITRF2000 terrestrial reference frame, in which Tigoconception position is not well determined. But it still remains a difference at the end of the data time span. In Figure 2, we plotted the Fourier spectrum of the Celestial Pole Offsets ($d\psi$, $d\epsilon$) we obtained, with respect to the IAU2000 nutation model. Depending on the data time span considered, we do not obtain the same periodical signals. The main ones are summarized in Table 1, investigating the longest data time span possible (between 1982 and 2004). For further studies about the Free Core Nutation effect (FCN), we will investigate a wavelet analysis on the prograde and retrograde parts of the Earth nutations. In the future, we will be able to use also the intensive VLBI sessions in our computations.

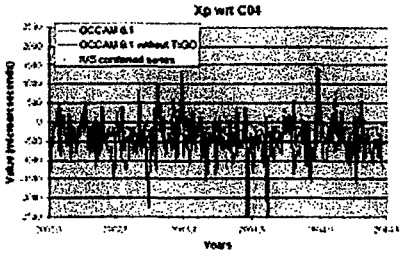

Figure 1: Polar motion x_p component, obtained with OCCAM 6.1 and compared to the IVS combined series.

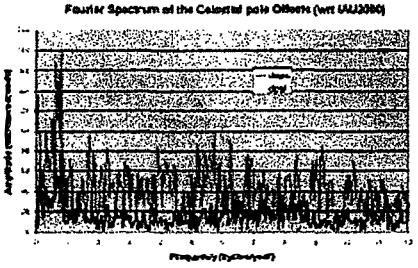

Figure 2: Fourier spectrum of the celestial pole offsets obtained with OCCAM 6.1, with respect to IAU2000 model.

Period	$d\epsilon$	$d\psi$
450 days	81 μas	181 μas
570 days	63 μas	168 μas

Table 1: Amplitudes of the biggest periodical signals for ($d\psi$,$d\epsilon$), with respect to IAU2000.

4. REFERENCES

Boehm, J., Schuh, H., 2004, "Vienna Mapping Functions in VLBI analyses", Geophys. Res. Lett., 31, doi: 10.1029/2003GL018984.

Heinkelmann, R., Boehm, J., Schuh, H., 2005, "IVS long-term series of tropospheric parameters", 6th IVS Analysis Workshop, April 21-23 2005, Noto Observatory, Sicily, Italy.

Koch, K.R., 1997, "Parameterschatzung und Hypothesentests in linearen Modellen", 3. Auflage, Ferdinand Dummlers Verlag, Bonn, pp. 381.

Mathews, P.M., Herring, T.A., Buffet, B.A., 2002, "Modeling of nutation and precession: New nutation series for nonrigid Earth and insights into the Earths's interior", J. Geophys. Res. (Solid Earth), 107, doi: 10.1029/2001JB000390.

Lieske, J.H., Lederle, T., Fricke, W., and Morando, B., 1977, "Expressions for the precession quantities based upon the IAU 1976 system of astronomical constants", A&A 58, pp. 1-16.

FIG. 3.2 – Proceedings of the poster presented at the Journées 2005 in Warsaw in the framework of the Descartes-Nutations prize.

4. Conclusion

Owing to the Descartes-Nutations prize, I could spend six months in Vienna, at the Institute of Geodesy and Geophysics (IGG) (TU Vienna). I worked there with the OCCAM software to compute VLBI data in order to determine Earth Orientation Parameters (EOP). These studies were the first ones to begin computing EOP with OCCAM and VLBI data at the IGG.

On one hand, this experience offered me to get more specialized with the VLBI technique and to investigate the EOP computation analyzing VLBI data. On the other hand, I could work with a lot of international scientists and this allowed me to begin some collaborations.

Appendices

A. EGU General Assembly 2005

"Length of day and polar motion, with respect to temporal variations of the Earth gravity field"

G. Bourda (1,2)

(1) Paris Observatory - SYRTE/UMR8630, FRANCE

(2) Now at: Vienna University of Technology - Institute of Geodesy and Geophysics, AUSTRIA

Geraldine.Bourda@obspm.fr

The masses distributions inside the Earth govern the behaviour of the rotation axis in the Earth (polar motion), as well as the Earth rotation rate (or equivalently, length of day). These masses distributions can be measured by space owing to artificial satellites, the orbitography of which provides the Earth gravity field determination. Then, the temporal variations of the Earth gravity field can be related to the variations of the Earth Orientation Parameters (EOP) (with the Inertia Tensor).

Nowadays, owing to the satellite laser ranging (SLR) technique and to the new gravimetric satellite missions (as CHAMP or GRACE), the temporal variations of the low degree coefficients of the Earth gravity field (i.e. Stokes coefficients) can be determined.

This paper is one of the first study using gravity variations data in the equations already established (e.g. Lambeck 1988, or Gross 2000) and linking the variations of the length of day and of the C20 Stokes coefficient (or, linking the polar motion and the C21 and S21 coefficients). This paper combines the Earth rotation data (mainly obtained from VLBI and GPS measurements) and the Earth gravity field variations ones (Lageos I and II data, or GRACE data), in order to complete and constrain the models of the Earth rotation. The goal is a better Earth global dynamics understanding, with possible application can be the constraint on the couplings into the Earth system (e.g. core-mantle couplings).

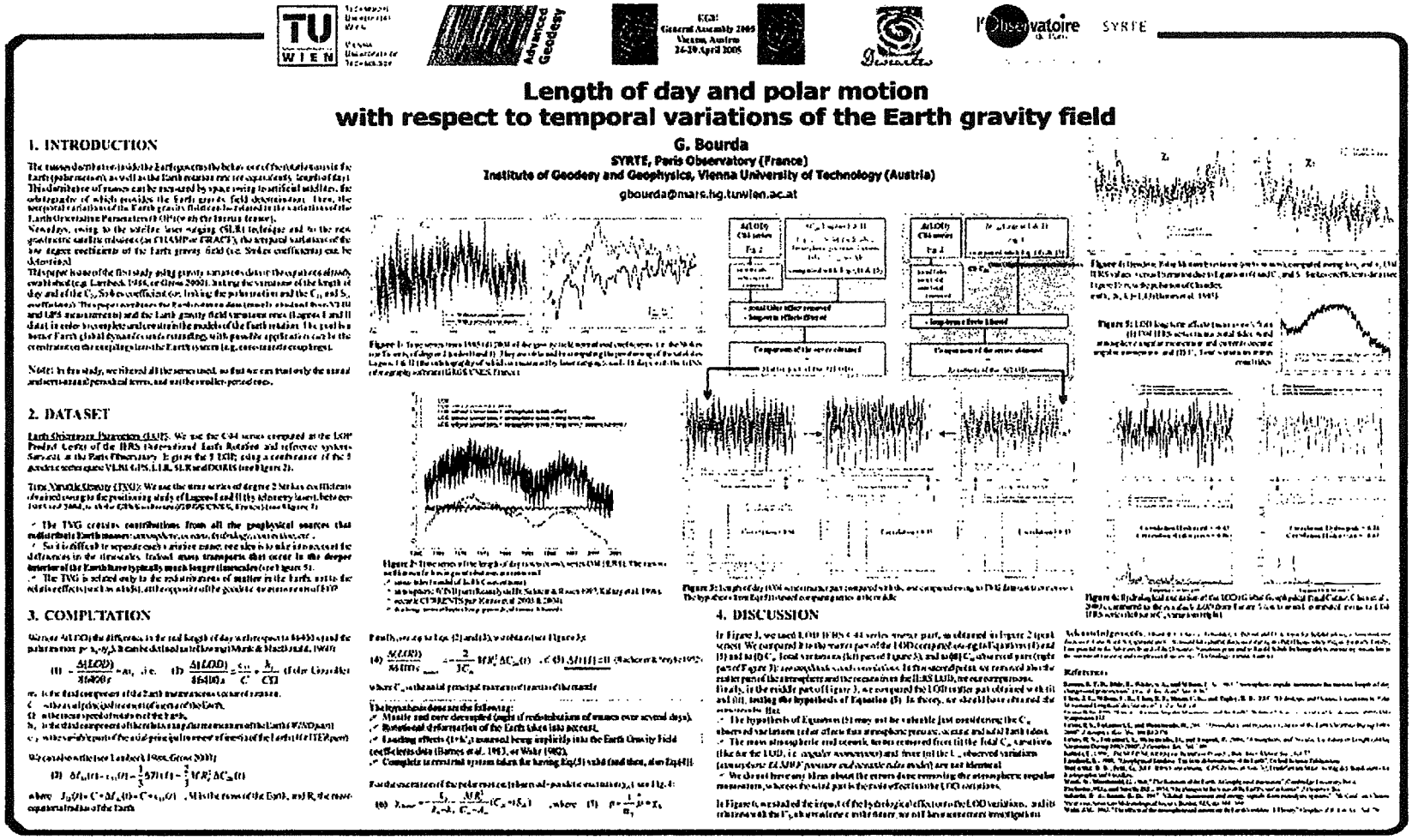

Length of day and polar motion with respect to temporal variations of the Earth gravity field

G. Bourda

SYRTE, Paris Observatory (France)

Institute of Geodesy and Geophysics, Vienna University of Technology (Austria)

gbourda@mars.hg.tuwien.ac.at

1. INTRODUCTION

2. DATA SET

3. COMPUTATION

4. DISCUSSION

European Geosciences Union General Assembly 2005, Vienna, Austria, 24 - 29 April 2005

FIG. 4.1 – Poster presented at the EGU General Assembly (April 2005).

B. IGG retreat

Figures 4.3 and 4.4 show the talk for the retreat, presenting the work I was doing at the Institute from the beginning of February.

FIG. 4.2 – Institute scientific members retreat.

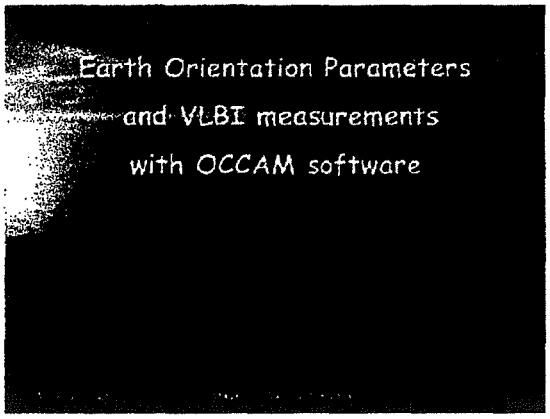

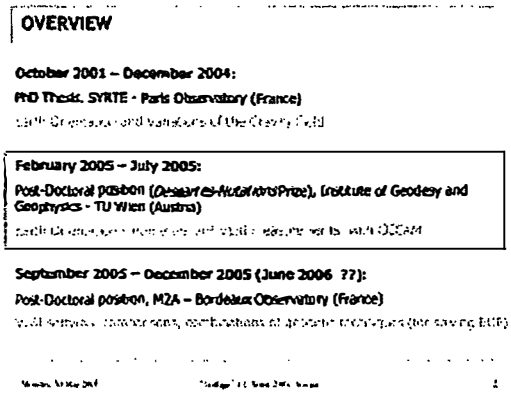

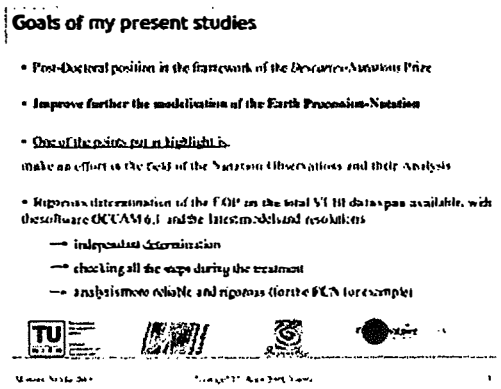

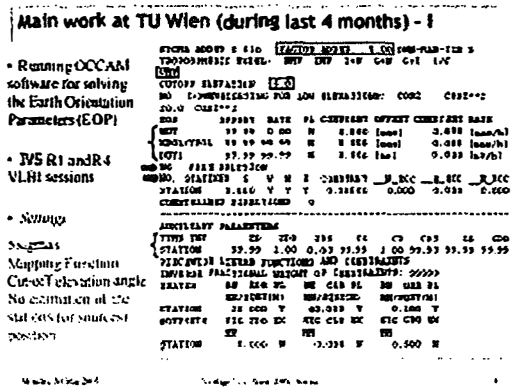

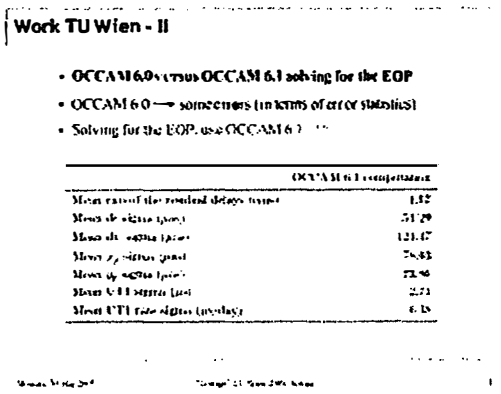

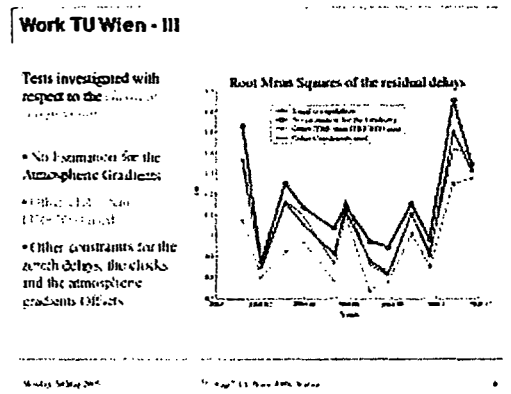

FIG. 4.3 – Retreat presentation.

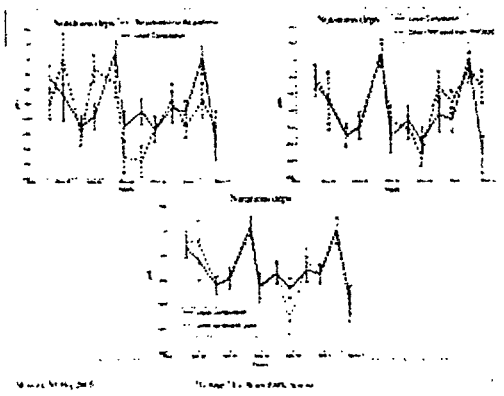

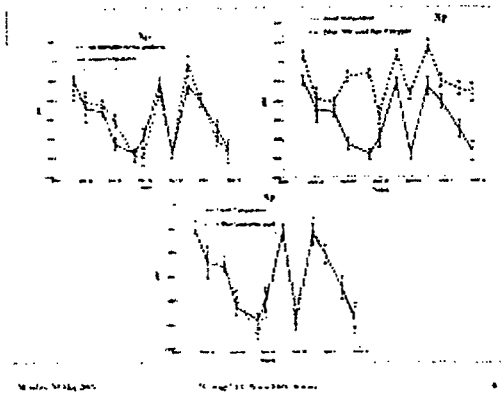

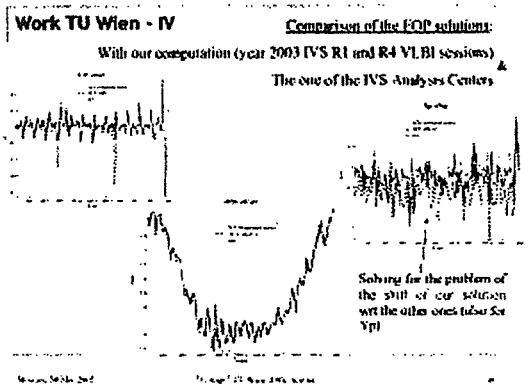

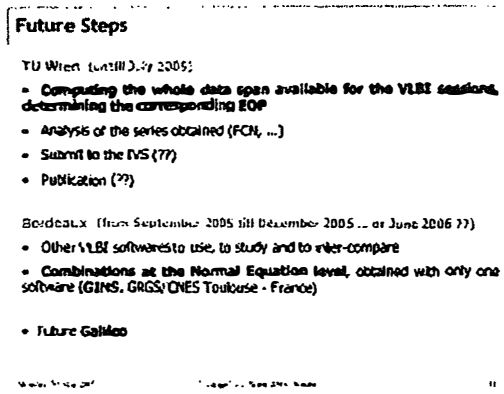

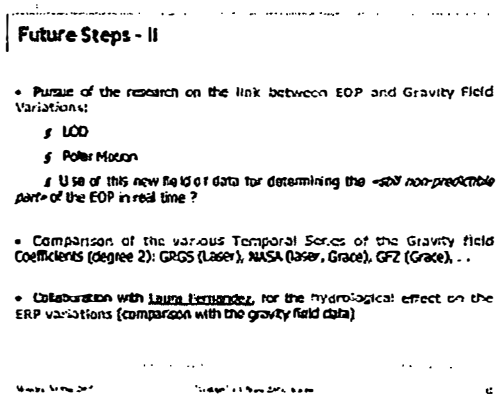

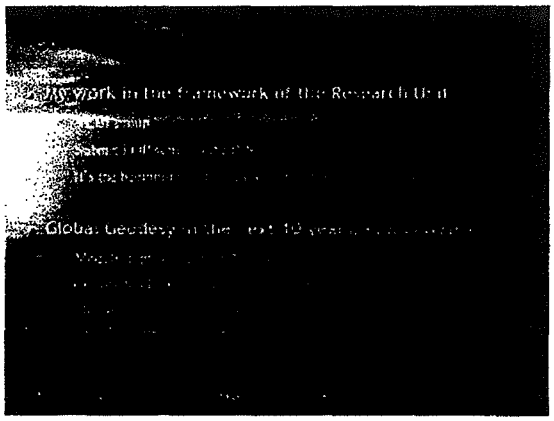

FIG. 4.4 – Retreat presentation.

C. Final Presentation

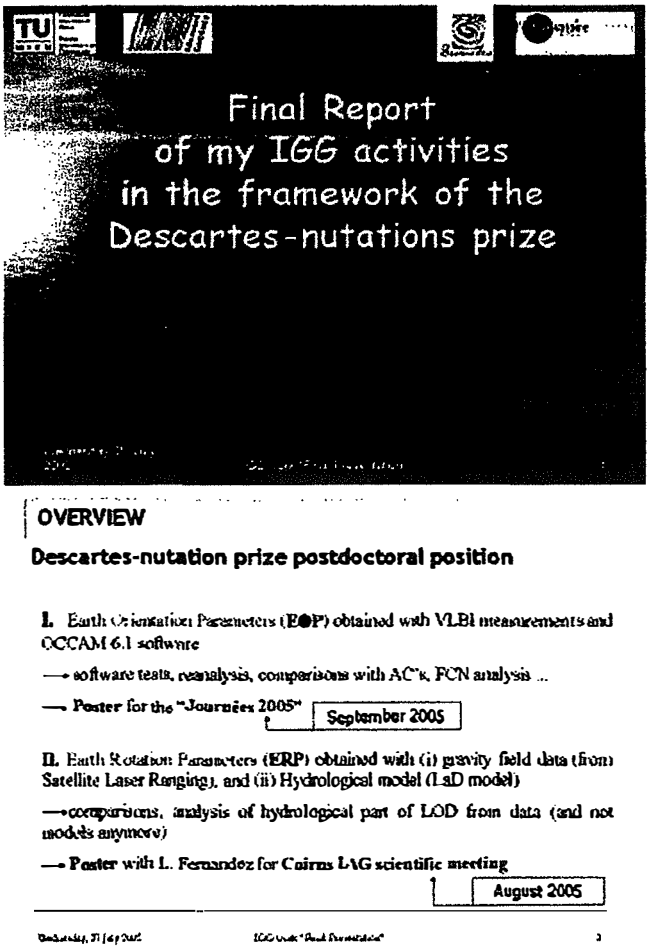

FIG. 4.5 – IGG final presentation.

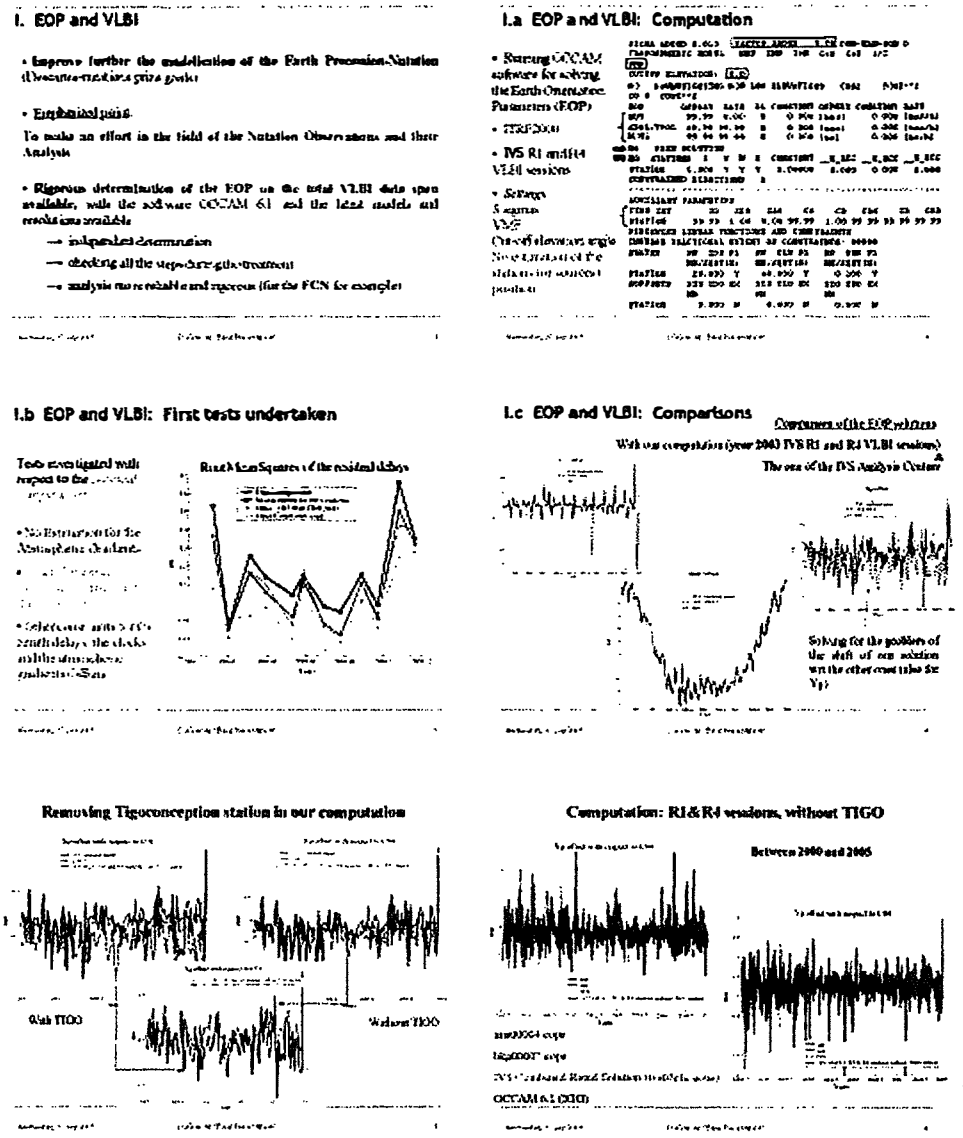

FIG. 4.6 – Final presentation.

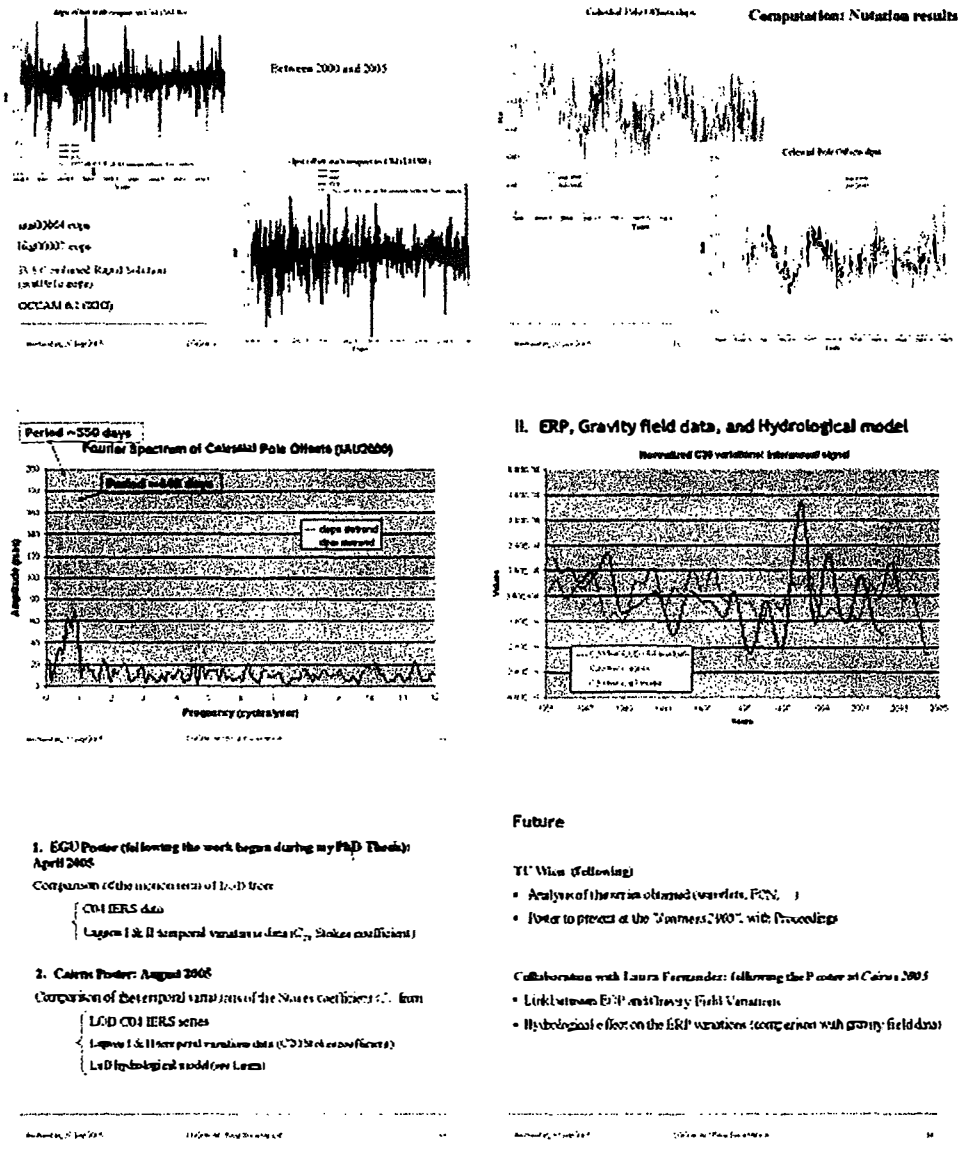

FIG. 4.7 – Final presentation.

D. IAG Scientific Assembly Colloquium "Dynamic Planet 2005"

"Earth gravity field and LOD variations related to hydrological excitations"

G. Bourda (1, 4), L. Fernández (2, 3, 4), and H. Schuh (4)

(1) Paris Observatory - SYRTE/UMR8630, FRANCE

(2) UN La Plata - Facultad de Cs. Astronómicas y Geofísicas, ARGENTINA

(3) Consejo Nacional de Investigaciones Científicas y Técnicas (CONICET)

(4) Vienna University of Technology - Institute of Geodesy and Geophysics, AUSTRIA

Geraldine.Bourda@obspm.fr; lauraf@fcaglp.unlp.edu.ar

Not only the motion terms but also the masses redistributions inside the Earth govern the behaviour of the Earth Rotation Parameters (ERP), and in particular of the Earth rotation rate or equivalently, length of day (LOD). Indeed, the dynamics of the internal processes that change the Earth's tensor of inertia also cause changes of the Earth's rotation. This distribution of masses can be measured from space by artificial satellites, the orbitography of which provides the Earth gravity field determination. Effectively, variations in the global mass distribution of the Earth cause changes in the gravitational field by changing the inertia tensor. Then, the temporal variations of the Earth gravity field can be related to the variations of the ERP. Nowadays the satellite laser ranging (SLR) technique and the new gravimetric satellite missions (as CHAMP or GRACE) provide the temporal variations of the low degree coefficients of the Earth gravity field (i.e. Stokes coefficients) with a good precision. In this work, variations of the Earth gravity field were analyzed for C_{20} estimated from (i) laser distances to Lageos I and II satellites, and (ii) from GRACE gravity measurements. After tidal and decadal signals were removed from LOD, the results were compared with C_{20} from geophysical model predictions focussing on the hydrological estimations from LaD-Danube (Milly & Shmakin, 2002) and NCEP/NCAR models.

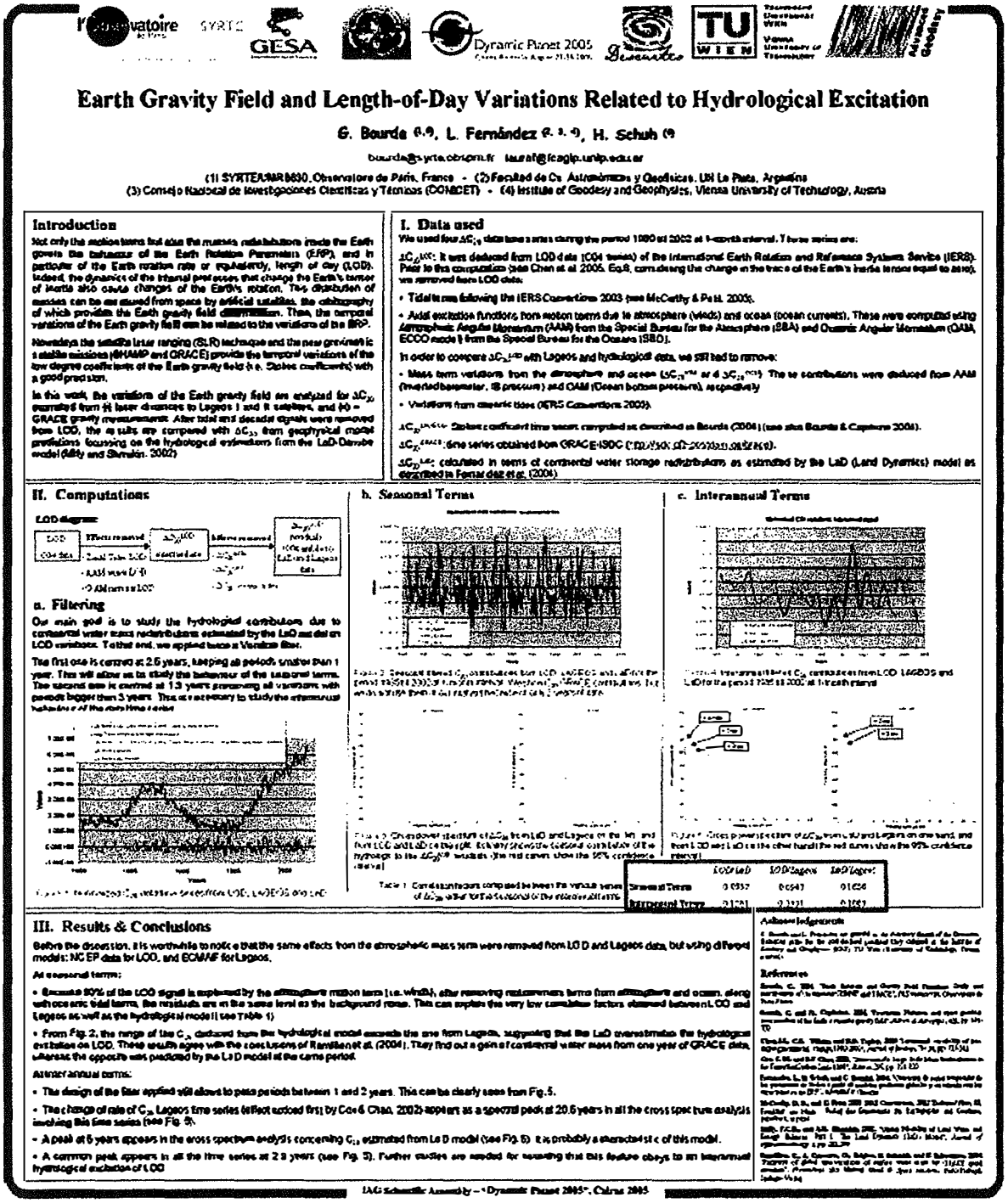

FIG. 4.8 – Poster presented at the IAG Scientific Assembly in Cairns (August 2005).

E. Journées 2005

"Analysis and comparison of precise long-term nutation series, strictly determined with OCCAM 6.1 VLBI software"

G. Bourda (1, 2, 3), J. Boehm (2), R. Heinkelmann (2), and H. Schuh (2)

(1) Paris Observatory - SYRTE/UMR8630, FRANCE

(2) Vienna University of Technology - Institute of Geodesy and Geophysics (IGG), AUSTRIA

(3) Bordeaux Observatory - L3AB/UMR5804, FRANCE

Geraldine.Bourda@obspm.fr

The IAU/IUGG Working Group on "Nutation for a non-rigid Earth", led by Véronique Dehant, won the European Descartes Prize in 2003, for its work developing a new model for the precession and the nutations of the Earth. This model (MHB2000, Mathews et al. 2002) was adopted by the IAU (International Astronomical Union) during the General Assembly in Manchester, in 2000. It is based (i) on some improvements for the precession model (with respect to the previous one of Lieske et al. 1977) owing to the VLBI technique, and (ii) on a very accurate nutation model, close to the observations. With this prize, the Descartes nutation project could offer for international scientists some grants, to be used for further improvements of the precession-nutation Earth model. At the IGG, with the OCCAM 6.1 VLBI analysis software and the best data and models available, we re-analyzed the whole VLBI sessions available (from 1985 till 2005) solving for the Earth Orientation Parameters (EOP). In this paper we present the results obtained for the EOP and more particularly for the nutation series. We compare them with the other IVS analysis centers results, as well as with the IVS combined EOP series from the analysis coordinator. The series are in good agreement, except for the polar motion coordinates that show a shift with respect to the other ones and that we discuss here. Finally, we analyse the nutation series in the framework of the free core nutation (FCN) study and modelisation.

F. IAU 2006

During the General Assembly of the IAU (International Astronomical Union), in August 2006, Véronique Dehant presented all the studies done in the framework of the Descartes-Nutations prize. For this reason I prepared a slide (see Fig. F.1) to show my work, the results and how the Descartes-prize could be useful for me.

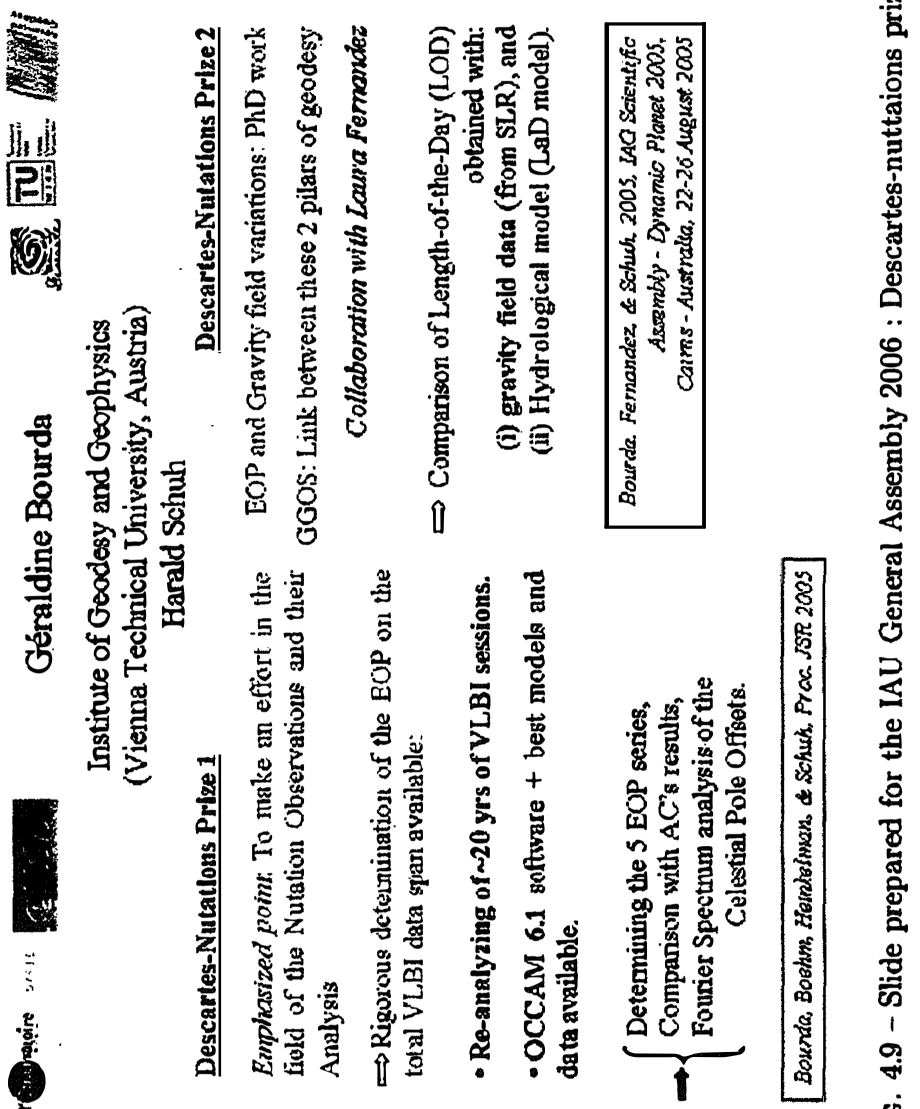

FIG. 4.9 – Slide prepared for the IAU General Assembly 2006 : Descartes-nuttaions prize.

References

Barnes, R. T. H., Hide, R., White, A. A., and Wilson, C. A., 1983, "Atmospheric angular momentum fluctuations, length-of-day changes and polar motion", Proc. R. Soc. Lond., Vol. A 387.

Biancale, R., Balmino, G., Lemoine, J.-M., Marty, J.-C., et al., 2000, "A new global Earth's gravity field model from satellite orbit perturbations: GRIM5-S1", Geophys. Res. Let., 27, pp. 3611--3614.

Bourda, G., and Capitaine, N., 2004, "Precession, Nutation, and space geodetic determination of the Earth's variable gravity field", Astron. Astrophys., 428, pp. 691-702.

Bourda, G., 2004, "Rotation terrestre et Variations du Champ de gravité : Etude et apport des missions CHAMP et GRACE", Thèse de Doctorat, Observatoire de Paris, France.

Chen, J. L., Wilson, C. R., Chao, B. F., Shum, C. K., and Tapley, B. D., 2000, "Hydrologic and Oceanic Excitations to Polar Motion and Length-of-day Variation", G. J. I., Vol. 141.

Chen, J.L., Wilson, C.R., and Tapley, B.D., 2005, "Interannual variability of low-degree gravitational change, 1980-2002", J. Geodesy, 78 (9), pp. 535-543.

Dehant, V., Brzezinski A., Report of the WG Precession-nutation of the Comission 19 of the IAU: http://www.astro.oma.be/IAU/.

Feissel-Vernier, M., 2003, "Selecting stable extragalactic compact radio sources from the permanent astrogeodetic VLBI program", Astron. Astrophys., 403, pp. 105-110.

Gross, R. S., 2000, "Gravity, Oceanic Angular Momentum and the Earth's Rotation", Gravity, Geoid and Geodynamics 2000, IAG Symposium 123.

Gross, R. S., Fukumori, I., and Menemenlis, D., 2003, "Atmospheric and Oceanic Excitation of the Earth's Wobbles During 1980-2000", J. Geophys. Res., Vol. 108 B8 2370.

Gross, R. S., Fukumori, I., Menemenlis, D., and Gegout, P., 2004, "Atmospheric and Oceanic Excitation of Length-of-Day Variations During 1980-2000", J. Geophys. Res., Vol. 109.

Gruber, T., Bode, A., Reigber, C., Schwintzer, P., et al., 2000, "GRIM5-C1: Combination solution of the global gravity field to degree and order 120", Geophys. Res. Let., 27, pp. 4005–4008.

Kalnay, E., 1996, "The NCEP/NCAR 40-year Reanalysis Project", Bull. Amer. Meteor. Soc., Vol. 77.

Lambeck, K., 1988, "Geophysical Geodesy: The slow deformations of the Earth", Oxford Science Publications.

Lieske, J. H., Lederle, T., Fricke, W., and Morando, B., 1977, "Expression for the Precession Quantities Based upon the IAU (1976) System of Astronomical Constants", Astron. Astrophys., 58, pp. 1--16.

McCarthy, D. D., Petit, G., 2003, IERS Conventions, IERS Technical Note 32, Frankfurt am Main: Verlag des Bundesamts für Kartographie und Geodäsie.

Mathews, P. M., Herring, T. A., and Buffett, B. A., 2002, "Modeling of nutation-precession: New nutation series for nonrigid Earth, and insights into the Earth's Interior", J. Geophys. Res., 107 B4, 10.1029/2001JB000390.

Munk, W., Macdonald, G., 1960, "The Rotation of the Earth: A Geophysical discussion", Cambridge University Press.

Rochester, M.G., and Smylie, D.E., 1974, "On changes in the trace of the Earth's inertia tensor", J. Geophys. Res.

Salstein, D. A., Rosen, R. D., 1997, "Global momentum and energy signals from reanalysis systems", 7th Conf. on Climate Variations, American Meteorological Society, Boston, MA, pp. 344--348.

Wahr, J.M., 1982, "The effects of the atmosphere and oceans on the Earth's wobble - I. Theory", Geophys. J. R. Astr. Soc., Vol. 70.

DESCARTES Project:

Integral influence of "geophysical fluids" to shape and rotation of the Earth

Laura Isabel Fernandez Monteagudo

Guest scientist at the IGG from

01-02-2005 to 31-07-2005

Following we will describe the activities developed during 6 months at the Institute of Geodesy and Geophysics (IGG) (TU Wien; Vienna University of Technology) in the frame of the master Descartes project "Pinpoint positioning in a wobbly world" The following points, which will be developed later, condense the principal achievements of this stage.

A. *Computation of a hydrological excitation time series (Hydrological angular Momentum, HAM) as estimated by the LaD model.*
B. *Analysis of the effectiveness of the Hydrology (LaD) in exciting inter-annual polar motion variations.*
C. *Comparison of LaD hydrological mass term excitation to polar motion at annual periods with respect to other model estimation.*
D. *Analysis of the polar motion budget at seasonal terms:*
   D1. Comparison of NCEP, LDAS and LaD.
E. *Study of the annual and inter-annual effects of the on LOD variations*
   E1. Comparison with the respective Stokes coefficients (2,0) from LAGEOS and GRACE

A. Computation of the HAM time series

1. Getting data: Reading of groundwater values from LaD model

Among all the output files from the Land Dynamics Model (hence after, LaD), I took the groundwater field, that is, the total water storage on spatial cells. (Milly and Shmakin, 2002)

The groundwater density distribution data has been generated within the Continental Water, Climate, and Earth-System Dynamics Project and is provided on a global 1° x 1° grid. Data outputs are available in monthly intervals for the period between January 1980 and May 2004. The numerical values refer to the first day of each month. Data quantities represent the mass of water per grid cell given in units of [kg/m2]. Frozen cells are assumed to be permanently glaciated and global ice melting and sublimation is considered.

The water storage within a non-glaciated cell is composed of a snow pack store w_s, a root zone store w_r, and a groundwater store w_g. Glaciated cells consist of the snow pack store and a glacier-ice store w_l. In general form, the total water storage W of a cell is given by

$$W = w_s + w_r + w_g + w_l \tag{1}$$

The whole information, is contained in 292 matrices of 180 x 360 values each, given at a large *.nc file format. Such file was read and converted into simple and easily manageable ASCII data files.

2. Data Time series calculation:

In order to compute the time series of Stokes coefficients ΔC_{20}, ΔC_{21} and ΔS_{21} variations due to the continental water storage mass redistributions from LaD model, a FORTRAN program was written.

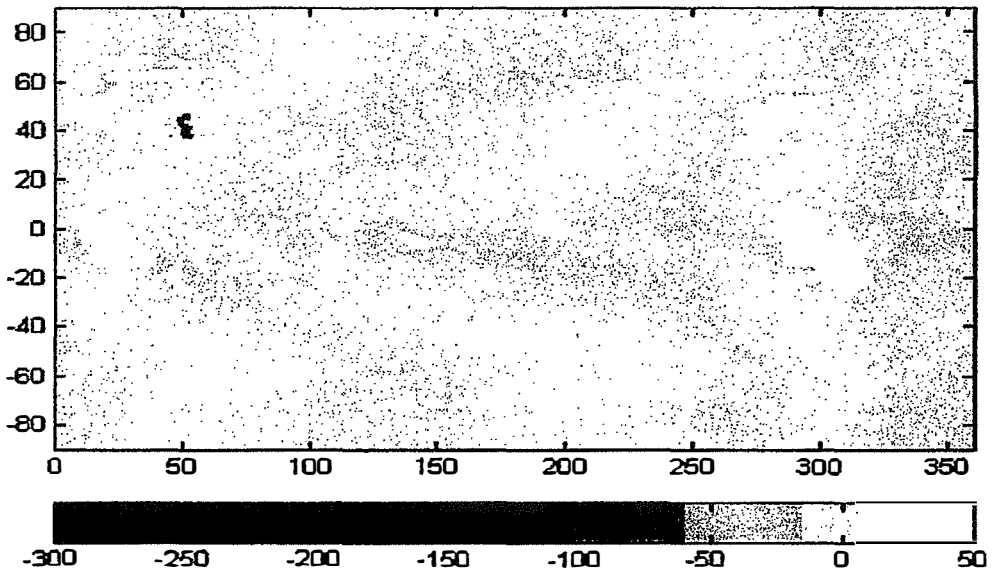

Figure 1: Shows an example of LaD groundwater data distribution. The white areas represent the continental water storage data distribution (in units of kg/m2) in latitude and longitude for the first epoch (1.2.1980).

According to Wahr et al. (1998), we must solve the following integral equations:

$$\Delta C_{20} = \frac{3(1+k_1)}{4\pi R_e \rho_{ave} 5} \int_S \Delta\sigma(\phi,\lambda)\, \overline{P}_{20}(\cos\phi)\, sin(\phi)\, d\phi\, d\lambda$$

$$\left.\begin{matrix}\Delta C_{21} \\ \Delta S_{21}\end{matrix}\right\} = \frac{3(1+k_1)}{4\pi R_e \rho_{ave} 5} \int_S \Delta\sigma(\phi,\lambda)\, \overline{P}_{21}(\cos\phi) \left\{\begin{matrix}cos\,\lambda \\ sin\,\lambda\end{matrix}\right\} sin\phi\, d\phi\, d\lambda \qquad (2)$$

where ρ_{ave} = 5517 kg/m3 is the average terrestrial density, Re = 6378136.6 meters is the equatorial Earth's radii and k_ℓ = -0.301 is the degree 2 load Love number (IAG Numerical Standards, 1999). φ refers to the latitude and λ to the longitude.

Referring the mass of the Earth as $M = 4/3\pi R^3_e \rho_{ave}$ = 5.976 E24 in kilograms and replacing the normalized associated Legendre Functions by

$$\overline{P}_{lm} = \sqrt{\frac{(2l+1)\,(l-m)!}{2\,(l+m)!}}\, P_{lm}$$

which in this case adopts the values

$$\overline{P}_{20}(\cos\phi) = \sqrt{\frac{5}{2}}\ \frac{1}{2}\ (3\ \cos^2\phi - 1)$$

and

$$\overline{P}_{21}(\cos\phi) = -3\cos\phi\sin\phi$$

Replacing in (2) we have

$$\Delta C_{20} = \frac{3\ R_e^2(1+k_1)}{2\sqrt{10}\,M} \int_0^{2\pi}\int_0^{\pi} \Delta\sigma(\phi',\lambda)\ (3\ \cos^2\phi' - 1)\ \sin(\phi')\ d\phi'\ d\lambda$$

$$\left.\begin{matrix}\Delta C_{21}\\ \Delta S_{21}\end{matrix}\right\} = \frac{-3\,R_e^2\,(1+k_1)}{5\,M} \int_0^{2\pi}\int_0^{\pi} \Delta\sigma(\phi',\lambda)\cos\phi'\sin^2\phi' \left\{\begin{matrix}\cos\lambda\\ \sin\lambda\end{matrix}\right\} d\phi'\,d\lambda \quad , \qquad (3)$$

where $\Delta\sigma(\varphi',\lambda)$ is the total water storage values in units of kg/m^2 from LaD model, provided in a 1° latitude x 1° longitude grid. The variable φ (latitude), which takes the extreme values - 90° (S) to 90° (N), was replaced by φ' between 0° and 180°.

The problem consists in solving numerically the surface integral in (3).

The integration was made in two steps. First, a numerical integration on latitude is performed addressing a two-dimensional interpolate scheme and then the integral was approximated by Gaussian quadratures.

The idea of this last is the approximation of the integral by a sequential sum of functional values evaluated at a set of equally spaced points and multiplied by weighting coefficients. In order to test the programs, a first computation was done using the $\Delta\sigma(\varphi',\lambda)$ continental water storage data from the NCEP (National Centers for Environmental Prediction, NOAA) reanalysis model.

In figure 2, the results of our numerical integration were compared with ΔC_{20}, ΔC_{21} and ΔS_{21} deduced from the excitation functions Ψ_z^{mass}, Ψ_x^{mass} and Ψ_y^{mass} given by the Special Bureau for Hydrology (SBH) of the Global Geophysical Fluid Centre (GGFC). The period of computation was January1st 1980 till December 31st 2002 at 1-day interval.

Figure 3 shows the application of the same FORTRAN programs but on LaD groundwater data for the period January 1980 till May 2004 at 1-month interval.

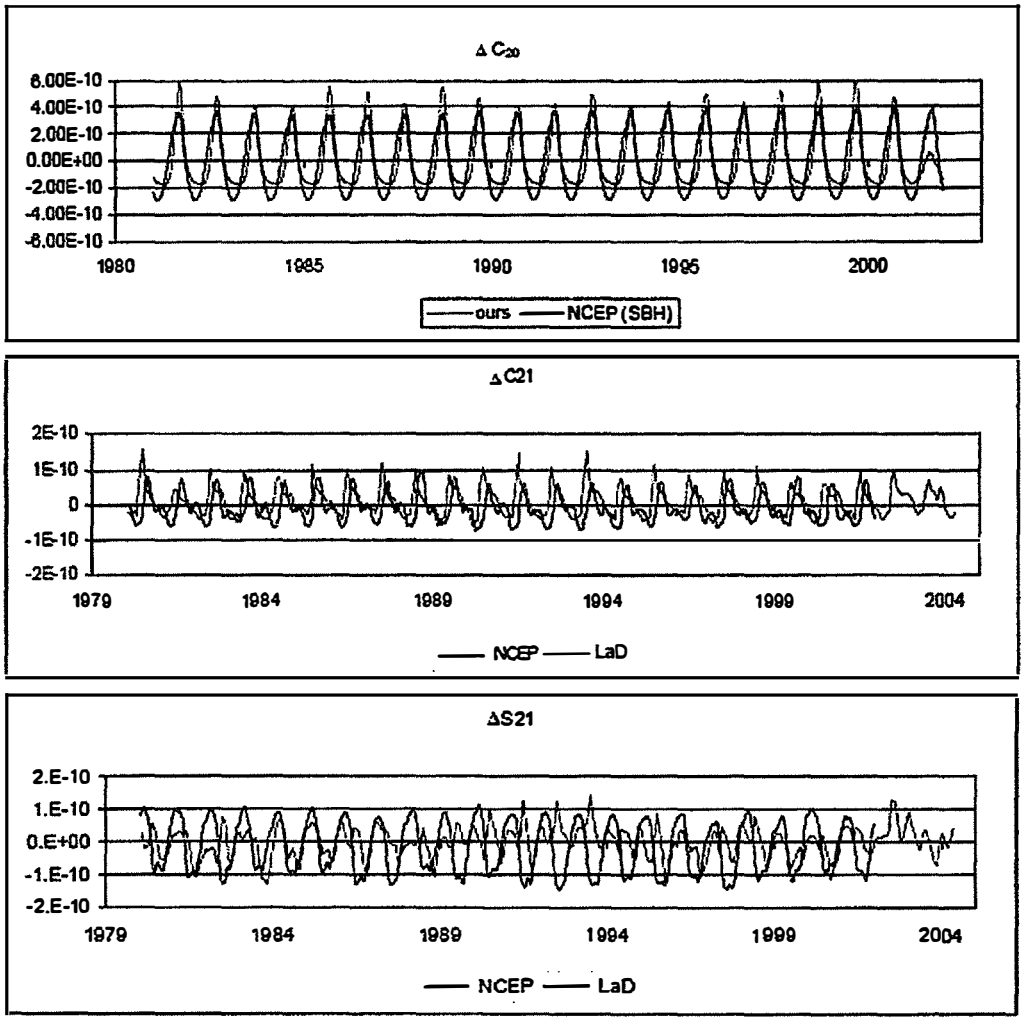

Figure 2: Testing the performance of the numerical integration programme. Red curve our computation of C_{21} and S_{21} variations based on NCEP/NCAR groundwater model. Blue curve: C_{20}, C_{21} and S_{21} time series computed from the continental water storage excitation functions (SBH, Sub bureau of Hydrology. IERS). Data is given daily.

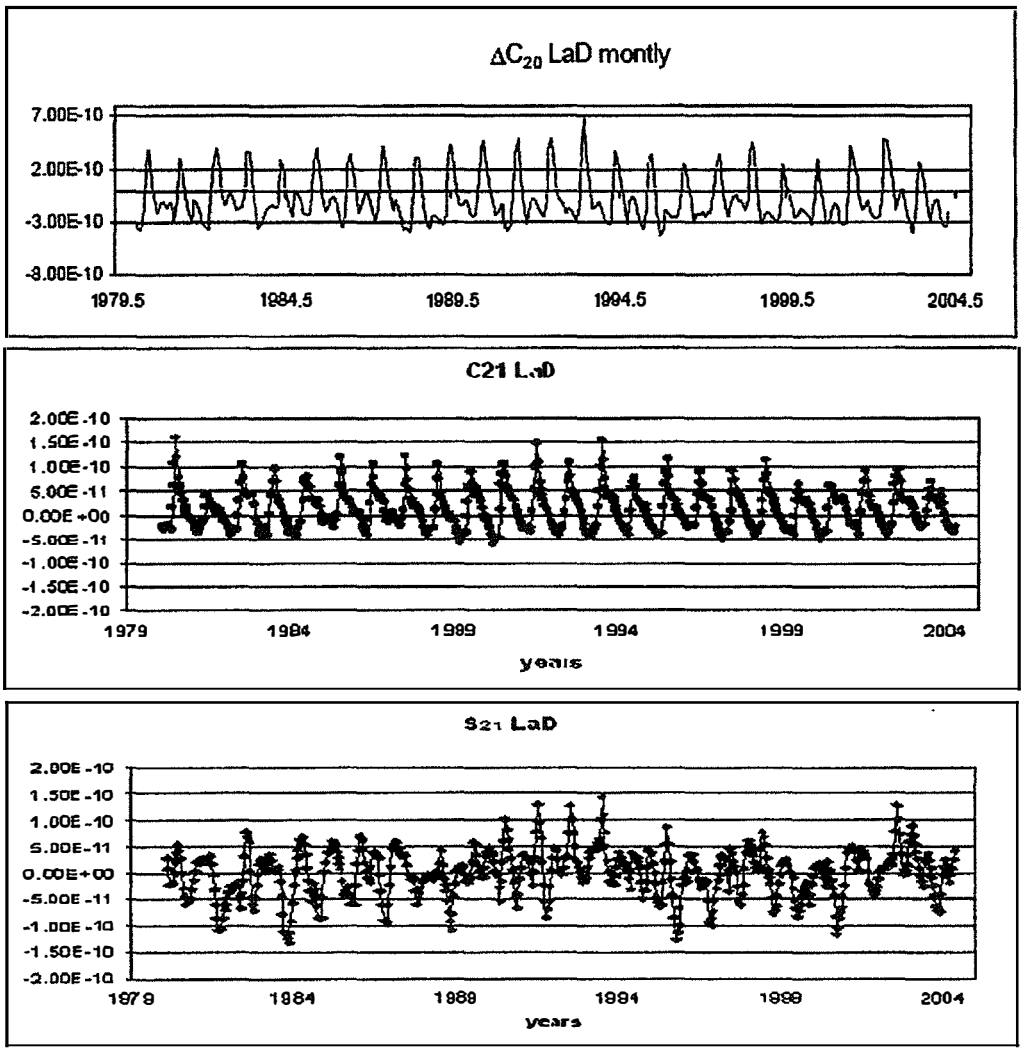

Figure 3: The numerical integration program applied in the computation of ΔC_{20}, ΔC_{21} and ΔS_{21} from LaD model. Data time interval is 1 month.

B. Hydrology (LaD) in exciting inter-annual polar motion variations.

With the purpose of qualifying the ability of the Hydrosphere to excite long term ERP (Earth Rotation Parameters) variations, we also estimates the Stokes coefficients, C_{21} and S_{21}, but from the Atmosphere and the Oceans.

1. Atmospheric excitation function

As a source for estimating the gravity variation signal from the Atmosphere, we used the atmospheric angular momentum (AAM). It is that derived from the NCEP/NCAR reanalysis project at 6-hours interval. AAM are real values multiplied by 10^7, with a 2.5°-by-2.5° spatial resolution.

They were also obtained from the IERS, but in this case from the Sub-bureau for the Atmosphere (SBA).

As atmospheric pressure forcing is not taken into account by the global ocean circulation model ECCO, an inverse barometric (IB) correction was applied to the pressure fields (i.e. the pressure

was set to zero over the oceans) prior to the computation of atmospheric angular momenta (AAM) (Salstein et al., 1993). The data set spans the time interval between January 1st 1980 and December 31st 2002 at daily intervals.

Following Barnes et al., (1983)

$$\Psi_x^w = \frac{-1.43\,R_e^3}{\Omega\,(C-A)\,g}\int_S (u\,sin\phi\,cos\phi\,cos\lambda - v\,cos\phi\,sin\lambda)\,d\lambda\,d\phi\,dp$$

$$\Psi_y^w = \frac{-1.43\,R_e^3}{\Omega\,(C-A)\,g}\int_S (u\,sin\phi\,cos\phi\,sin\lambda + v\,cos\phi\,cos\lambda)\,d\lambda\,d\phi\,dp \qquad (4)$$

$$\Psi_x^P = \frac{-1.00\,R_e^4}{(C-A)\,g}\int_S p_s\,\sin\phi\,\cos^2\phi\,\cos\lambda\,d\lambda\,d\phi$$

$$\Psi_y^P = \frac{-1.00\,R_e^4}{(C-A)\,g}\int_S p_s\,\sin\phi\,\cos^2\phi\,\sin\lambda\,d\lambda\,d\phi \qquad (5)$$

where the super-index w refers to the wind (or motion) terms and p to the pressure (or mass) terms. R_e = 6378136.6 meters is the equatorial Earth's radii, g the acceleration of gravity, C and A the axial and equatorial moment of inertia of Earth and p_s is the surface pressure values, u(φ,λ,p,t) and v(φ,λ,p,t) are the eastward and northward components of the wind velocity at pressure level p. Finally, φ refers to the latitude and λ to the longitude.

Thus, the atmospheric Stokes excitation functions, the add of the mass + motion atmospheric terms, were taken for the period January 1st 1980 till December 31st 2002 at daily intervals.

2. Oceanic excitation time series

In this case we used the global oceanic angular momentum (OAM) as estimated by Gross et al. (2003). The data were obtained from the IERS, Special Bureau for the Oceans (SBO).

The global OAM mass term used in our computations is based on the Massachusetts Institute of Technology (MIT) model. The last is named as Estimating the Circulation and the Climate of the Ocean (ECCO) Program ocean general circulation model (Gross et al. 2003).

Calculation is performed at one day interval, on a grid of 72.5° S to 72.5° N. The grid points are 1/3° far apart at the equator and 1° at the poles. However, they are 1° of space between longitudinal grid points. Some other specific features of the MIT model can be found in Gross et al. (2003) and references therein.

The ocean angular momentum can be expressed as Gross et al. (2003)

$$(\Psi_x + i\,\Psi_y)_{ocean}^{currents} = -\int_V \rho(r,t)\,r\,[sin\phi\,u(r,t) + i\,v(r,t)]\,e^{i\lambda}\,dV \qquad (6)$$

$$(\Psi_x + i\,\Psi_y)_{ocean}^{mass} = \frac{-1.00}{(C-A)}\int_V \rho(r,t)\,r^2\,sin\phi\,cos\phi\,e^{i\lambda}\,dV \qquad (7)$$

where φ refers to the north latitude, λ is the east longitude, u(**r**,t) and v(**r**,t) are the eastward zonal and the northward meridional currents throughout the volume V of the modelled oceans. Finally, ρ(**r**,t) is the density of some mass element located at position **r**. Daily values were weighted average mass terms of the oceanic excitation function in units of [kg m^2/s].

As before the total oceanic angular momentum, computed as the addition of the mass and motion terms, was taken for the period January 1980 till middle 2002 at daily values.

3. The polar motion excitation functions

Conservation of angular momentum within the Earth system implies that polar motion and LOD will be excited by torques acting on the Earth as well as variations in the Earth inertia tensor. Whereas the torques are caused by changes in winds and currents, the variations in the Earth inertia tensor are caused by global mass redistributions.

In effect, the linearized conservation of the angular momentum equation is, (Munk and MacDonald, 1960; Lambeck, 1980)

$$\mathbf{m}(t) + \frac{\mathrm{i}}{\sigma_0}\frac{d\mathbf{m}(t)}{dt} = \Psi(t) - \frac{\mathrm{i}}{\Omega}\frac{d\Psi(t)}{dt} \tag{8}$$

where $\sigma_0 = 2\pi/T\,(1 + i/2\,Q)$ is the complex-valued frequency of the Chandler wobble, determined by period T and quality factor Q, Ω = 7.292115 E-05 rad/s. (IAG Numerical Standards, 1999) refers to the angular velocity of the Earth. $\mathbf{m}(t) = m_x(t) + i\,m_y(t)$, where $m_x(t)$ and $m_y(t)$ are the direction cosines of the Earth's rotation axis relative to the axis of the rotating, body-fixed reference frame.

Thus, if $\omega = (\omega_x,\omega_y,\omega_z)$ represents the instantaneous angular velocity of the Earth, the excursions of ω from a uniform rigid rotation with angular velocity Ω can be written in terms of 3 small dimensionless quantities m_i; (Munk and MacDonald, 1960; Lambeck, 1980)

$$\omega_x = m_x\,\Omega;\quad \omega_y = m_y\,\Omega;\quad \omega_z = (1 + m_z)\,\Omega \tag{9}$$

hence the m_i represent the direction cosines of ω (instantaneous rotation axis) relative to the z-axis of a fixed-body reference frame.

$\Psi = \Psi_x + i\,\Psi_y$ are the polar motion excitation functions. In absence of external torques is valid, (Wahr, 1982; Gross, 2000)

$$\Psi(t) = \frac{1.61}{\Omega\,(C - A)}\left[\mathbf{h}(t) + \frac{\Omega\,(\Delta I_{xz}(t) + i\,\Delta I_{yz}(t))}{1.44}\right] \tag{10}$$

where $\mathbf{h}(t) = h_x(t) + i\,h_y(t)$ is the relative angular momentum, ΔI_{xz}, $\Delta\, I_{yz}$ are the respective variations of the Earth's inertia tensor and C, A the axial and equatorial principal moments of inertia of the entire Earth. The factors 1.44 accounts for the yielding of the solid Earth to impose surface loads, and 1.61 takes into account the core-mantle decoupling (Gross, 2000; Gross et al. 2003).

Hydrological effects on inter-annual polar motion are mainly expected from variations of water storage, whereas the contribution from motions of continental water are viewed as inferior. Therefore relative angular momenta are neglected in our study ($\boldsymbol{h}(t) = 0$). Eqs. (10) can be written into complex formulation as: (Lambeck, 1980; Barnes et al., 1983; Chen et al., 2000; Gross, 2001)

$$\Psi_x(t) + i\;\Psi_y(t) = -\frac{1.61\,MR^2}{(C - A)}(\Delta\bar{C}_{21}(t) + i\,\Delta\bar{S}_{21}(t)) = \Psi(t), \tag{11}$$

$i = \sqrt{-1}$. This equation relates the excitation functions to mass variations in the Earth system which are described by time series of the second-degree and first-order Stokes coefficients.

The whole previous formalism relates changes in the Earth angular momentum to changes in the Earth's rotation pole. However, the observed Earth rotation Parameters as given by the International Earth Rotation Service (IERS), are referred to the location of the celestial ephemeris pole within the rotating body-fixed terrestrial reference frame (Gross, 1992; Brzezinsky, 1992).

So that, re-writing equation (8) in terms of the ERP as reported by IERS,

$$\mathbf{p}(t) + \frac{\mathrm{i}}{\sigma_0}\frac{d\mathbf{p}(t)}{dt} = \Psi(t) \tag{12}$$

where $\mathbf{p}(t) = p_x(t) - \mathrm{i}\, p_y(t)$ with $p_x(t)$ and $p_y(t)$ the respective x and y components of the polar motion, following the convention of $p_y(t)$ (Y_{pole}) being positive toward 90° W longitude.

Addressing equations (11) and (12), daily Earth Rotation Parameters (ERP) excitations for the period January 1980- May 2004 are computed from the multi technique combined C04solution from the IERS. In particular, we applied the IERS Earth Orientation Parameters Product Center (EOP-PC) online interactive tool (http://hpiers.obspm.fr/eop-pc/geophysicalexcitation/observed excitation). We set the Chandler period (T) at 433 days and the quality factor Q at 175. No filtering was applied to the output data series.

4. Homogenization of data

In order to homogenise the different time series, a Savitzky-Golay filter was adopted to smooth the LaD hydrological Stokes coefficients at 30-day interval. The same procedure was applied to NCEP/NCAR hydrological, atmospheric, oceanic and the polar motion (observed) time series.

The criteria followed for the adoption of this method as well as all the preliminary analysis was addressed in the internal report Nº2 (March 2005).

5. ΔC21 and ΔS21 geodetic time series computed from observed polar motion

From the above discussion, we could also deduce an atmospheric and oceanic C_{21} and S_{21} time series by using the mass terms of the excitation functions data series formerly described.

From Chen et al. (2000)

$$\left(\Psi_x + \mathrm{i}\,\Psi_y\right)^{\mathrm{mass}} = -1.098\,\frac{\mathrm{MR}_e^2}{(\mathrm{C}-\mathrm{A})}\left(C_{21} + \mathrm{i}\,S_{21}\right) \tag{13}$$

where Ψ_x and Ψ_y are the excitation functions due to mass redistributions of X and Y of polar motion and C_{21} and S_{21} the Stokes coefficients of degree 2 and order 1.

This computation was performed for the Atmosphere, the Oceans and also for the observed polar motion data. The period of the computation was January 1980 till 2003 at daily values. Figure 4 show us that the addition of the mass contributions from Atmosphere and Oceans can explain mostly of the features observed in the Stokes coefficients variations of the polar motion.

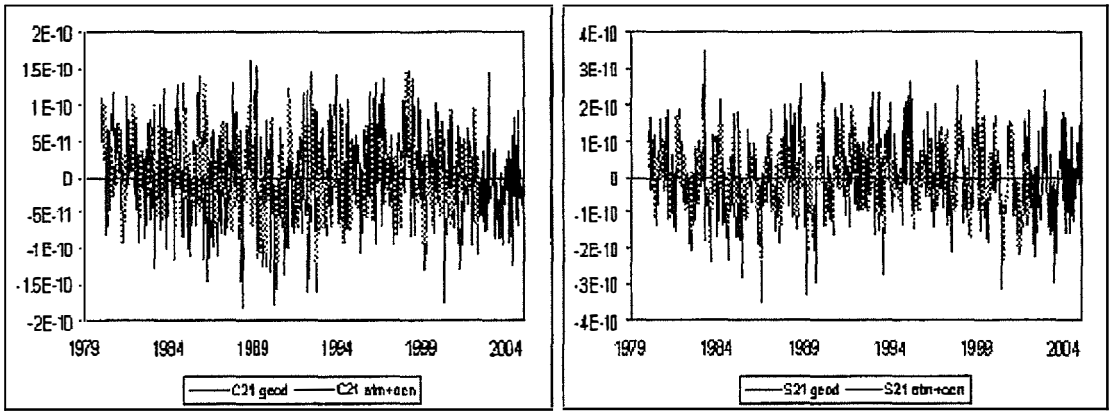

Figure 4: C_{21} and S_{21} temporal variations from ERP IERS C04 (blue curves) and atmospheric + oceanic models (red curve) at 15-day interval.

6. Computation of "Ψ free"

We computed the "free" excitation function as the subtraction of the geodetic (observed) excitation minus the atmospheric + oceanic contribution. Afterwards, we compared the free excitation with respect to the hydrological excitation functions due to mass redistributions.

Figure 5 shows the free excitation function, that is the observed polar motion excitation free of oceanic and atmospheric influence, for the period 1980-2002 at 30-days interval.

7. Data Filtering

Seasonal variations of the Stokes coefficients must be attributed to similar mass changescaused by variations of the ocean dynamics as well as the atmospheric mass redistribution and the global hydrological cycle.

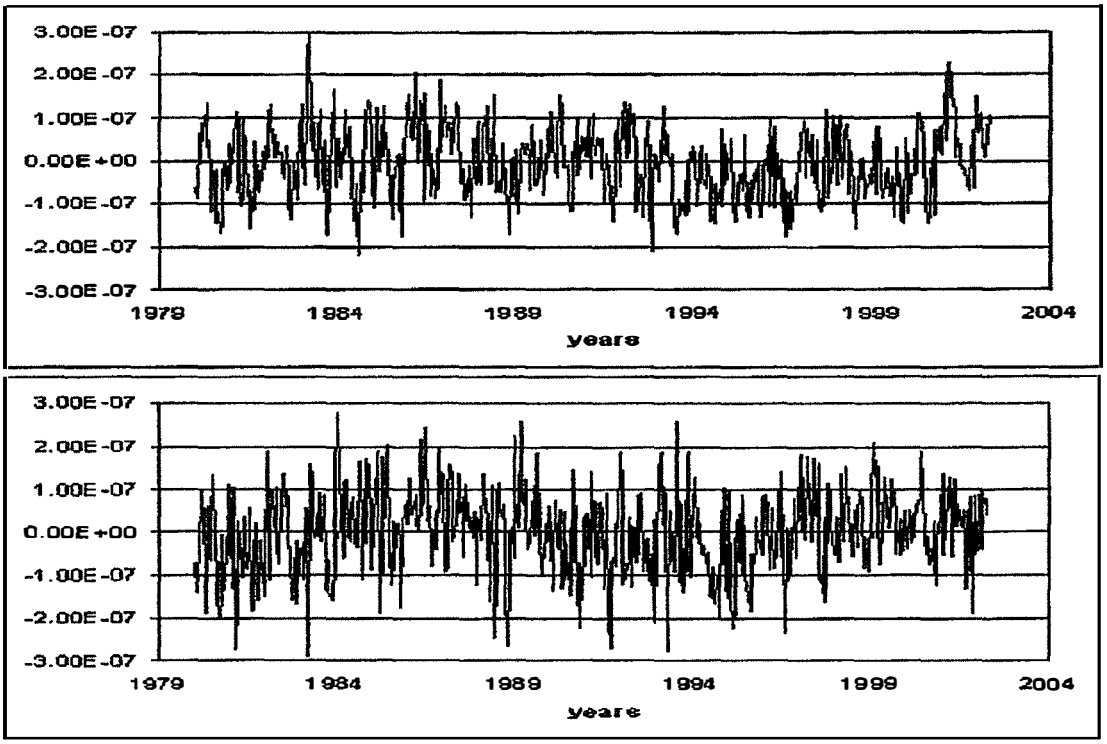

Figure 5: Ψ^f_x (up) and Ψ^f_y (down) components of the Ψ_{free} excitation function in radians as function of time in years.

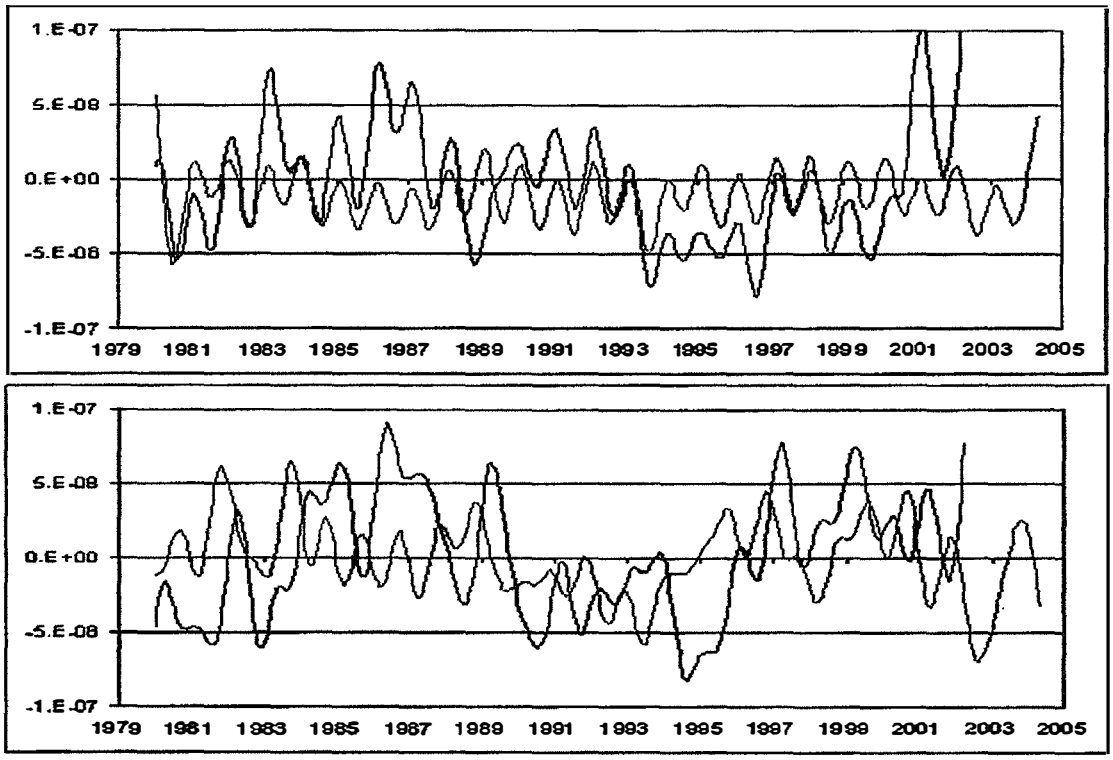

Figure 6: Inter-annual temporal variations of the mass excitation functions of polar motion. Ψ_x (up) and Ψ_y (down) in radians versus time in years. The blue curve represents the free excitation function while the red curve is the hydrological one from LaD model.

In order to study the possible hydrological excitements to the inter-annual variations of the polar motion, we eliminate the high frequency components from each data series by using a low pass filter.

To accomplish with this, we applied a Vondrak filter with $\varepsilon = 35604.92$ (Vondrak, 1977). It corresponds to a cut-off frequency of 1 cycle in 2.37 years, which is approximately twice the Chandler wobble.

Figure 6 shows the two components of the excitation functions ($\Psi = \Psi_x + i\,\Psi_y$) in radians as a function of time in years. In this case, each plot shows both: the free excitation function (blue) and the hydrological excitation function from LaD model. The Vondrak filtering was applied to all of them. The period for this plotted data is January 1st 1980 – May 2004 at 30-day interval.

8. Time-frequency analysis: Wavelets

In order to analyze the behaviour of the filtered series in the frequency domain, we applied a mathematical tool that allows us to do this, but also to scan the performance of the time series along the full time interval: January 1980 – May 2004.

We applied Wavelet analysis of filtered Ψ_{free} and $\Psi_{hydrological}$ time series. In particular we used the FORTRAN codes morlet.f and coherence.f from M. Schmidt (Deutsches Geodatisches Forschungsinstitut, DGFI).

Morlet.f was applied to produce the prograde and retrograde wavelet scalogram for both mass excitation time series. The mother wavelet was Morlet with a $\omega_0 = 2\pi$.

In order to evaluate the relative importance of the maximums, we applied a significance test on the scalogram values; using $\sigma = 2$ following Schmidt (2002).

Figures 7 and 8 show the application of the morlet.f code to the filtered time series: "free" (observed polar motion deprived of the oceanic and atmospheric excitations) and hydrological mass excitations values.

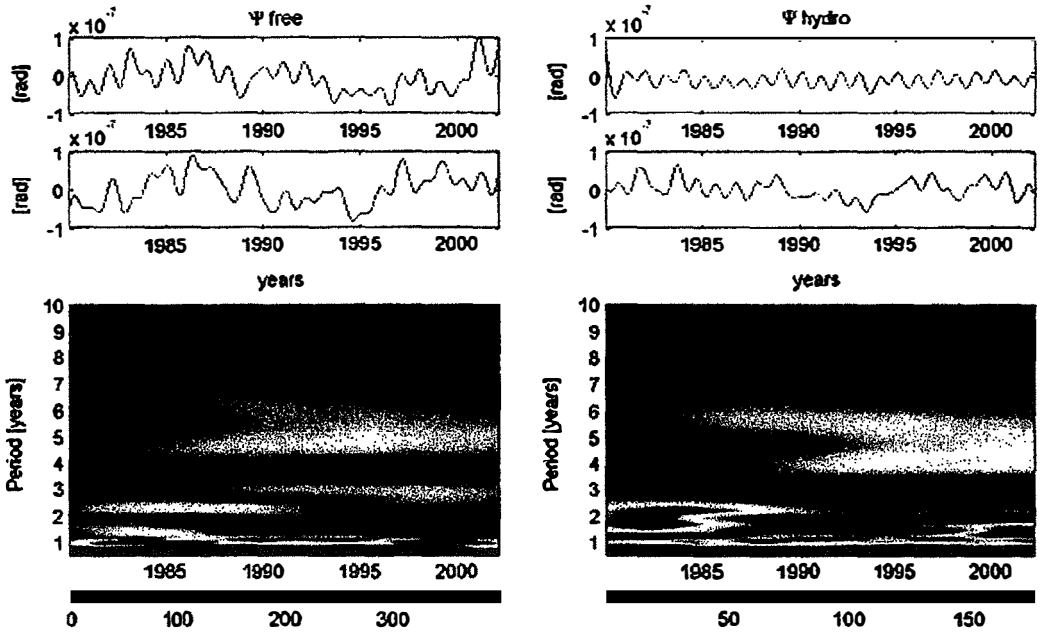

Figure 7: Prograde wavelet scalogram of the inter-annual temporal variations of the free mass excitation function (left) and the hydrological one (right).

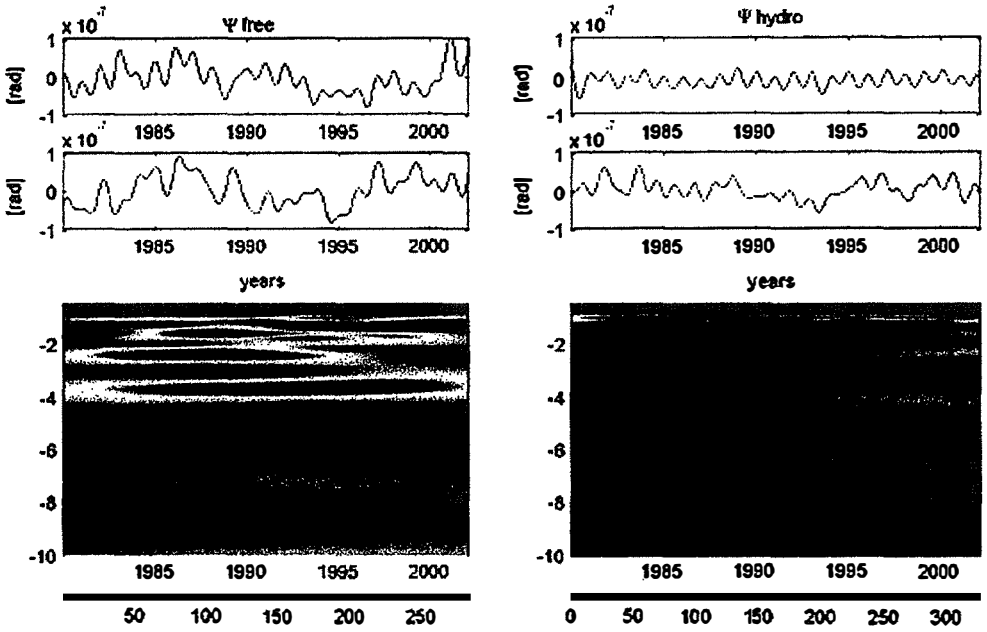

Figure 8: Retrograde wavelet scalogram of the inter-annual temporal variations of the free mass excitation function (left) and the hydrological one (right).

Note that for the prograde component the annual remnant variation reaches a maximum at the free excitation, but this peak appears by apart 15 years. Because the time span is not enough to see a complete Markowitz period, we speculate that this feature should be related to that effect.

Afterwards, we used the coherence.f program (also from M. Schmidt, DGFI) in order to compute the cross wavelet scalogram as well as the normed coherence values. Again, these values were computed in agreement with the Schmidt (2002) procedure.

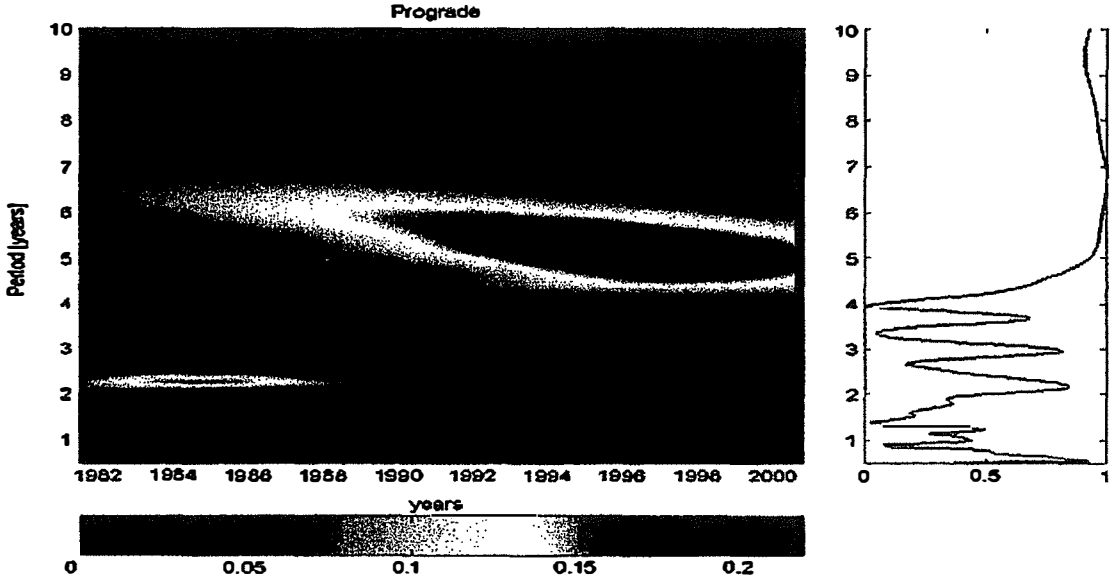

Figure 9: The square of cross wavelet scalogram (left) and normed coherency (right) for the prograde free and hydrological mass excitation functions.

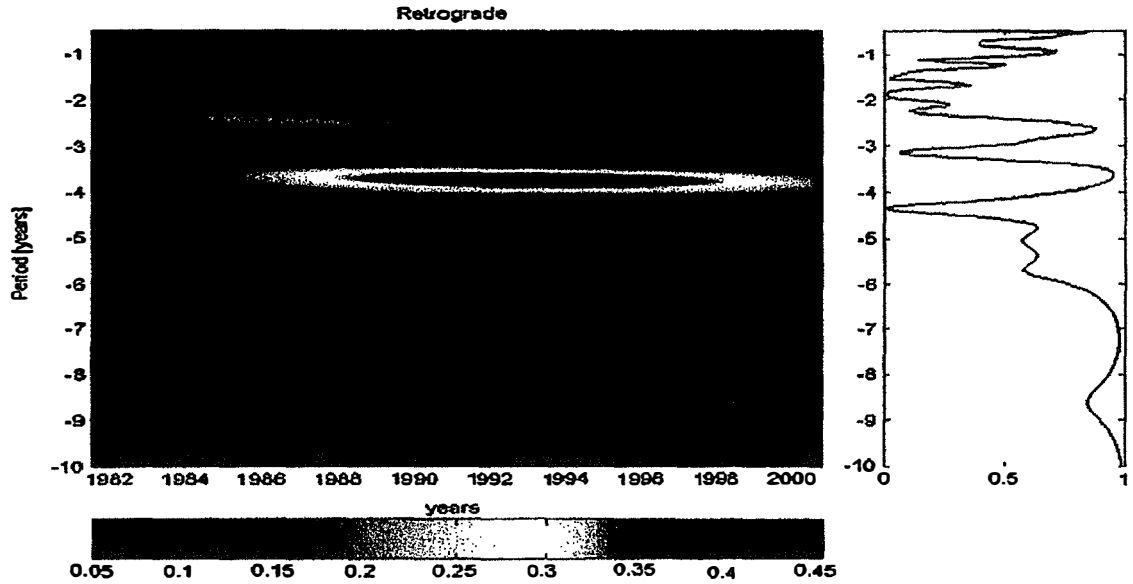

Figure 10: The square of cross wavelet scalogram (left) and normed coherency (right) for the retrograde free and hydrological mass excitation functions.

Figures 9 and 10 show us the square of cross wavelet scalogram and the normed coherence values for the prograde and retrograde components, respectively. From these figures we can conclude that: At one hand, for the prograde components we can see the hydrological influence with a period near 4-5 years, which is demonstrated by a normed coherence of 0.99.

On the other hand, for the retrograde, groundwater redistributions excite variations at 4 years. However the irregular variations between 1.5 and 2.5 years are not clearly explained by hydrological excitation. They should obey to oceanic or atmospheric mis-modelling.

C. Comparison of LaD excitation to polar motion at annual periods with respect to other model estimation

The seasonal polar motion excitation is a set of 12 excitation functions. It is the sum of sinusoidal variations at 1, 2, 3, 4, 5 and 6 cycles per year (c.p.y.). We defined annual excitation to mean the 1 c.p.y. sinusoidal component of the seasonal excitation. It is considered a pure sinusoid and thus, it correspond to a discrete line spectrum in the frequency domain.

The annual excitation describes an ellipse centered at the North Pole, which can be written as the sum of prograde (west to east) and retrograde circular components,

$$\Psi_a(t) = \Psi^+ e^{i\nu t+\lambda^+} + \Psi^- e^{-i\nu t+\lambda^-} \tag{14}$$

with ν = 1 cpy the frequency, t the time in months from January 1st and λ the phase-lag.

We estimated the contribution to the annual excitation in polar motion from continental water mass redistributions. For that, by using a least squares adjustment, we fitted an annual sinusoid to the hydrological excitation functions time series.

Table 1 shows annual contribution from other several hydrological models by (Chao and O'Connor, 1988), (Hinnov and Wilson, 1988), (Kuehne and Wilson, 1988), (Jochmann, 1999) and

(Cheng and Wilson, 2005). Hereafter these models will be named as: CHOC, HW, KW, JOCH and LDAS, respectively.

The values for NCEP/NCAR model were taken from (Cheng and Wilson, 2005) as well as the results for LDAS model. The results of the least squares adjustment applied on LaDDanube model were mentioned as LaD.

	Abbrev.	Prograde	Retrograde
(Chao et al., 1987) snow	CH	(4.9, -109°)	(4.8, -28°)
Chao & O'Connor, 1988	CHOC	(1.9, -74°)	(3.3, 29°)
Hinnov & Wilson, 1988	HW	(7.27, 55.87°)	(6.33, 85°)
Kuehne & Wilson, 1991	KW	(1.79, -22.69°)	(6.84, 175°)
Jochmann, 1999	J	(11.2, -0.59°)	(12.4, 156.74°)
NCEP/NCAR*	NCEP	(12.6, -115°)	(8.72, -30°)
LDAS*	LDAS	(5.11, -9°)	(7.39, 116°)
LaD	LaD	(2.98, -8.21°)	(7.46, -45.47°)

*values from [Chen and Wilson, 2005]

Table 1: Continental water storage excitation functions of the annual wobble of the polar motion. Units of amplitude are milliarcseconds and phase in degrees. The reference phase for date is January 1.

Almost all the authors listed in Table 1 also considered the snow contribution along with the liquid water but (Chao et al., 1987) (CH). This last work only studies the snow pack effect on the Earth rotation and low degree zonal gravitational field. This contribution was also included to the comparison for being the first one of this type.

In Figure 11 we have plotted the annual hydrological excitation functions as estimated by the before mentioned references, along with the LaD estimation.

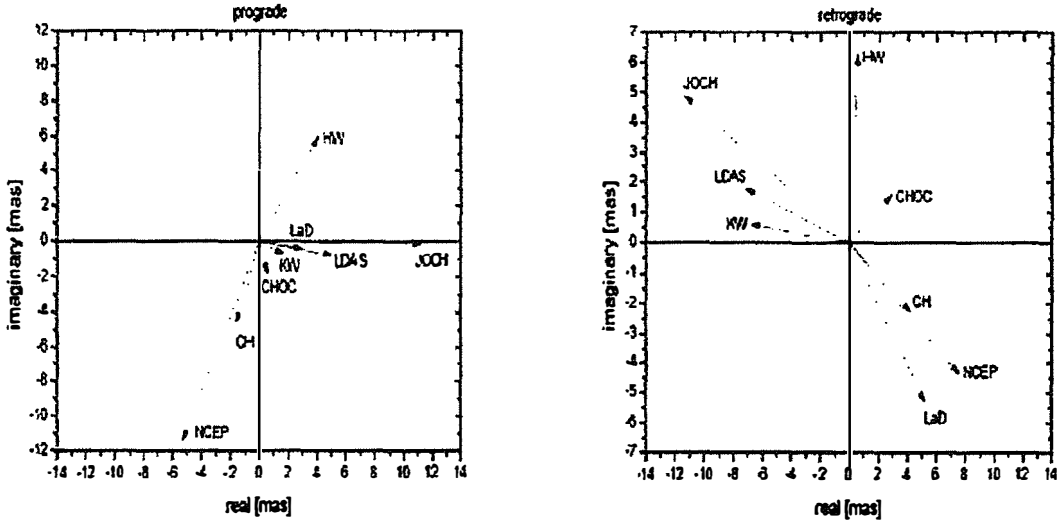

Figure 11: Phasor diagrams for the comparison of the annual prograde and retrograde wobble excitation induced by continental water variations. The reference date for the phase is 1st January For the prograde annual component almost all the contributions have negative phase lag but HW's value, while phases are quite different for the annual retrograde excitation.

Taking into account only their amplitude, NCEP values are similar to HW or J. Regarding at the last developed two models, phases for LDAS and LaD are quite close for the prograde components. However, LaD is larger than twice the amplitude of LDAS. For the retrograde component, these models show a better agreement in amplitude.

D. Analysis of the polar motion budget at seasonal terms:

Besides the annual terms, the seasonal variations also alludes to the semiannual (2 c.p.y.) and ter-annual (3 c.p.y.) terms. With the purpose of qualifying the ability of the hydrosphere to excite long term ERP, we corrected the polar motion time series from atmospheric and oceanic excitations. After that, we evaluate the efficiency of NCEP, LaD and LDAS in closing the seasonal polar motion budget.

The annual, semi-annual and ter-annual signals are subsequently extracted from the excitation functions by a least-squares fit. Finally the results are converted into prograde and retrograde components for January 1st 1990.

The least squares adjustment was applied on the mass term contributions to the atmospheric, oceanic and hydrological excitation functions; but also to the geodetic time series. Previously, the Chandler wobble was eliminated from the last one. The respective amplitude and phase for Chandler are 29.24 milliarcseconds and -150º.15, respectively.

The polar motion observed values were transferred into corresponding terms of the excitation function according to (Gross 1992) and named as geodetic $\psi geod$.

The amplitudes and phases of annual, semiannual and ter-annual variations estimated by least squares are listed in Table 2 discriminated by source.

Figure 12 shows the annual phasor diagrams. For the prograde component there is a very good agreement in closing the polar motion budget, although the add of vectors of the geophysical contributions is not enough to explain the observed polar motion.

For the retrograde component the amplitudes seem to agree, but the phases are such the vector add is far of justifying the polar motion variation at that period.

Annual	Prograde	Retrograde
Geodetic (IERSC04)	(22.12, -76.49°)	(6.19, -142.92°)
AAM (wind + pressure)	(20.1, -90.28)	(16.6, 98.83°)
OAM (currents + ocean bottom pressure)	(6.64, 53.81°)	(4.84, 88.22°)
LaD	(2.98, -8.21°)	(7.46, -45.47°)
NCEP	(12.6, -115°)	(8.72, -30°)
LDAS	(5.11, -9°)	(7.39, 116°)

Semi-annual	Prograde	Retrograde
Geodetic (IERSC04)	(6.97, 115°)	(7.34, 149.57°)
AAM (wind + pressure)	(3.03, -72.51)	(4.46, 118.28°)
OAM (currents + ocean bottom pressure)	(1.96, 160.89°)	(2.89, -139.87°)
LaD	(4.33, -142.97°)	(2.61, 98.89°)
NCEP	(3.88, 89°)	(2.6, -83°)
LDAS	(0.20, -81°)	(0.75, 24°)

Terannual	Prograde	Retrograde
Geodetic (IERSC04)	(2.38, 142.34°)	(2.21, -38.67°)
AAM (wind + pressure)	(1.28, 147.68)	(0.93, -1.59°)
OAM (currents + ocean bottom pressure)	(1.48, 133.87°)	(1.78, -75.69°)
LaD	(0.6, 28.42°)	(0.31, -11.37°)

Table 2: Annual, semi-annual and ter-annual wobble excitations due to mass redistribution. Amplitude are in milliarcseconds (mas); phase in degrees.The reference phase for date is January 1, 1990

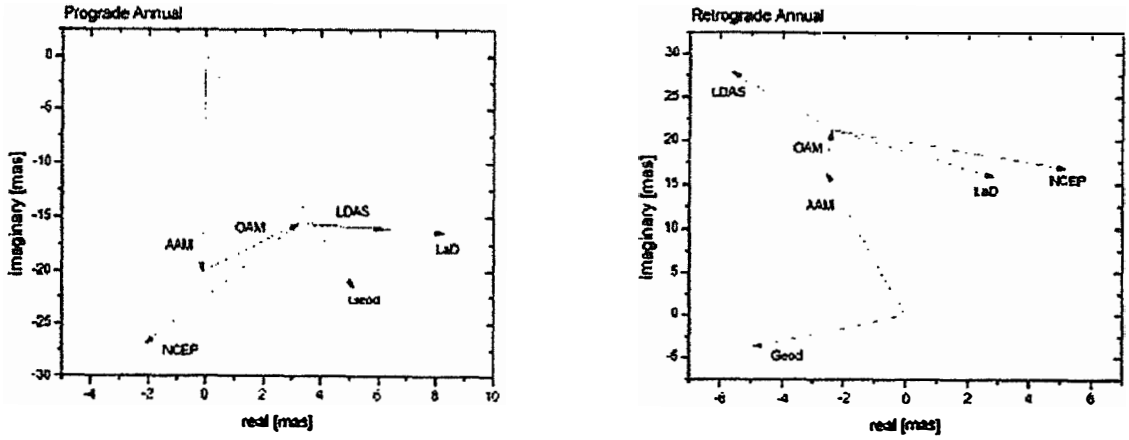

Figure 12: Phasor diagrams of the prograde (left) and retrograde (right) of the geodetic (geod), atmospheric (atm), oceanic (ocn) and our estimate of the continental water (hyd) excitation functions at the annual frequency. Units are milliarcseconds. These contributions were calculated from the C_{21} and S_{21} Stokes coefficients respectively. So that, they only consider the mass redistributions effects. The oceanic bottom pressure values are from [Gross et al., 2003]. The reference date for the phase is 1 January 1990, 0 UTC.

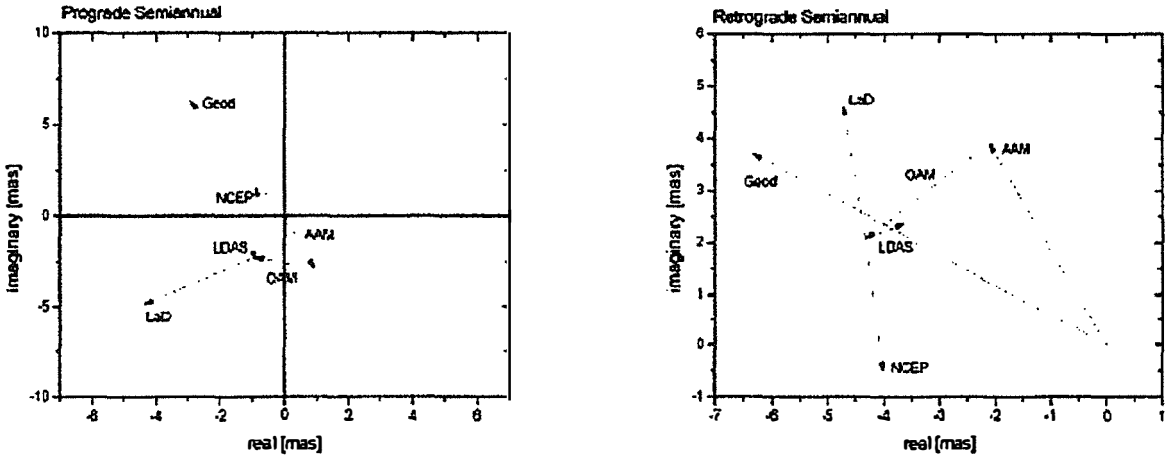

Figure 13: The same as in figure 16 but for the semiannual excitation functions due to mass redistributions.

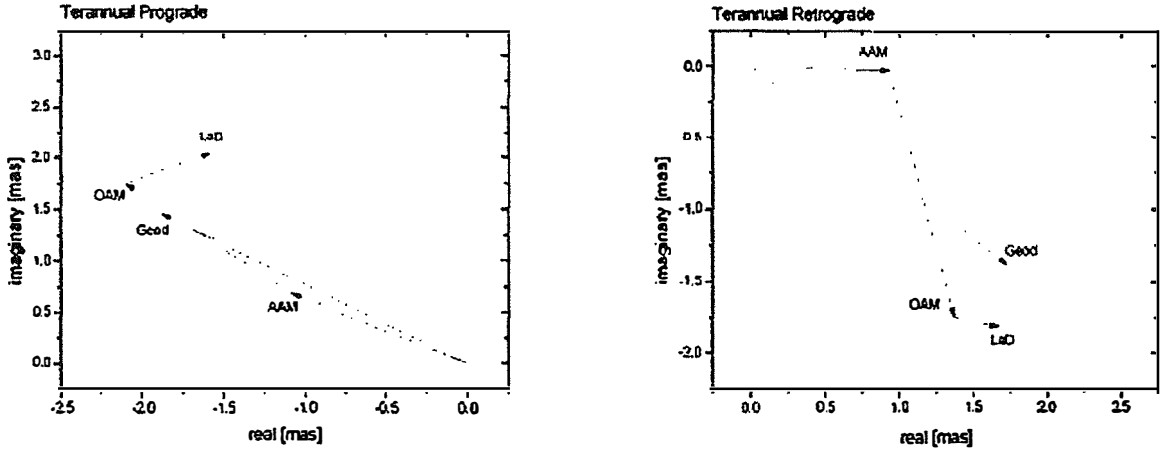

Figure 14: The same as in figure 16 but for the ter-annual excitation functions due to mass redistributions.

Figure 13 and 14 show the same as in figure 12, but for the semiannual and the ter-annual components. For the semiannual prograde terms the agreement is fairly good. The vector add resultant for the geophysical excitation is 2.35 milliarcseconds smaller in amplitude (a 36% less), and less than 10 degrees of difference in phase lag, with respect to the geodetic excitation.

In the case of the semiannual retrograde, the situation is different. The amplitude of the resultant is just 48% of the amplitude of the semiannual retrograde polar motion variation.

For both ter-annual polar motion diagrams, the resultant amplitude for the vectorial sum of geophysical causes is only 53% for the prograde and 36% for the retrograde with respect to the observed polar motion.

The phase lag for the prograde ter-annual terms is almost 12 degrees, while for the retrograde is larger than 180 degrees.

E. Study of the annual and inter-annual effects of the on LOD variations: Comparison with the respective Stokes coefficients C20 from LAGEOS and GRACE

The main objective of this work is to compare seasonal and inter-annual hydrological mass redistributions from LAGEOS with the estimations from LaD and to evaluate seasonal and inter-annual hydrological effects to LOD.

To that end we compared seasonal and inter-annual hydrological mass redistributions from LAGEOS data with the estimations from LaD. The techniques applied were: Vondrák filtering, cross power spectrum and the computation of correlation factors.

Variations of the Earth gravity field were analyzed for ΔC_{20} estimated from (i) laser distances to Lageos I and II satellites, and (ii) from GRACE gravity measurements.

After tidal and decadal signals were removed from LOD, the results were compared with ΔC20 from geophysical model predictions focussing on the hydrological estimations from LaD-Danube (Milly & Shmakin, 2002) and NCEP/NCAR models.

After removing tides and atmospheric + oceanic contribution, the LOD residuals appears just hardly to distinguish from the background noise. Low correlation factors were obtained.

At seasonal periods (annual and semi-annual), the hydrological global mass redistribution can be clearly seen so much in LAGEOS as in LOD residual data series.

At inter-annual time scales, the very well known and controversial change of rate in C_{20} LAGEOS's time series can be seen as a spectral peak (~20y).

Although, we found out some evidence of hydrological excitation with a period of 2.92 years to the length-of-day, some more studies are still needed for affirming it categorically.

Production

As a result, all the activities before described produced several papers and scientific meeting presentation, besides the internal presentations, even after the period informed in the present report

Fernández L., Schuh H. (2005). Low degree gravitational effects of water storage variations on polar motion. EGU 2005, Vienna, Austria.

Bourda G., Fernández L., Schuh H. (2005). Earth gravity field and LOD variations related to hydrological excitations. IAG meeting Dynamic Planet 2005. Cairns, Australia

Fernández L., Schuh H. (2005). Polar motion excitation analysis due to global continental water redistribution. Proceedings Journées 2005 Systèmes de Référence Spatio-

Temporels: "Earth dynamics and reference systems: five years after the adoption of the IAU 2000 Resolutions", Warsaw, Poland.

Fernández L., Schuh H., Brunini C. (2005) Obtención de series Temporales de los parámetros de Stokes a partir de modelos Geofisicos globales y su relación con las variaciones en los ERP. Geoacta, 30, 93 - 102. ISSN 0326-7237

Fernández L.I., Schuh H., Schmidt M., Seitz F. (2006). Effects of inter-annual water storage variations on polar motion. Accepted in Geophysical Journal Internacional. ISSN 0956-540X 16

Fernández L., Schuh H., Brunini C. (2006). Hydrological excitations to polar motion. EGU 2006, Vienna, Austria.

Fernández L., Brunini C. (2006). Excitación hidrológica al movimiento del polo. XXIII meeting A.A.G.G. (Asociación Argentina de Geofísicos y Geodestas), Bahía Blanca, Argentina (poster presentation).

Fernández L., Brunini C. (2006) Excitación hidrológica al movimiento del polo, submited to Geoacta, ISSN 0326-7237.

References

Barnes R.T.H., Hide R., White A.A., Wilson C.A., 1983. Atmospheric Angular Momentum fluctuations, Length-of-Day changes and polar motion. Proc. R. Soc. London, A, 387, 31-73.

Brzezinski A. 1992. Polar motion excited by variations of the effective angular momentum function: Considerations concerning deconvolution problem. Manuscripta Geod. 17, 3-20.

Chen J.L., Wilson C.R., Eanes R.J., Tapley B.D., 2000. A new assessment of long-wavelength gravitational variations. J. Geophys. Res. 105, 16271-16277.

Gross R.S., 1992. Correspondence between theory and observations of polar motion. Geophys. J. Int. 109, 162-170.

Gross R.S., 2001. Gravity, oceanic angular momentum and the Earth's rotation. In: Sideris M.G. (ed), Gravity, Geoid and Geodynamics 2000, Springer, Berlin, 153-158.

Gross R.S., Fukumori I., Menemenlis D., 2003. Atmospheric and Oceanic Excitation of the Earth's Wobbles During 1980-2000. J. Geophys. Res., 108 (B8), doi: 10.1029/2002JB002143, 20031992.

Lambeck K., 1980. The Earth's variable rotation: geophysical causes and consequences. Cambridge University Press. Cambridge.

Milly and Shmakin, 2002), "Global Modeling of Land Water and Energy Balances: Part I: The Land Dynamics Model (LaD)" Journal of Hydrometeorology, Pp. 283-299.

Munk W.H., MacDonald G.J.F., 1960. The Rotation of the Earth: a geophysical discussion. Cambridge University Press, New York.

Salstein D.A., Kann D.M., Miller J.A., Rosen R.D., 1993. The Sub-Bureau for Atmospheric Angular Momentum of the International Earth Rotation Service: A meteorological data center with geodetic applications. Bull. Am. Meteorol. Soc., 74, 67-80.

Schmidt, M., Schuh, H., 2000. Abilities of Wavelet Analysis for Investigating Short-Period Variations of Earth Rotation. IERS Technical Note No 28, 73-80

Vondrák J., 1977. Problem of smoothing observational data II. Bull. Astron. Inst Czech. 28, 84-89.

Research Report:

A phase delay connection for delta VLBI observations – estimation of maximum gap limits

Tetsuro Kondo

Guest scientist at the IGG from

01-03-2006 to 31-08-2006

This report consists of research work sections of 6 monthly reports which were issued every month during my stay in Vienna.

Acknowledgements

I am deeply grateful to Prof. Harald Schuh-san for providing me this nice and fruitful opportunity to stay in Vienna for 6 months. I thank Hobiger-san and Joe-chan for taking care of me everyday. I also thank all staff members of the HG for all they have done to make my stays memorable.

My stay was supported by the research project P16136-N06 "Investigation of the ionosphere by geodetic VLBI" founded by the Austrian Science Fund (FWF).

Monthly Report (March, 2006)

1. Kashima-Gifu VLBI experiment dedicated to the detection of TID

A test VLBI experiment was carried out on the Kashima-Gifu baseline (Fig.1) on Mar. 16 in cooperation with the Gifu University and NICT. In this experiment, one strong source, 3C273B, was continuously observed for 1 hour (but divided into 12 scans each consisting of one 5 minute scan). After the experiment, 2 scans of raw data of each station were transferred from Kashima to Vienna through the Internet using SFTP and/or SCP programs. Data were correlated in Vienna using a K5 software correlator, and a good fringe was successfully found after the first trial (Fig.2). Thereafter, all scan data were processed at Kashima also using a software correlator, and correlated results were transferred to Vienna for further analysis. All raw data were transferred to Vienna to estimate the turn-around time of data processing if all were carried out in Vienna. We found that it was possible to process all data within a few days in case of one-baseline and one-hour observation with a data rate of 16 Mbps.

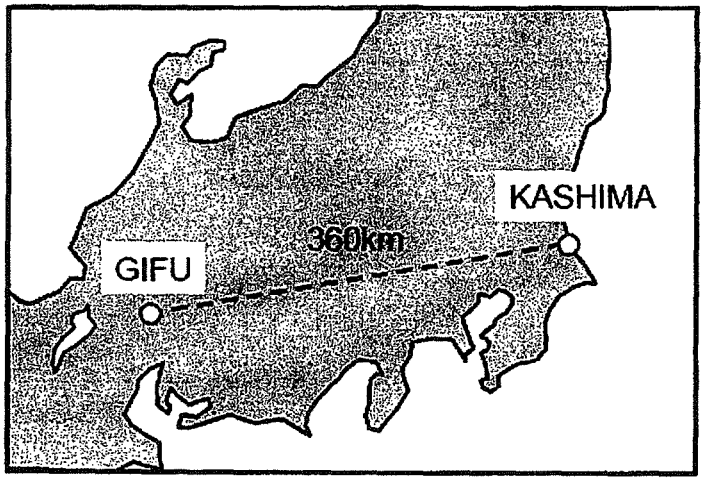

Fig.1: Kashima-Gifu baseline.

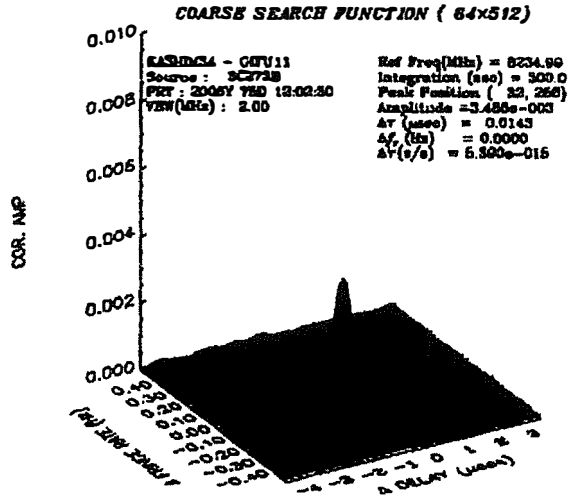

Fig.2: Fringes detected by the software correlator.

A preliminary analysis result does not show any evidence of the detection of TID event. Further analysis is going on to establish a method necessary to connect phase delays between scans. A fringe phase plot is shown in Fig.3 as one example of the result of phase delay connection. Vertical bars show the boundary of scans.

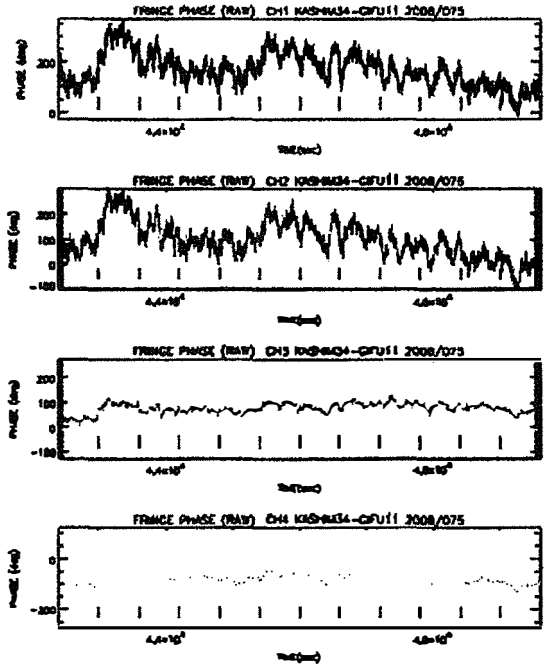

Fig.3: Observed fringe phases for 1 hour period. Upper 2 panels are for X band and lower 2 for S band.

A next experiment with a longer observation period will be scheduled in April.

Monthly Report of April, 2006

1. Kashima-Gifu VLBI Experiment (TID Experiment)

As has already reported in the last monthly report, no TID event was detected in the Kashima-Gifu VLBI data observed on March 16, 2006. Therefore a further analysis was made to investigate the relation between a scan length and an available scan gap to connect phase delays between adjacent scans. This issue is quite important for a differential VLBI technique that observes a spacecraft and a quasar alternately to measure their position difference. If we can connect observed phase delays from scan to scan, the accuracy of measurement will drastically improve.

We have connected phase delays from a scan "A" to the next scan "B" by extrapolating a phase delay observed in scan A to that at the beginning of scan B using an observed delay rate from scan A. Hence the error of the extrapolated delay ($\Delta\tau$) caused by the error of the delay rate ($\Delta\dot{\tau}$) can be written as

$$\Delta\dot{\tau} = t\Delta\tau$$

where t is a scan gap length (sec). We compute a delay rate from the changing rate of fringe phase (fringe rate), so that the fluctuation of the fringe phase affects the accuracy of the determined delay rate. Assuming fluctuations caused by both, thermal noise and natural atmospheric characteristics, we can express $\Delta\dot{\tau}$ as

$$\Delta\dot{t} = \sqrt{(\Delta\dot{t}_{snr})^2 + (\Delta\dot{t}_{atm})^2} \tag{1}$$

where $\Delta\tau_{snr}$ is the error caused by thermal noise, i.e., computed the signal to noise ratio (SNR), $\Delta\tau_{atm}$ is the error due to the characteristics of the atmosphere. $\Delta\dot{\tau}$ can be computed from observed fringe phases, and $\Delta\tau_{snr}$ can be theoretically computed from an observed correlation amplitude. Fig.1 shows $\Delta\dot{\tau}$ and $\Delta\tau_{snr}$ for Kashima-Gifu VLBI data. From Eq.(1), $\Delta\dot{\tau}$ should be always greater than $\Delta\tau_{snr}$, however, $\Delta\tau_{snr}$ takes larger value than $\Delta\dot{\tau}$ for X-band at the range of scan lengths less than or equal to 2 seconds. This is thought to be due to the underestimation of correlation amplitude, because we use that at 300 sec for computing $\Delta\tau_{snr}$. Using $\Delta\dot{\tau}$ we can compute the phase error after extrapolating the phase for t seconds as follows.

$$\Delta\phi = 2\pi f t \Delta\dot{t} \tag{2}$$

where f is frequency. We assume that if the phase error is less than 1 radian, i.e., $\Delta\Phi<1$ we can connect phase delays over scan gap t. In this case the condition where scan gap t should satisfy can be written as follows.

$$t < \frac{1}{2\pi f \Delta\dot{t}} \tag{3}$$

Fig.2 shows a maximum gap t obtained from the actual VLBI data.

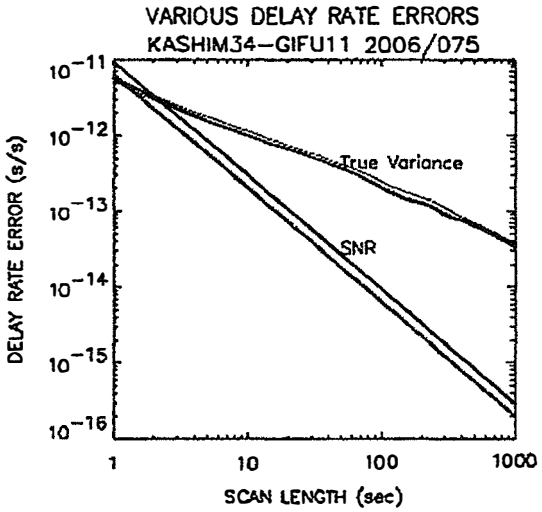

Fig.1: Delay rate errors computed from SNR (signal-to-noise ratio) and from true phase variance for S-band (red lines) and X-band (dark green lines) data.

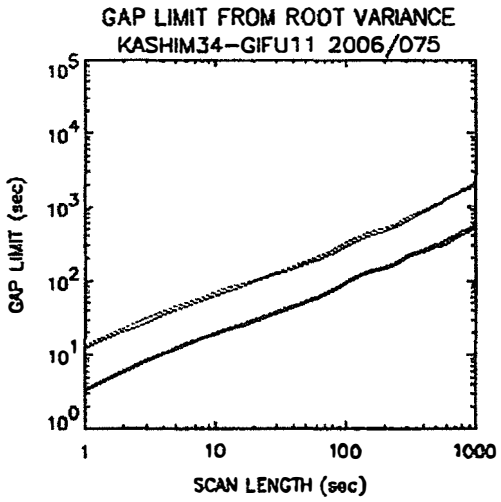

Fig.2: Gap limit obtained from fringe phase variance for S-band (red lines) and X-band (dark green lines) data.

In the meantime Eq.(2) is based on the propagation of error caused from Gaussian noise. If fringe phase variation does not follow this type, we cannot apply a simple error propagation to evaluate the connectivity of phase delays. Actually, phase fluctuations attributed to the atmosphere is known to be a random walk or flicker-noise type fluctuations at a time range concerned in this study. We hence compute the structure function of fringe phase to investigate the scan gap length independently from the discussion about $\Delta\dot{\tau}$. The structure function at time τ is defined as follows.

$$\sigma^2(\tau) = 4\pi^2\tau^2 f^2 I^2(\tau) \tag{4}$$

where I^2 is the true phase variance. Fig.3 shows $\rho(\tau)$ obtained from the VLBI data. We can assume that if $\rho(\tau)$ is less than 1 radian, we can connect scans like the assumption in the discussion about a $\Delta\dot{\tau}$. This condition limits the maximum gap lengths. By taking this condition into the discussion about $\Delta\dot{\tau}$ we obtain more realistic gap limits as shown in Fig. 4.

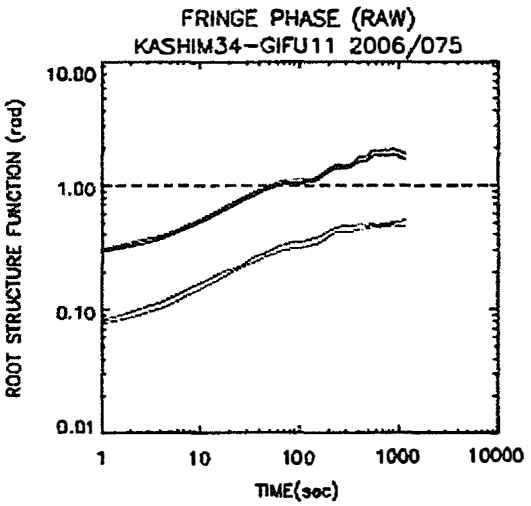

Fig.3: Root structure function obtained from the VLBI data for S-band (red lines) and X-band (dark green lines) data.

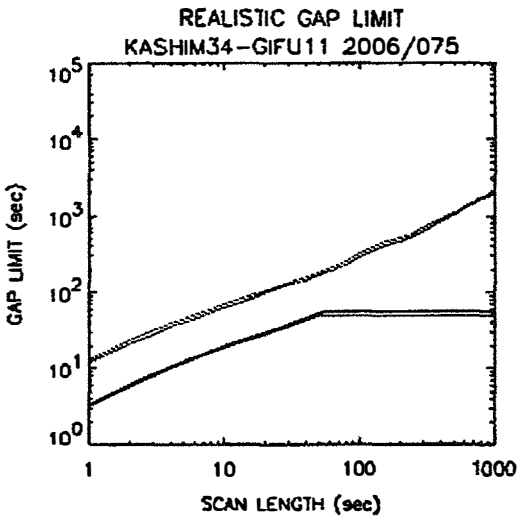

Fig.4: Realistic gap limit taking both, the structure function and delay rate error into account. S-band data are red lines and X-band data are dark green lines.

A report describing details is being prepared.

Second TID VLBI experiment was carried out on April 19, 2006 for two hours. Unfortunately, S-band data acquisition at Kashima failed. So that the data cannot be used for the analysis of TID. Now analysis is being made from the view point of atmospheric stability.

Monthly Report of May, 2006

1. Kashima-Gifu VLBI Experiment (TID Experiment)

So far four experiments have been carried out since March, among those two were failed in S-band observations (Table 1). Therefore two experiments can be used for a TID analysis.

	Date	Comments
No.1	12-13 UT, March 16, 2006	Rainy
No.2	12-15 UT, April 19, 2006	No S-band data at Kashima
No.3	12-15 UT, May 10, 2006	No S-band data at Gifu
No.4	12-15 UT, May 11, 2006	

Table 1: Kashima-Gifu TID VLBI Experiments

I have reported about a method to connect phase delays between scans and about available gap limits in the last two monthly reports. The method to connect scans was applied to the fourth experiment conducted on May 11. Some bugs in a program calculating a fringe phase at each PP, which is a unit integration period in a software correlator, were found in the process of scan connection. These bugs were fixed, and how to evaluate results of connections has been established.

1.1 Phase delay connection and its evaluation

A phase delay connection between scans is carried out as follows (only the essence of a method is described here). In Fig.1, let t_a be the time at the boundary of scan #1 and #2, and coarse delay and residual fringe phase observed for scan #1 at t_a be t_1 and F_1, and those for scan #2 at t_a be t_2 and F_2, respectively. We can connect phase delays of both scans by adding t_{add} given by

$$\tau_{add} = \tau_1 - \tau_2 + \frac{\phi_1 - \phi_2}{2\pi f} \tag{1}$$

to scan #2, where f is a RF frequency. t_{add} appears because the coarse search delay is less accurate compared with that of a phase delay and it should be an integer number times of an ambiguity of phase delay (=1/f). Hence we can evaluate phase delay connections by using the ambiguity number *n* defined as

$$n = f \cdot \tau_{add} = f \cdot (\tau_1 - \tau_2) + \frac{\phi_1 - \phi_2}{2\pi} \tag{2}$$

A fractional part of *n* should be zero.

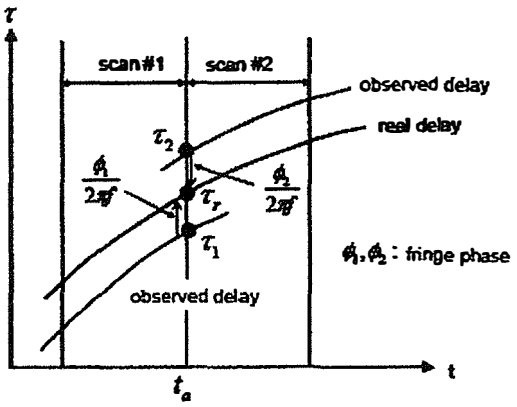

Fig.1: Connection of phase delays.

Fig.2 shows fringe phases after phase-delay connections for the fourth experiment. Fig.3 shows a fractional part of *n* calculated from *n-NINT(n)* where *NINT* is a function converting input to the nearest integer. We can see that almost all ambiguity numbers are integers. This means that phase delay connection goes well.

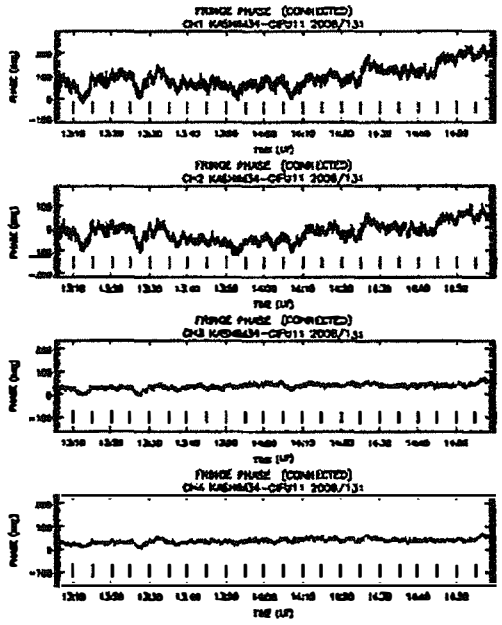

Fig.2: Plots of fringe phases after phase delay connections for fourth experiment (May 11)

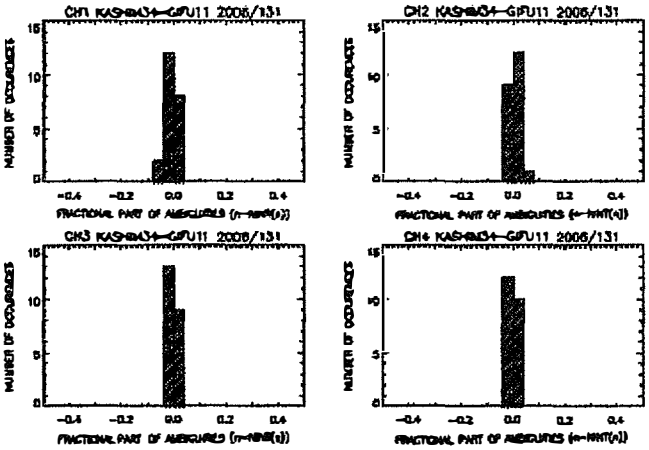

Fig.3: Occurrence frequency plot of a fractional part of ambiguity numbers.

Now I am working on the investigation of available gap limits between scans by using actual data listed in Table 1.

Monthly Report of June, 2006

1. Kashima-Gifu VLBI Experiment (TID Experiment)

A method to connect phase delays between scans has been evaluated by using the 2 hour period data observed on May 11, 2006.

1.1.1 An evaluation method

A phase difference, $\Delta\Phi$, between an estimated phase Φ_C and an actual phase Φ_0 is evaluated statistically, where Φ_C is a phase calculated using the data with the period of t_S for the time separated by t_G from the data span as shown in Fig.1. The data span used for estimation of phase is shifted by 10 sec and the calculation of the phase difference is repeated.

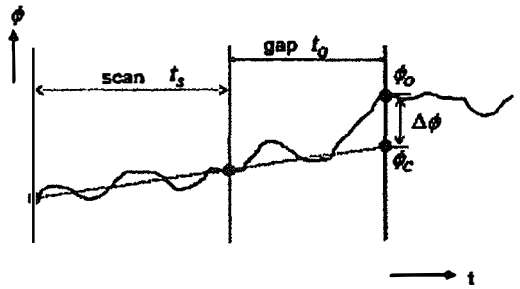

Fig.1: How to evaluate phase difference.

Fig.2 shows an example of occurrence distribution of $\Delta\Phi$ in the case of t_S=100sec and t_G=10sec for 8234.99 MHz data. Standard deviation is 17.6 deg in this case. Fig.3 shows the relation between gap length and standard deviation of $\Delta\Phi$ in the case of t_S=100sec. Standard deviation increases as gap length increases, and it reaches 1 rad (=57.3 deg) at t_G=116sec.

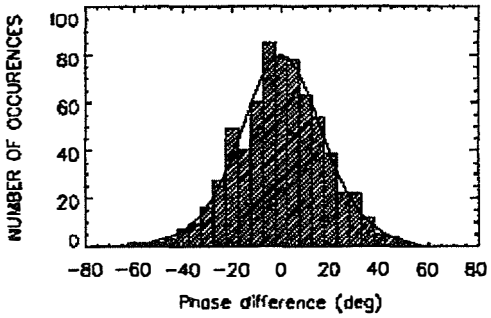

Fig.2: An example of occurrence distribution of $\Delta\Phi$ in the case of t_S=100sec and t_G=10sec for 8234.99 MHz data. Standard deviation is 17.6 deg.

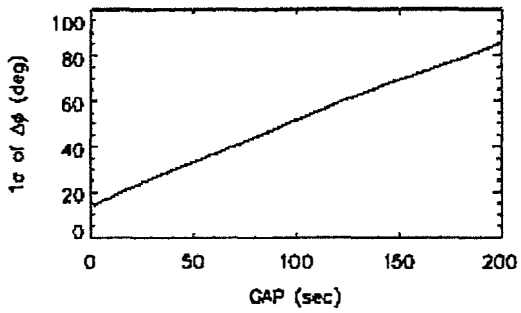

Fig.3: The relation between gap length and standard deviation of $\Delta\Phi$ in the case of t_S=100sec. Standard deviation reaches 1 rad (=57.3 deg) at t_G=116sec.

Assuming that the standard deviation of 1 rad gives the limit of gap length, we can obtain the relation between span length and gap length as shown in Fig.4. In the figure, the symbols are those obtained in this way and the solid lines are for those obtained by the method described in the previous report (April Monthly Report). Both coincided well with each other for S-band data

(red lines and square symbols), but discrepancy can be seen for X-band at spans from several tens to several hundreds of seconds, i.e., results obtained this time are less than previous estimations. This means that the assumption used for previous estimations is not correct for these span lengths. In the previous estimation, the Gaussian distribution of phase fluctuations is assumed for all time ranges. Actually it is not a Gaussian distribution (white phase fluctuation) but rather a random walk fluctuation for X-band at the time scales from several tens to several hundreds of seconds as shown in Fig.5. Thus it is important to evaluate an available gap limit by using the method used this time.

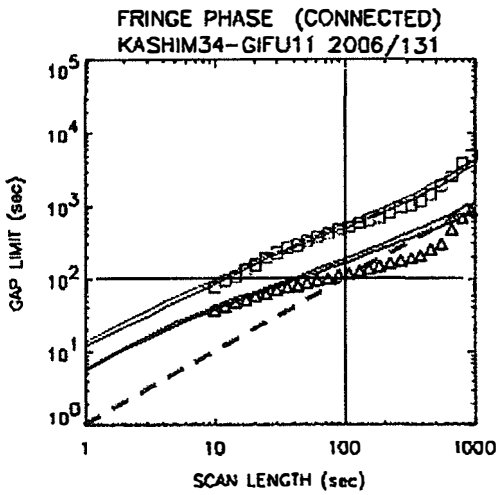

Fig.4: Gap limit obtained from the fringe phase variations (solid lines: red for S-band, dark green for X-band) and those obtained from this study (symbols: square for S-band, triangle for X-band). A green dashed line represents (scan length) = (gap length)

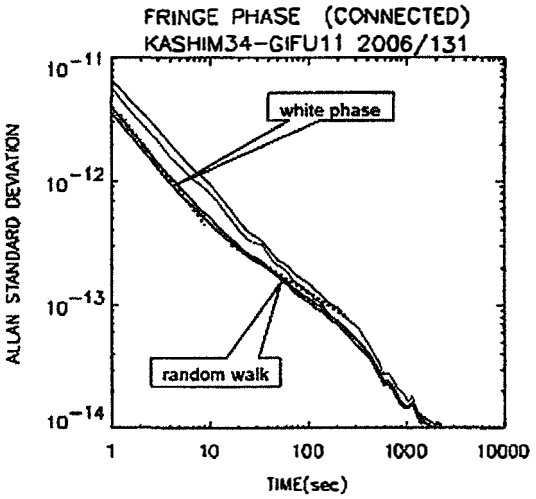

Fig.5: Results of Allan standard deviation analysis. S-band (red lines) shows white phase characteristics for all time range, while X-band (dark green lines) shows random walk characteristics at 10-200sec

A green dashed line in Fig. 4 represents (scan length) = (gap length). Hence, it is possible to do a phase-delay connection after switching VLBI observations only in the case when gap length is located on the left-side from this line because gap length can be longer than scan length. Considering that, 100 sec is a limit scan length (switching period) for X-band switching observations. As for S-band, no limitation appears from an atmospheric stability. Of course, this depends on the condition of the atmosphere, so that current one just shows a case study result. Moreover we may take a 3-sigma criterion (i.e., $3\rho=\pi$) to make a phase connection more robust. In this case, switching period becomes shorter.

Monthly Report of July, 2006

1. Kashima-Gifu-Koganei VLBI Experiment (last TID Experiment)

The fifth TID VLBI experiment (maybe the last one) was carried out on July 21, 2006. Koganei station was involved in this experiment besides Kashima and Gifu. Table 1 summarizes all TID VLBI experiments. The data transfer from Gifu and correlation processing for the fifth experiment was carried out by using PCs at Kashima, which were remotely executed from Vienna.

	Date	Stations	Source	Comments
No.1	12-13 UT March 16, 2006	Kashima(34m) Gifu(11m)	3C273B	Rainy
No.2	13-15 UT April 19, 2006	Kashima(34m) Gifu(11m)	3C273B	No S-band data at Kashima
No.3	13-15 UT May 10, 2006	Kashima(34m) Gifu(11m)	3C273B	No S-band data at Gifu
No.4	13-15 UT May 11, 2006	Kashima(34m) Gifu(11m)	3C273B	
No.5	15-17 UT July 21, 2006	Kashima(34m) Gifu(11m) Koganei(11m)	3C454.3	Rainy at Gifu? GPS 1Hz observation except for Gifu (failed at Gifu)

Table 1: Summary of TID VLBI Experiments

Scan #4 in Kashima data has a problem in header data. Header data were accidentally corrupted due to a sampling board problem. Detailed investigation of corrupted header showed that it was possible to recover header data, then a new program "data_recov" has been developed for this purpose. However correlation results using header recovered data shows a sub-peak shifted in delay domain by -2 micro seconds (corresponding to 8-bit data) (Fig. 1). This means that data were somewhat affected (corrupted) at a sampled data field as well as a header field. The correlation amplitude at the main-peak was diminished by 44% compared with other scans, but it shows a correct delay and fringe phases. Therefore we can use the data for a phase-delay connection.

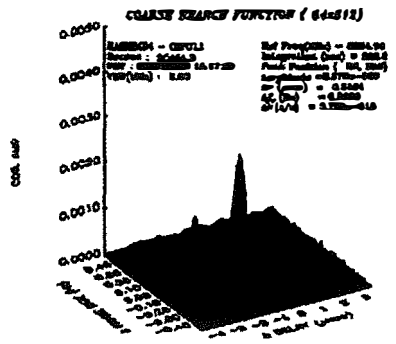

Fig.1: Coarse search function for header recovered data. See in the text for details.

Fig.2 shows gap limits obtained for three experiments on the Kashima-Gifu baseline by using the method described in the June report. Weather condition and elevation angle during the experiments are summarized in Table 2.

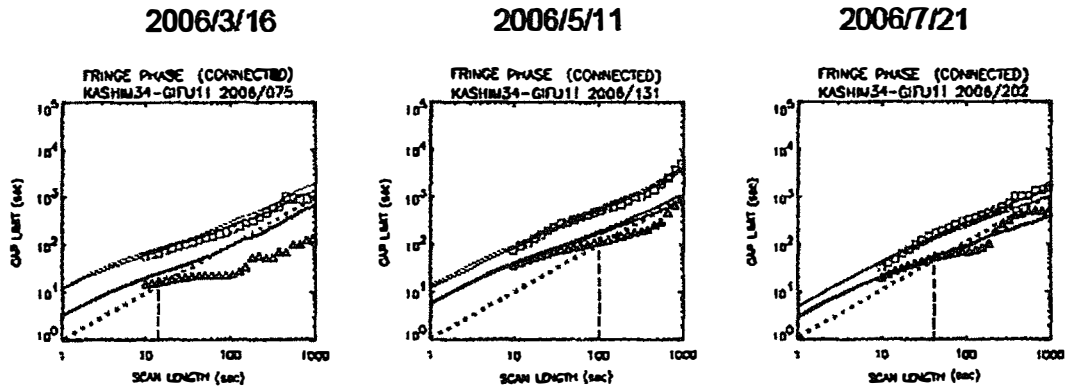

Fig.2: Gap limit obtained from fringe phase variations (solid lines: red for S-band, dark green for X-band) and those obtained from this study (symbols: square for S-band, triangle for X-band). A green dashed line represents (scan length) = (gap length).

		T (deg)	P (hP)	H (%)	Weather	Elevation angle (deg)
2006/3/16 (12-13h UT) 3C273B	Kashima	13.3	997.6	88.5	Rainy	36.2
	Gifu	10.2	991.4	97.0	Rainy	33.6
2006/5/11 (13-15h UT) 3C273B	Kashima	15.1	1015.8	83.9	Cloudy	44.7
	Gifu	15.9	1017.3	55.9	Cloudy	47.3
2006/7/21 (15-17h UT) 3C454.3	Kashima	20.7	999.2	91.9	Cloudy	61.2
	Gifu	21.5	999.7	99.9	Rainy	58.8

Table 2: Weather condition and elevation angle at experiments. Meteorological data are averaged over each observation period. Elevation angle is at a center of observation period.

Besides the May 11 experiment it was rain of either one of stations. Gap limits by means of the method described in the June report are 13 sec, 100 sec, and 40 sec for March 16, May 11, and July 26 experiments, respectively. We can say that gap limit is easily affected by weather condition even though we consider the difference in elevation angle.

Fig.3 shows an analysis result as same as Fig.2 but for Kashima-Koganei baseline. Gap limit is obtained at about 90 sec. In the mean time, as for Koganei-Gifu baseline, we exclude it from this analysis because the signal to noise ratio at the unit integration period of 1 sec is too low to obtain a reliable result.

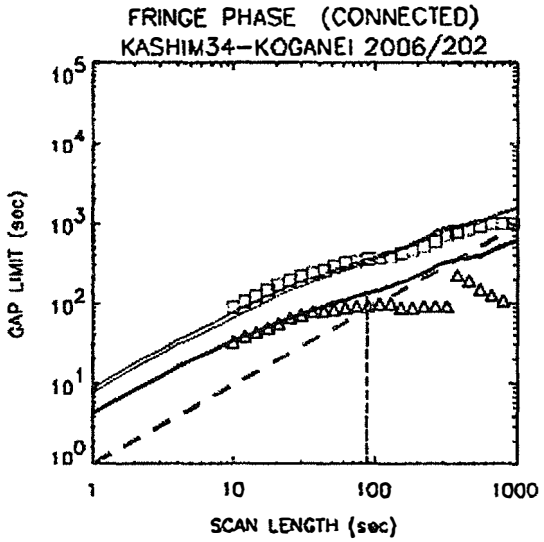

Fig.3: Same as Fig.2 but for Kashima-Koganei baseline on July 21 experiment.

Inhomogeneous distribution of water vapor is a main cause of fluctuations in fringe phase. The scale size of inhomogeneous distribution is about a few kilometers, so that the fluctuation of fringe phases on a baseline longer than this scale is affected by local weather condition rather than the difference of baseline lengths.

Monthly Report of August, 2006 (DRAFT)

1. Summary of VLBI Experiment

Five VLBI sessions dedicated to detect TID events were carried out during March – July, 2006. Each session observed a strong source, 3C273B or 3C454.3, for 1 or 2 hours continuously using 4 channels of geodetic-VLBI backend outputs of which RF frequencies are set to 8234.99 and 8584.99 MHz in X band and 2269.99 and 2344.99 MHz in S band with video bandwidth of 2 MHz. Kashima 34m antenna and Gifu 11m antenna participated in all sessions, but Koganei 11m antenna participated only in the last session. At all stations a hydrogen maser oscillator was used as a system reference signal. We failed to observe at S band in the two sessions among five, and also failed in continuous observation in these two sessions. Therefore three session data were analyzed for detecting TID events. However no TID event was detected. By the way, a continuous observation of one source enables us to investigate the fluctuations of fringe phases at various time scales. We have therefore analyzed the three session data to investigate an adequate switching time in a delta VLBI observation.

Delta (or differential) Very Long Baseline Interferometry (VLBI) is a technique to measure the angular separation between two nearby celestial radio-sources accurately by observing each source alternately. Common error sources such as those introduced by the receiving systems, clocks, propagating media, and station locations are nearly cancelled by differencing observed delays between sources. If the position of one source is well-known, we can measure the position of the other source through the well-known source position. The technique has been used for the navigation of a spacecraft (SC) cruising in deep space by observing an SC and a nearby extragalactic radio source (EGRS) alternately since the late 1970's (e.g., Brunn et al., 1978; Christensen et al., 1980). Since an antenna tracks SC and EGRS alternately, gaps in each data stream are inevitable. Consequently fringe phase of each data segment (scan) has an ambiguity of 2π. When observations are carried out with a narrow bandwidth like reception of carrier signals emitted from an SC, it is an important issue for improving the accuracy of measurements to connect fringe phases of corresponding scans. Wu (1979) developed a scheme to connect fringe phases among consecutive scans based on the iterative adjustment of integer ambiguity numbers. He applied the method to delta VLBI observations of Voyager 1 and OJ287 and concluded that when there was no sizable localized phase fluctuation mainly due to atmospheric disturbances the scheme connected VLBI fringe phases faultlessly. Both scan and gap lengths were about 5 minutes in this case. A limitation about gap lengths was not mentioned in his paper.

Recently the position measurements of NOZOMI, which is a Japanese Mars explorer (Yamamoto and Tsuruda, 1998), and HAYABUSA, which is a Japanese mission for near-earth-asteroid sample return (Fujiwara et al., 1999), by means of delta VLBI were carried out in Japan (Ichikawa et al., 2004; Sekido et al., 2004; Ichikawa et al., 2006). In the measurements the connection of fringe phases among consecutive scans is recognized again as an important issue to improve the measurement accuracy. Fluctuated fringe phases limit a gap length over which fringe phases can be connected. Thus one antenna switching period should be less than this limit length. Therefore the maximum limit of gap length as well as source strength is a critical parameter for preparing an observation schedule. This parameter thought to be strongly related to weather condition and locality. A number of researchers investigated statistical characteristics of atmospheric phase fluctuations by using radio interferometry including VLBI (e.g., Rogers and Moran, 1981; Rogers et al.,1984; Kasuga et al., 1986; Liu et al., 2005). Some hints regarding a gap limit may be obtained from their results of Allan variance and/or structure function, but it is not a straightforward one and the location of antenna is different from our concerned one. We have therefore analyzed the TID session data to investigate an adequate switching time in a delta VLBI observation.

Firstly, we developed a scheme to connect phase delays (fringe phases) over a short gap by using observed delay and delay rate (see the May report for details). By using this scheme, we can obtain fringe phase data connected over 1 or 2 hours. The fringe data were further analyzed statistically to estimate the maximum gap length to connect fringe phases by using the two methods as follows.

Method A: using the true variance of fringe phase fluctuations (see the April report for details)

Method B: using the linear fitting of fringe phases (see the June report for details)

Gap limits obtained by the two methods are summarized in Table 1 and depicted in Fig.1 for X band. As for S-band, maximum gap limit is longer than 1000 s for both methods. As for X band, they varies from 60 to 486 s for method A and from 16 to 126 for B. Furthermore gap limits obtained from method B are always shorter than those obtained from method A by about 28-74 % as shown in Fig.1. This means that the assumption used in method A is not correct for these scan lengths. In method A, the Gaussian distribution of phase fluctuations is assumed for all time ranges to propagate the errors over a gap. However it is not a Gaussian distribution (white phase fluctuation) at time scales from several tens to several hundreds of seconds as shown in Fig.2. Hence the available gap limits estimated by using linear fitting of fringe phases are thought to reflect a more actual condition.

Session	Frequency Band	Gap Limit (sec)	
		Method A	Method B
March 16, 2006 Kashima-Gifu	X	60	16
	S	>1000	>1000
May 11, 2006 Kashima-Gifu	X	486	126
	S	>1000	>1000
July 21, 2006 Kashima-Gifu	X	80	58
	S	>1000	>1000
July 21, 2006 Kashima-Koganei	X	335	96
	S	>1000	>1000

Table 1: Summary of gap limits

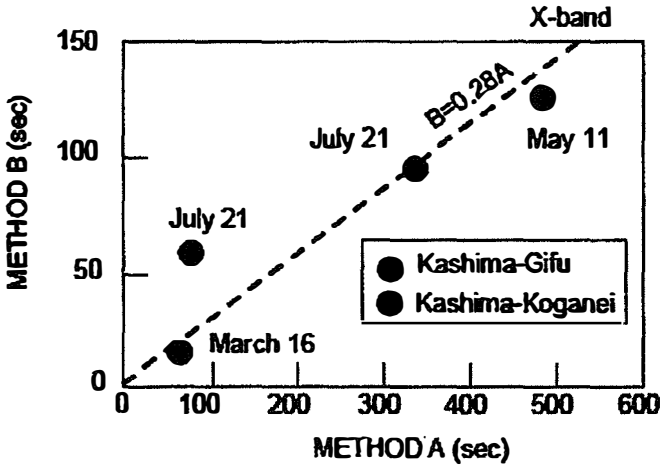

Fig.1: Gap limits (comparison of method A and B).

It was raining at least at one station except for the May 11 session. Drastic shortening of the maximum gap limits occurred when it was raining as we can see for the Kashima-Gifu baseline. So far we have no data observed with weather condition of clear sky. We would like to conduct a session regularly at least once a month to investigate the relation between scan length and maximum gap length statistically under wider range of weather conditions.

References

Brunn, D.L., R.A. Preston, S.C.Wu, H.L. Siegel, D.S. Brown, C.S. Christensen, and D.E. Hilt, Delta VLBI spacecraft tracking system demonstration: Part I. design and planning, DSN Progress Report 42-45, 111-132, 1978.

Christensen, C.S., B. Moultrie, P.S. Callahan, F.F. Donivan, and S.C. Wu, Delta VLBI spacecraft tracking system demonstration: Part II: data acquisition and processing, TDA Progress Report 42-60, 60-67, 1980.

Fujiwara, A., T. Mukai, J. Kawaguchi, and K.T. Uesugi, Sample return mission to NEA: MUSES-C, Advances in Space Research, 25, 231-238, 1999.

Ichikawa, R., M. Sekido, H. Osaki, Y. Koyama, T. Kondo, T. Ohnishi, M. Yoshikawa, W. Cannon, A. Novikov, M. Berube, and NOZOMI DVLBI GROUP, An evaluation of VLBI observations for the deep space tracking on the interplanetary spacecrafts, in International VLBI Service for Geodesy and Astrometry 2004 General Meeting Proceedings, Edited by Nancy R. Vandenberg and Karen D. Baver, NASA/CP-2004-212255, 253-257, 2004.

Ichikawa, R., M. Sekido, Y. Koyama, and T. Kondo, An evaluation of atmospheric path delay correction in differential VLBI expriments for spacecraft tracking, in International VLBI Service for Geodesy and Astrometry 2006 General Meeting Proceedings, Edited by D. Behrend and K.D. Baver, 2006. (in press)

Kasuga, T., M. Ishiguro, and R. Kawabe, Interferometric measurement of tropospheric phase fluctuations at 22 GHz on antenna spacings of 27 to 540 m, IEEE Trans. Antennas Propag., AP-34, 797-803, 1986.

Liu, Q., M. Nishio, K. Yamamura, T. Miyazaki, M. Hirata, T. Suzuyama, S. Kuji, K. Iwadate, O. Kameya, and N. Kawano, Statistical characteristics of atmospheric phase fluctuations observed by a VLBI system using a beacon wave from a geostationary satellite, IEEE Trans. Antennas Propag., AP-53, 1519-1527, 2005.

Rogers, A.E.E. and J.M. Moran, Coherence limit for very long baseline interferometry, IEEE Trans. Instrum. Meas., IM-30, 283-286, 1981.

Rogers, A.E.E., A.T. Moffet, D.C. Backer, and J.M. Moran, Coherence limits in VLBI observation at 3-millimeter wave length, Radio Sci., 19, 1552-1560, 1984.

Sekido, M, R. Ichikawa, H. Osaki, T. Kondo, Y. Koyama, M. Yoshikawa, T. Ohnishi, W. Cannon, A. Novikov, M. Berube, and NOZOMI DVLBI GROUP, VLBI observation spacecraft navigation (NOZOMI) - data processing and analysis status report, in International VLBI Service for Geodesy and Astrometry 2004 General Meeting Proceedings, Edited by Nancy R. Vandenberg and Karen D. Baver, NASA/CP-2004-212255, 258-262, 2004.

Wu, S.C., Connection and validation of narrow-band delta VLBI phase observations, DSN Progress report 42-52, 13-20, 1979.

Danke Schön

GEOWISSENSCHAFTLICHE MITTEILUNGEN

Bisher erschienen:

Heft 1 Kolloquium der Assistenten der Studienrichtung Vermessungswesen. 1970 - 1973, Dezember 1973.

Heft 2 EGGER-PERDICH-PLACH-WAGENSOMMERER, Taschenrechner HP 45 und HP 65, Programme und Anwendungen im Vermessungswesen. 1. Auflage, März 1974, Special Edition in English, Juli 1974, 2. verbesserte Auflage, November 1974.

Heft 3 Kolloquium der Assistenten der Studienrichtung Vermessungswesen 1973 - 1974, September 1974.

Heft 4 EGGER-PALFINGER-PERDICH-PLACH-WAGENSOMMERER, Tektronix-Tischrechner TEK 31, Programmbibliothek für den Einsatz im Vermessungswesen, November 1974.

Heft 5 K.LEDERSTEGER, Die horizontale Isostasie und das isostatische Geoid, Februar 1975.

Heft 6 F.REINHART, Katalog von FK4 Horrebow-Paaren für Breiten von +30 bis +60, Oktober 1975.

Heft 7 Arbeiten aus dem Institut für Höhere Geodäsie, Wien, Dezember 1975.

Heft 8 Veröffentlichungen des Instituts für Photogrammetrie zum XIII. Internationalen Kongreß für Photogrammetrie in Helsinki 1976, Wien, Juli 1976.

Heft 9 W.PILLEWIZER, Felsdarstellung aus Orthophotos, Wien, Juni 1976.

Heft 10 PERDICH-PLACH-WAGENSOMMERER, Der Einsatz des programmierbaren Taschenrechners Texas Instruments SR-52 mit Drucker PC100 in ingenieurgeodätischen Rechentechnik, Wien, Mai 1976.

Heft 11 Kolloquium der Assistenten der Studienrichtung Vermessungswesen 1974 - 1976, November 1976.

Heft 12 Kartographische Vorträge der Geodätischen Informationstage 1976, Wien, Mai 1977.

Heft 13 Veröffentlichung des Instituts für Photogrammetrie anläßlich des 80. Geburtstages von Prof.Dr.h.c.K.Neumaier, Wien, Januar 1978.

Heft 14 L.MOLNAR, Self Checking Analytical Relative Orientation and Strip Formation, Wien, Dezember 1978.

Heft 15 Veröffentlichung des Instituts für Landesvermessung anläßlich des 80. Geburtstages von Prof.Dr.Alois Bavir, Wien, Januar 1979.

Heft 16 Kolloquium der Assistenten der Studienrichtung Vermessungswesen 1976 - 1978, Wien, November 1979.

Heft 17 E.VOZIKIS, Die photographische Differentialumbildung gekrümmter Flächen mit Beispielen aus der Architekturbildmessung, Wien, Dezember 1979.

Heft 18 Veröffentlichung des Instituts für Allgemeine Geodäsie anläßlich des 75. Geburtstages von Prof.Dipl.Ing.Dr.F.Hauer, Die Höhe des Großglockners, Wien, 1981.

Heft 19 H.KAGER, Bündeltriangulation mit indirekt beobachteten Kreiszentren, Wien, April 1981.

Heft 20 Kartrographische Vorträge der Geodätischen Informationstage 1980, Wien, Mai 1982.

Heft 21 Veröffentlichung des Instituts für Kartographie anläßlich des 70. Geburtstages von Prof.Dr.Wolfgang Pillewizer: Glaziologie und Kartographie, Wien, Dezember 1982.

Heft 22 K.TEMPFLI, Genauigkeitsschätzung digitaler Höhenmodelle mittels Spektralanalyse, Wien, Mai 1982.

Heft 23 E.CSAPLOVICS, Interpretation von Farbinfrarotbildern, Wien, November 1982.

Heft 24 J.JANSA, Rektifizierung von Multispektral-Scanneraufnahmen - Entwicklung und Erprobung eines EDV-Programms, Wien, Mai 1983.

Heft 25 Zusammenfassung der Diplomarbeiten, Dissertationen und Habilitationen an den geodätischen Instituten der TU Wien, Wien, November 1984.

Heft 26 T.WUNDERLICH, Die voraussetzungsfreie Bestimmung von Refraktionswinkeln, Wien, August 1985.

Heft 27 G.GERSTBACH (Hrsg.), Geowissenschaftliche/geotechnische Daten in Landinformationssystemen - Bedarf und Möglichkeiten in Österreich, Juni 1986.

Heft 28 K.NOVAK, Orientierung von Amateuraufnahmen ohne Paßpunkte, Wien, August 1986.

Heft 29 Veröffentlichung des Instituts für Landesvermessung und Ingenieurgeodäsie, Abt. Ingenieurgeodäsie, anläßlich des 80. Geburtstages von Prof.Dipl.Ing.Dr.F.Hauer, Wien, Oktober 1986.

Heft 30 K.-H.ROCH, Über die Bedeutung dynamisch ermittelter Parameter für die Bestimmung von Gesteins- und Gebirgseigenschaften, Wien, Februar 1987.

Heft 31 G. HE, Bildverbesserung mittels digitaler Filterung, Wien, April 1989.

Heft 32 F.SCHLÖGELHOFER, Qualitäts- und Wirtschaftlichkeitsmodelle für die Ingenieurphotogrammetrie, Wien, April 1989.

Heft 33 G.GERSTBACH (Hrsg.), Geowissenschaftliche/geotechnische Daten in Landinformationssystemen - Datenbestände und Datenaustausch in Österreich, Wien, Juni 1989.

Heft 34 F.HOCHSTÖGER, Ein Beitrag zur Anwendung und Visualisierung digitaler Geländemodelle, Wien, Dezember 1989.

Heft 35 R.WEBER, Lokale Schwerefeldmodellierung unter Berücksichtigung spektraler Methoden zur Geländereduktion, Wien, April 1990.

Heft 36 o.Prof.Dr.Hans Schmid zum 70. Geburtstag. Veröffentlichung der Abteilung für Landesvermessung, Wien, Oktober 1990.

Heft 37 G.GERSTBACH, H.P.HÖLLRIEGL und R.WEBER, Geowissenschaftliche Informationsbörse - Eine Nachlese zu GeoLIS II, Wien, Oktober 1990.

Heft 38 R.ECKER, Rastergraphische Visualisierungen mittels digitaler Geländemodelle, Wien, August 1991.

Heft 39 Kartographische Forschungen und Anwendungsorientierte Entwicklungen, herausgegeben von W.Stams und F.Kelnhofer zum 80. Geburtstag von Prof.Dr.W.Pillewizer, Wien, Juli 1991.

Heft 39a W.RIEGER, Hydrologische Anwendungen des digitalen Geländemodelles, Wien, Juli 1992.

Heft 40 K.STEINNOCHER, Methodische Erweiterungen der Landnutzungsklassifikation und Implementierung auf einem Transputernetzwerk, Wien, Juli 1994.

Heft 41 G.FORKERT, Die Lösung photogrammetrischer Orientierungs- und Rekonstruktionsaufgaben mittels allgemeiner kurvenförmiger Elemente, Wien, Juli 1994.

Heft 42 M.SCHÖNER, W.SCHÖNER, Photogrammetrische und glaziologische Untersuchungen am Gàsbre (Ergebnisse der Spitzbergenexpedition 1991), Wien, Mai 1996.

Heft 43 M.ROIC. Erfassung von nicht signalisierten 3D-Strukturen mit Videotheodoliten, Wien, April 1996.

Heft 44 G.RETSCHER, 3D-Gleiserfassung mit einem Multisensorsystem und linearen Filterverfahren, Wien, April 1996.

Heft 45 W.DAXINGER, Astrogravimetrische Geoidbestimmung für Ingenieurprojekte, Wien, Juli 1996.

Heft 46 M.PLONER, CCD-Astrometrie von Objekten des geostationären Ringes, Wien, November 1996.

Heft 47 Zum Gedenken an Karl Killian "Ingenieur" und "Geodät" 1903-1991, Veröffentlichung der Fachgruppe Geowissenschaften, Wien, Februar 1997.

Heft 48 A.SINDHUBER, Ergänzung und Fortführung eines digitalen Landschaftsmodelles mit multispektralen und hochauflösenden Fernerkundungsaufnahmen, Wien, Mai 1998.

Heft 49 W.WAGNER, Soil Moisture Retrieval from ERS Scatterometer Data, Wien, Dezember 1998.

Heft 50 R.WEBER, E.FRAGNER (Editoren),Prof.Bretterbauer, Festschrift zum 70.Geburtstag, Wien, Juli 1999.

Heft 51 Ch.ÖHRENEDER, A Similarity Measure for Global Image Matching Based on The Forward Modeling Principle, Wien, April 1999.

Heft 52 M.LECHTHALER, G.GARTNER, Per Aspera ad Astra, Festschrift für Fritz Kelnhofer zum 60. Geburtstag, Wien, Jänner 2000.

Heft 53 F.KELNHOFER, M.LECHTHALER, Interaktive Karten (Atlanten) und Multimedia - Applikationen, Wien, März 2000.

Heft 54 A.MISCHKE, Entwicklung eines Videotheodlit-Meßsystems zur automatischen Richtungsmessung von nicht signalisierten Objektpunkten, Wien, Mai 2000

Heft 55 Veröffentlichung des I.P.F. anlässlich der Emeritierung von Prof.Dr. Peter Waldhäusl, Wien.

Heft 56 F.ROTTENSTEINER, Semi-automatic Extraction of Buildings Based on Hybrid Adjustment Using 3D Surface Models and Management of Building Data in a TIS, Wien, Juni 2001.

Heft 57 D.LEGENSTEIN, Objektrekonstruktion aus perspektiven Bildern unter Einbeziehung von Umrisslinien, Wien, Mai 2001.

Heft 58 F.KELNHOFER, M.LECHTHALER und K.BRUNNER (Hrsg.), Telekartographie und Location Based Services, Wien, Jänner 2002.

Heft 59 K.BRETTERBAUER, Die runde Erde eben dargestellt: Abbildungslehre und sphärische Kartennetzentwürfe, Wien, 2002.

Heft 60 G.GARTNER, Maps and the Internet 2002, Wien 2002.

Heft 61 L.DORFFNER, Erzeugung von qualitativ hochwertigen 3D Photomodellen für Internetbasierte Anwendungen mit besonderem Augenmerk auf Objekte der Nahbereichsphotogrammetrie, Wien, Jänner 2002.

Heft 62 CHMELINA, Wissensbasierte Analyse von Verschiebungsdaten im Tunnelbau Wien 2002

Heft 63 A.NIESSNER, Qualitative Deformationsanalase unter Ausnutzung der Farbinformation, Wien 2002

Heft 64 K.BRETTERBAUER; R.WEBER, A Primer of Geodesy for GIS-Users, Wien im Herbst 2003

Heft 65 N.PFEIFER, 3D Terain Models on the basis of a triangulation, Wien, Jänner 2002.

Heft 66 G.GARTNER (Hrsg), Lacation Based Services & Telecartography, Wien, 2004

Heft 67 I.KABASHI, Gleichzeitig-gegenseitige Zenitwinkelmessung über größere Entfernungen mit automatischen Zielsystemen, Wien, 2004

Heft 68 J.BÖHM, Troposphärische Laufzeitverzögerungen in der VLBI, Wien 2004

Heft 69 R.WEBER, W.SCHLÜTER, U.SCHREIBER, O. TITOV
Evolving Space Geodesy Techniques (EGS XXVII General Assembly, Nice, France, 2002), Wien 2004

Heft 70 G. WEINWURM, Amalthea's Gravity Field and its Impact on a Spacecraft Trajectory, Wien 2004

Heft 71 Forschungsgruppe Ingenieurgeodäsie, Festschrift anlässlich des 65. Geburtstages von Herrn o.Univ.Prof.Dr.-Ing. Heriber Kahmen, Wien 2005

Heft 72 A. REITERER, A Knowledge-Based Decision System for an On-Line Video-Theodolite-Based Multisensor System, Wien 2005

Heft 73 M. HABERLER, Einsatz von Fuzzy Methoden zur Detektion konsistenter Punktbewegungen, Wien 2005

Heft 74 G. GARTNER, Location Based Services & Telecartography, Proceedings of the Symposium 2005, Wien 2005

Heft 75 Th. HOBIGER, VLBI as a tool to probe the ionosphere, Wien 2006

Heft 76 E. KLAFFENBÖCK, Troposphärische Laufzeitverzögerung von GNSS-Signalen – Nutzen aktiver Referenzstationsnetze für die Meteorologie, Wien 2007

Heft 77 P.J. MENDES-CERVEIRA, Tidal and non-tidal contributions to surface loading processes on station coordinates, Wien 2006